Design and Evaluation of Integrated Waste to Energy Multigenerational Systems

by

Ugur Kahraman

A thesis submitted to the
School of Graduate and Postdoctoral Studies in partial
fulfillment of the requirements for the degree of

Master of Applied Science in Mechanical Engineering

Faculty of Engineering and Applied Science

University of Ontario Institute of Technology (Ontario Tech University)

Oshawa, Ontario, Canada

April 2022

Thesis Examination Information

Submitted by: **Ugur Kahraman**

Master of Applied Science in Mechanical Engineering

Thesis title: Design and Evaluation of Integrated Waste to Energy Multigenerational Systems

An oral defense of this thesis took place on April 12, 2022, in front of the following examining committee:

Examining Committee:

Chair of Examining Committee	Prof. Dr. Ghaus Rizvi
Research Supervisor	Prof. Dr. Ibrahim Dincer
Examining Committee Member	Assoc Prof. Haoxiang Lang
Examining Committee Member	Dr. Dipal Patel
Thesis Examiner	Dr. Sayyed Ali Hosseini

The above committee determined that the thesis is acceptable in form and content and that a satisfactory knowledge of the field covered by the thesis was demonstrated by the candidate during an oral examination. A signed copy of the Certificate of Approval is available from the School of Graduate and Postdoctoral Studies.

Abstract

This thesis study develops three renewable energy-based waste-to-energy multigeneration systems and examine them thermodynamically and economically. The first system uses solar-based energy and animal manure waste, and the second system utilizes waste tires with geothermal energy. Finally, the third system is an underground coal gasification system in which low-grade lignite is considered waste and used as fuel. Hydrogen, ethanol, electricity, heating, cooling, and sulfuric acid are produced for the communities in Konya in Turkey, Tuscany in Italy, and Kutahya in Turkey. All suggested systems are developed, modelled, and analyzed using thermodynamic-based sensitive simulations and software. According to the calculations, multigeneration system 2 provides the best performance results, and the overall system energy and exergy efficiencies are 71.45% and 69.87%, respectively. Integration of waste-to-energy systems with renewable energy sources leads to the prevention of waste generation and the development of more environmentally benign systems.

Keywords: ethanol; gasification; geothermal; hydrogen; power; solar

Author's Declaration

I hereby declare that this thesis consists of original work of which I have authored. This is a true copy of the thesis, including any required final revisions, as accepted by my examiners.

I authorize the University of Ontario Institute of Technology (Ontario Tech University) to lend this thesis to other institutions or individuals for the purpose of scholarly research. I further authorize University of Ontario Institute of Technology (Ontario Tech University) to reproduce this thesis by photocopying or by other means, in total or in part, at the request of other institutions or individuals for the purpose of scholarly research. I understand that my thesis will be made electronically available to the public.

UGUR KAHRAMAN

Statement of Contributions

Part of the work described as multigeneration system 1 is published as:

U. Kahraman and I. Dincer, “Performance analysis of a solar based waste to energy multigeneration system,” Sustainable Energy Technology and Assessments, vol. 50, no. August 2021, p. 101729, 2022, doi: 10.1016/j.seta.2021.101729.

Acknowledgements

I would like to express my heartfelt appreciation to my supervisor, Prof. Dr. Ibrahim Dincer, for his steadfast support, guidance, and tolerance, which helped me complete my thesis. I would also like to express my gratitude to him for this once-in-a-lifetime opportunity and igniting my research passion.

I would like to express my gratitude to my mother, father, sister, and friends. Their unwavering support and encouragement are significant motivators for me to pursue my career. It is not easy to put their immense impact and significance on me into words.

I would also like to thank Mohamed Ismail and Mert Temiz for their help during my master's and extend my appreciation to my colleagues and friends within the clean energy research laboratory and ACE 3030B.

Table of Contents

List of Tables

List of Figures

Nomenclature

CE	chemical exergy (kJ/kg)
COC	cost of capital ($)
e	specific energy (kJ/kg)
E	energy (kJ)
e_{mix}	chemical exergy of mixed waste (kJ/kg)
ex	specific exergy (kJ/kg)
Ex	exergy (kJ)
$\dot{E}x$	exergy rate (kW)
ex_{CH}	standard chemical exergy (kJ/kg)
ex_{dest}	specific exergy destruction rate (kJ/kg)
$\dot{E}x_d$	exergy destruction rate (kW)
Ex_Q	exergy transfer associated with heat transfer (kJ)
$\dot{E}x_{\dot{Q}}$	exergy transfer rate associated with heat transfer rate (kW)
G	Gibbs free energy (J)
g	gravitational acceleration (m s^{-2})
HHV	higher heating value (kJ/kg)
h	specific enthalpy (kJ/kg)
H	enthalpy (kJ)
HV	heating value (kJ/kg)
LHV	lower heating value (kJ/kg)
m	mass (kg)
$\dot{m}$	mass flow rate (kg/s)
P	pressure (kPa)
r	discount rate
q	specific heat transfer (kJ/kg)
Q	heat transfer (kJ)
$\dot{Q}$	heat transfer rate (kW)
s	specific entropy (kJ/kg.K)
S	entropy (kJ /K)
$\dot{S}$	entropy rate (kW/K)

t	time (s)
T	temperature (^{o}C or K)
w	water, specific work (kJ/kg)
W	total work (kJ)
$\dot{W}$	work rate (kW)
x	vapor quality

Subscripts

c	compressor
d	destruction
exv	expansion valve
gen	generation
H	high
hex	heat exchanger
i	inlet
j	outlet
L	low
mc	maintenance cost
oc	operating cost
P	pump
t	total
T	turbine
TV	throttling valve
w	water

Greek Letters

η	energy efficiency
ρ	density
ψ	exergy efficiency

Acronyms

ARC	absorption refrigeration cycle
ASU	air separation unit

BFB	bubbling fluidized bed
BR	Boudouard reaction
CC	combustion chamber
COMP	compressor
COND	condenser
CS	cyclone separator
EES	engineering equation solver
EXV	expansion valve
EV	evaporator
GEN	generator
GF	gasifier
HEX	heat exchanger
HRSG	heat recovery steam generator
HTTS	higher temperature thermal storage
LTTS	lower temperature thermal storage
IGCC	integrated gasification combined cycle
IRR	internal rate of return
IPCC	Intergovernmental Panel on Climate Change
M	Million
MED	multi-effect distillation
NASA	National Aeronautics and Space Administration
NPV	net present value
OECD	Organisation for Economic Co-operation and Development
PBP	payback period
PRS	primary Rankine cycle
PTC	parabolic trough collector
PV	photovoltaic
PV/T	photovoltaic/thermal
REC	rectifier
SAP	sulfuric acid production

ST	steam turbine
TES	thermal energy storage
TRC	the third Rankine cycle
UCG	underground coal gasification
WGSR	water gas shift reactor

Chapter 1. Introduction

Throughout history, energy has undoubtedly been one of the most critical needs of humanity. Today, it undergoes a revolution under the perspective of sustainability by countries and organizations all over the world. Sustainable development is accomplishable goal. However, various variables should be considered. Consideration should be given to the capacity to phase out fossil fuels as an energy source, ensuring the transition to green energy sources with lower emissions, increasing energy production efficiency, and energy consumption reduction [1]. Renewable energy sources such as geothermal, wind, solar, and tidal have grown to prominence in recent years as viable solutions for fossil fuels. However, these resources, whose efficiency changes depending on various factors such as solar radiation and wind speed, also bring some sustainability concerns. Therefore, incorporating renewable energy sources into systems poses particular sustainability challenges due to environmental conditions [2]. To address these obstacles, integrated systems that combine energy sources and produce alternative fuels such as ethanol and hydrogen, in addition to cooling, electricity generation, and heating, seem to be a reasonable solution.

1.1 Environmental Issues

Undeniably, climate change is one of the most serious concerns of our age. Since the early twentieth century, the temperature of the world's atmosphere has grown by 1.18 °C on average due to the increase in human activities and carbon dioxide emissions [3]. While rising air temperatures endanger nature and life, the use of fossil fuels and their environmental consequences are becoming increasingly controversial. Global carbon pollution is expected to grow by approximately 52% by the mid 21st century, according to OECD forecasts. Nevertheless, growth will be faster outside the OECD area; the OECD's share of global green gas emissions will drop to 33% in 2050 from 40% today, depending on renewable energy consumption [4].

According to a study [5], paleo sea-level data from warm times over the last three million years indicate that the global average sea level surpassed 5 metres during periods when the global average temperature was up to 2 ° C higher than pre-industrial levels. Moreover, according to the Climate Change 2021 report issued by the IPCC (Intergovernmental Panel on Climate Change) [6], a worldwide sea-level rise of 0.6 to 1.1 meters by 2100 (or around

15 millimetres per year) is predicted in its 2021 report (RCP8.5). In the worst-case scenario, by 2300, sea levels might rise by up to 5 meters. If nations considerably reduce their emissions (RCP2.6), the IPCC projects a 0.3 to 0.6-metre increase in sea level by 2100. The study's findings were used to create Figure 1.1, which depicts the rise in sea level up to the year 2300 as a function of emissions. The results demonstrate unequivocally that emissions will significantly impact global sea levels.

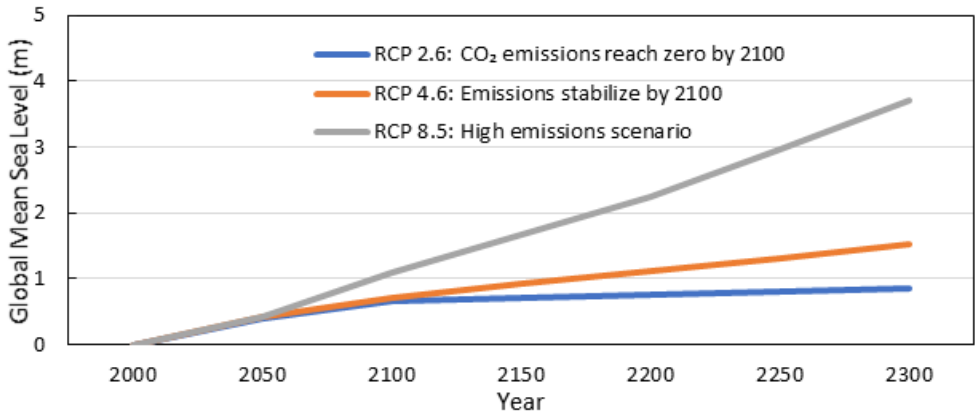

Figure 1.1 Sea level change as a result of increased emissions

(data from [6, 7])

Global warming has several negative consequences for the environment and human life, but it also poses significant economic risk factors. A recent analysis [8] assessed the effects of climate change on 22 different sectors of the economy under two alternative scenarios: if earth temperatures rised around three Celsius over pre-industrial levels in 80 years, or if they reached 4.5 degrees Celsius. According to the research, if the scenario of increased temperatures happens, climate change effects on these 22 industries may cost the United States $520 billion annually. If temperature change can be limited to 2.8 degrees Celsius, it will cost the world $224 billion less. In any event, the US, according to another analysis [9], expects to incur significant economic losses as a result of climate change, second only to India.

As a result of all these environmental effects, global warming due to increased emissions seriously damage global economic equality. Global warming has very certainly exacerbated global economic disparity, including a 25% rise in population-weighted inequality across countries over the last 50 years [10]. To prevent all these adverse effects, biofuel, hydrogen, and renewable energy sources stand out as promising methods as

alternatives to fossil fuels. The inadequacy of renewable energy sources in terms of sustainability is the most distinguishing feature of hydrogen compared to other sources, and it intensifies the studies on hydrogen [11].

1.2 World's Energy Perspective and The Importance of Green Fuels

According to the World Energy Outlook 2021 report [12], while the electricity generation in the world was 6,131 TWh in 1973, it increased approximately four and a half times until 2018, reaching 26,619 TWh. The sources used in electricity generation in 1973 are listed in Figure 1.2, where fossil fuel resources such as natural gas, oil, and coal make up the majority of all sources with 38%, 25%, and 21%, respectively. The rest is mainly met by renewable energy sources such as hydro, nuclear, solar power and wind, constituting 13% of the total resources used in energy production. While non-hydro renewable energy sources provide only 1% of this energy production, this rate has reached the order of 10% until 2021, as shown in Figure 1.2b. In opposition, oil consumption has reduced to 3%, far from being the primary source of electricity production.

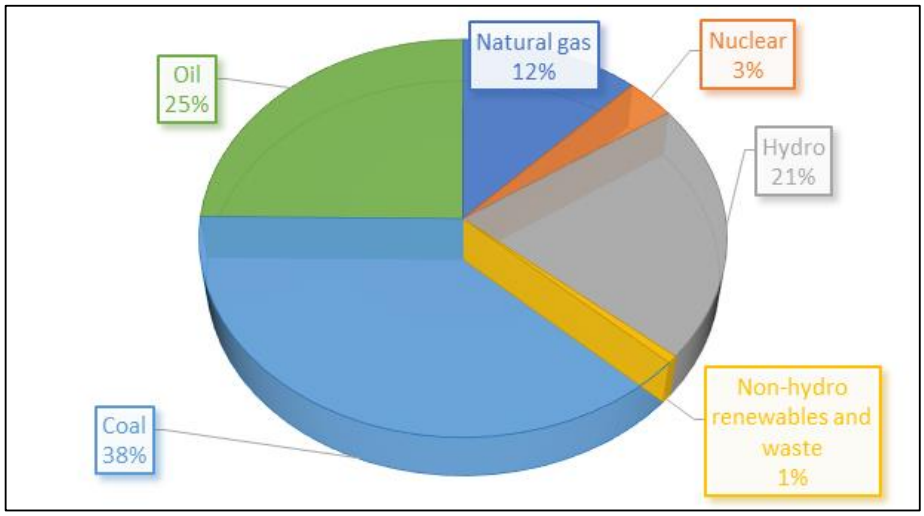

Figure 1.2a: Global share of electricity generation in 1973 (data from [13])

Numerous nations intend to diversify their energy sources and grow renewable energy in their overall energy supply. Due to their clean and renewable nature, renewable energy sources have garnered great deal of interest as a possible future substitute for fossil fuels.

Apart from renewable energy sources, fuels such as ethanol and hydrogen benefit from being both a medium for storing energy and a carrier of clean energy when created using

clean energy sources. Figure 1.3 shows the change in demand for pure hydrogen between 1975 and 2021. This implies that burning these fuels produces fewer pollutants while also allowing for extra power in hydrogen and hydrogen-rich fuels, including ethanol and methanol, which is more efficient than utilizing existing fossil fuels.

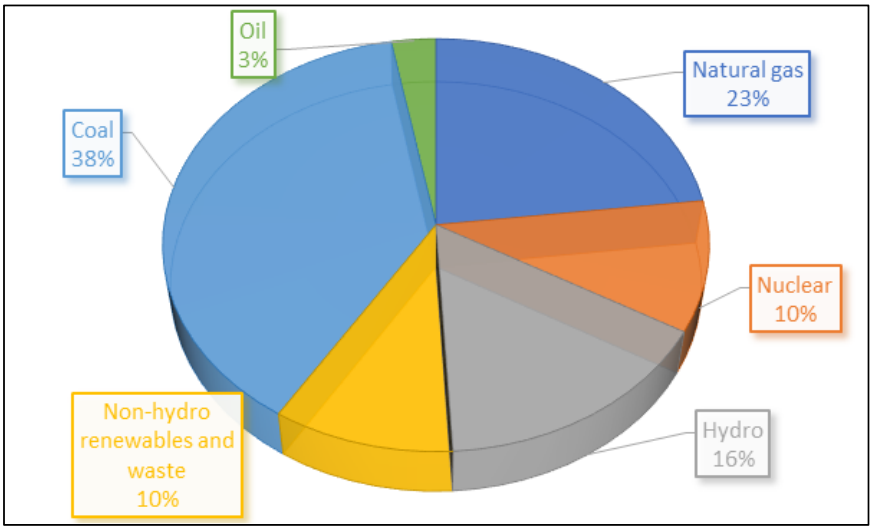

Figure 1.2b: Global share of electricity generation in 2021 (data from [13])

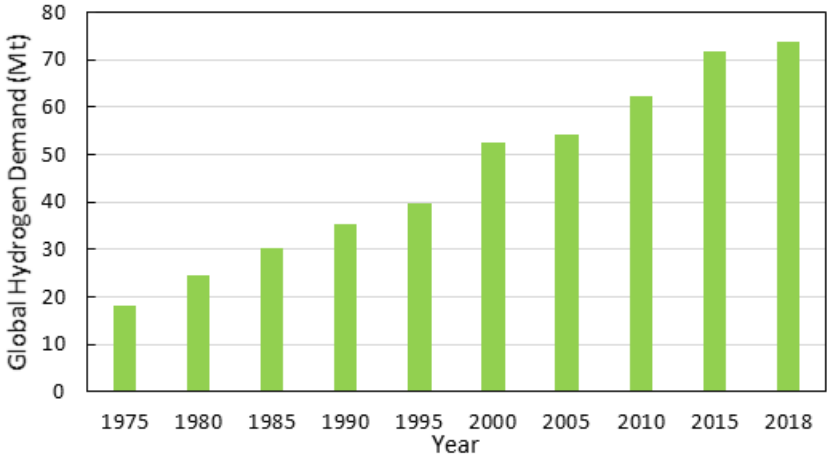

Figure 1.3: Global demand for pure hydrogen, 1975-2018 (data from [14])

As seen in the figure, demand for hydrogen is constantly growing. One of the primary reasons for this is that hydrogen's combustion products are water and oxygen. Another major factor is that hydrogen is a high-energy carrier [15]. In summary, hydrogen is a sensible potential for the long-term viability of future energy systems, providing clean, efficient power and generating heat with various transit, fixed, and portable energy

applications. The general use of hydrogen and ethanol technologies has many benefits for the environment, energy security, local economies, and end consumers [16].

1.3 Waste to Energy

Globally, approximately two billion tonnes of municipal solid waste are produced yearly, with at least one third of it not being handled in an ecologically sustainable way, according to the World Bank [17]. Globally, garbage created per capita averages almost 1 kilo daily but varies significantly between 0.11 and 4.54 kilograms. In spite of the fact that they account for just 16% of the global population, high-income nations account for around 34%, or slightly less than 700 million tonnes, of global waste. According to Figure 1.4, global waste is anticipated to reach almost 3.5 billion tonnes in a 30 year period, more than double the rate of population increase over the same time. Most of these waste sources consist of plastic and organic wastes, and they are quite suitable for economic evaluation due to their high carbon content.

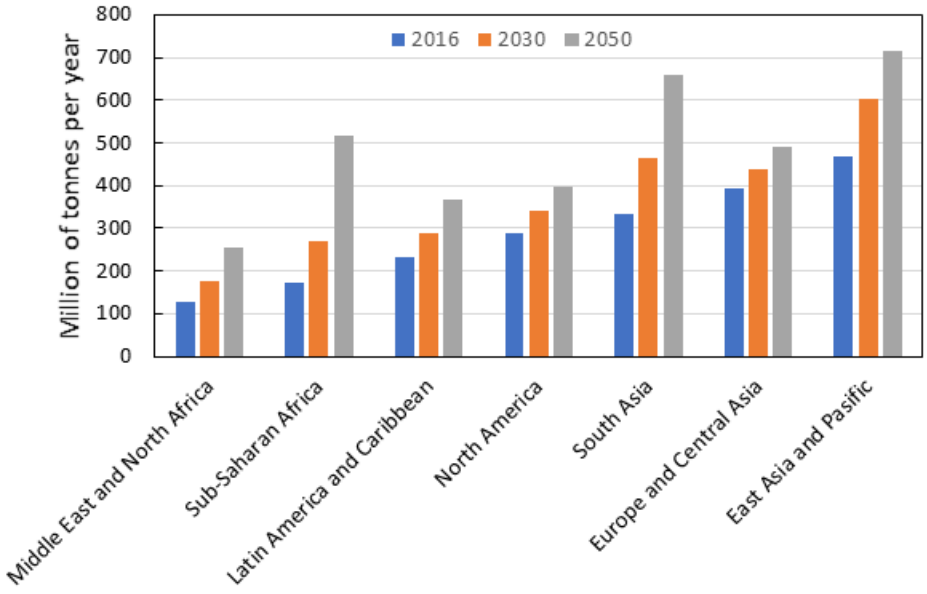

Figure 1.4: Projected waste generation (data from [17])

Numerous studies estimate that between 1 billion and 1.7 billion old tires are disposed of globally each year. This accounts for around 2–3% of the total waste collected. The United States alone discards approximately 300 million end-of-life tires each year. Waste to energy technologies such as gasification, incineration, and pyrolysis can be utilized to generate electricity and heat. Moreover, energy-dense, environmentally benign alternative

green energy resources such as hydrogen and ethanol can be produced using these technologies.

According to a United Nations global methane assesment report [18], livestock emits almost 15% of all greenhouse gases such as fluorinated gases, NOx, carbon dioxide, and methane gases discharged into the atmosphere are emitted by livestock, with more than half of it are accounted for by cattle. Utilizing this manure in the gasification process may assist in decreasing greenhouse gas emissions while also producing clean energy sources such as hydrogen and ethanol with a high energy density.

Unlike other coal types, lignite has a low heating value and can be challenging to evaluate economically. Especially for countries like Turkey, where 60% of their coal consists of lignite and its derivatives, it is of vital economic importance to benefit from this energy source. However, most coal seams are pretty deep, and the mining process is impractical. As a result, on-site exploitation of Turkish lignites by underground coal gasification is quite a cost-effective and logical approach. In addition, hydrogen and ethanol produced as a result of gasification can be stored and transported to other places. These systems are remarkably feasible for countries like Turkey with insufficient petro and natural gas resources. Utilizing this manure in the gasification process may assist in decreasing greenhouse gas emissions while also producing clean energy sources such as hydrogen and ethanol with a high energy density.

1.4 Solar Energy

No living creature can exist without solar energy, a vital source that enables plants, humans, and animals to produce all the nutrients they need. Around 2500 years ago, solar radiation was first utilized. The ancient Greeks oriented their dwellings southerly in order to maximize the utilization of solar radiation to heat their homes, particularly during the winter months [19].

NASA initially employed solar photovoltaic energy on its Vanguard spacecraft in 1958. It lasted more than five years and had a maximum output of one watt. Solar photovoltaic energy was at first prohibitively expensive; it was basically employed for space missions throughout the 1960s. The 1973 oil crisis affected solar photovoltaic research and development, resulting in solar photovoltaic deployment to modest roofs and off-grid

telecommunications networks. Between 1980 and 1990, solar photovoltaic cell costs decreased from 32 $/W to under 10 $/W as investment increased. Solar photovoltaic technology has grown in popularity in recent years due to regulatory support, subsidies, and feed-in tariffs [20]. Solar photovoltaic module costs have recently decreased to below 0.25$/W, making them very economical as of Q1 2020 in the U.S.

Solar photovoltaic (PV) output climbed by a record 156 TWh (23%), reaching 821 TWh in 2020 [21]. It increased at the second-fastest pace of absolute generation increase among all renewable energy sources in 2020, after only wind but ahead of hydroelectric. Ahead of regulatory deadlines in China, the United States, and Vietnam, an extraordinary surge in photovoltaic capacity expansions, a record 134 GW, occurred. Solar photovoltaic energy is becoming the most cost-effective method of generating power in the majority of the globe, which is projected to drive investment in the future years. As can be seen from the Figure 1.5, the investments made by countries in solar energy are increasing day by day with the falling costs and increasing PV panel efficiency.

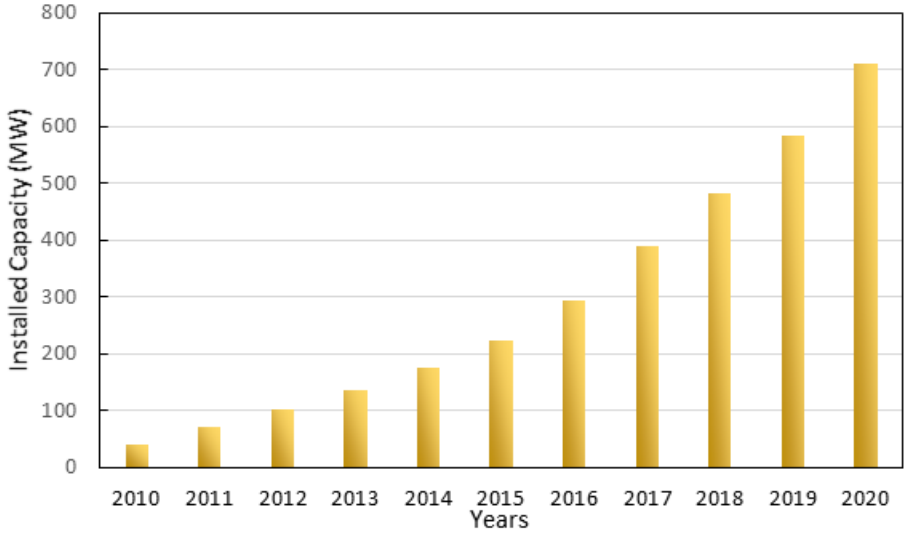

Figure 1.5: Solar PV installed capacity of the (data from [22])

Solar radiation's accessibility is erratic owing to cyclical and aperiodic situations and meteorological conditions. Consequently, solar energy cannot be utilized as a sole source of supply in cases of increasing demand. As required, shortfall power should be balanced by an alternative flexible energy generating system. Additionally, if the solar power generation plant generates surplus electricity, the excess energy may be utilized through an energy storage medium. Storage systems guarantee sustainability in the nights when solar

radiation is lacking, and the presence of storage systems is vital for the sustainability of solar energy.

1.5 Geothermal Energy

Briefly defined, geothermal resources include ground heat, hot water, steam, and gases containing compounds created by heat collected in different depths of the earth's crust. On the other hand, geothermal energy encompasses any advantage derived from geothermal resources. A lot of different things can be done with geothermal energy. It can be utilized to provide direct heat for district and space heating, hot water production, electricity generation, agriculture, and farming and industrial activities. Additionally, geothermal energy refers to the extraction of energy from the earth's consistent temperatures at shallow depths using ground-source heat pumps.

There are several geothermal technologies, each with a particular maturity level. Direct use technologies such as geothermal heat pumps, district heating, and greenhouses are extensively employed and may be called mature. The technique for generating energy from inherently high-permeability hydrothermal reservoirs is likewise established and dependable, having been in operation for a hundred years. Most of today's power plants are dry steam plants or flash plants that can generate temperatures exceeding about 200°C. Nonetheless, mid-temperature areas are progressively utilized to produce power or heat due to the development of binary cycle technology, where geothermal energy is utilized to heat a working fluid in a closed system using heat exchangers [23].

Furthermore, new technologies, such as Enhanced Geothermal Systems (EGS), are being improved and demonstrated. Geothermal energy is heat stored in or released from the earth's crust that can be utilized to produce power and supply direct heat for various purposes, including space and district heating, water heating, aquaculture, agriculture, and industrial activities. Additionally, geothermal energy refers to extracting energy from the earth's consistent temperatures at depths near the surface using ground-source heat pumps.

1.6 Motivation

Since the discovery of fire, energy has been a common need of all societies throughout history. Therefore, one of the most formidable obstacles to today's society is energy-based problems, as in the past. While energy is a primary driving force of contemporary

civilization, fossil-fuel combustion contributes to global climate change and poses concerns about energy security. Alternative energy research indicates that there is no only one remedy to all energy-related obstacles. Green energy-based systems provide sustainable and environmentally friendly energy due to low emissions. However, these systems' economic potential is debatable. Intermittent renewable energy availability is a significant concern since it has a detrimental impact on system flexibility, preventing the grid from fulfilling the necessary energy demand on time. Current storage methods are neither feasible nor commercially viable for large-scale use.

For the factors stated before, it is critical to developing waste-to-energy multigeneration systems where many useful outputs such as cooling, heating, and electricity generation are produced. Multiple generation systems utilize renewable resources to generate useful outputs and store them till they are used. In this respect, solar and geothermal energy integrated gasification systems are potential alternative fuel and useful output production methods using high-grade thermal energy obtained from waste. However, these solutions do not yet have the requisite economic viability. It is crucial to enhance the feasibility and commercial viability of integrated waste-to-energy multigeneration systems and their development and assessment with various techniques.

Some conventional waste treatment methods such as incineration are not environmentally friendly. However, renewable energy-based waste energy multigeneration systems have a much less detrimental effect on the environment since the main power supplier is renewable energy sources and syngas is utilized environmentally benign. In the proposed three systems, carbon monoxide is converted to carbon dioxide, and this carbon dioxide is used for ethanol production. Therefore, carbon emissions are minimized by means of the chemical transformation of carbon hydrogenation. In this way, ethanol, a good hydrogen carrier, is obtained and carbon emissions are prevented. Furthermore, this increases the H/C ratio of the fuel, which means presenting a more environmentally benign alternative.

1.7 Objectives

This thesis research mainly focuses on integrating waste into energy systems with geothermal and solar resources. The suggested three systems comprise distinct thermal

energy integration technologies for transforming waste into energy and different hydrogen and ethanol production methods.

- To design geothermal and solar energy systems that are combined with waste-to-energy multigeneration systems in order to produce electricity, cooling, heating, sulfuric acid, ethanol, as well as hydrogen.
- To perform parametric analyses of power production, gasification outputs, heat generation, and overall system efficiency as a function of altering steam feed rates, gasifier temperatures, and oxygen feed rates within the gasification component.
- To determine the overall energetic and exergetic efficiency of the proposed systems and the subsystems' exergy destruction.
- To investigate the impact of various operational circumstances on the performance of subsystems and the overall system. Parametric analyses are conducted on the overall system and many subsystems.
- To compare energy and exergy efficiencies of all three systems depending on operating conditions and comparison of useful outputs produced per unit waste and production amounts of green fuels such as hydrogen and ethanol.

Numerous researchers have conducted extensive research on multigeneration systems that utilize renewable resources. The demand for environmentally benign energy production techniques has increased the number of studies on these systems even more. In comparison to renewable-energy-based multigeneration systems, waste-to-energy multigeneration systems have higher commercial viability in terms of sustainability due to their continuous energy and fuel production throughout the day. However, there are relatively few studies examining multigeneration systems powered by renewable energy derived from various wastes. Moreover, there are few comprehensive studies on multigeneration systems' efficiency and emission production based on waste types and system configurations. This study differs from other studies in terms of designing and analyzing multigeneration systems that produce many useful outputs such as cooling, heating, sulfuric acid, hydrogen, electricity and ethanol integrated with renewable energy sources by using different waste sources and comparing the systems according to the results. The findings resulting from

the analyses shed light on the development of such systems and guide further studies to be performed.

A comprehensive literature review is provided on waste-to-energy systems, particularly those utilizing manure, waste tires, and low-grade lignite as an energy source. Moreover, the literature study discusses environmentally friendly technologies for hydrogen generation, including thermochemical cycles, solar towers, geothermal systems, absorption refrigeration cycles, and the Brayton-Rankine combine cycle.

Chapter 2. Literature Review

A comprehensive review of the literature is presented on waste-to-energy systems, particularly those utilizing manure, waste tires, and low-grade lignite as an energy source. Moreover, the literature study discusses environmentally friendly technologies for hydrogen generation, including thermochemical cycles, solar towers, geothermal systems, absorption refrigeration cycles, and the Brayton-Rankine combine cycle.

Dincer and Acar [24] studied sustainable energy options. They evaluated opportunities and compared the technological, economic, and environmental potential and performance of different energy sources. Additionally, they addressed and demonstrated multigeneration systems. The study established the benefits of integrated systems with various outputs by demonstrating decreased energy needed, decreased emissions, reduced system costs, and reduced exergy destruction and energy waste.

Dincer and Zamfirescu [25] discussed future energy usage and associated environmental difficulties in detail and suggested prospective solutions to existing environmental problems, such as renewable energy.

The global need for energy has boosted innovative new power plants. Innovation, however, does not imply reducing the conventional background involved in developing power plants. While there is some interest in utilizing renewable energy to power facilities, the availability of coal and the volatility of oil prices generate a need for Integrated Gasification Combined Cycle power plants (IGCC). In comparison to other coal and waste-powered combustion plants, the Integrated Gasification Combined Cycle has the lowest environmental effect in terms of both the amount of waste material generated and the potential to leach harmful compounds underground. Furthermore, the integration of these systems with renewable energy sources ensures that they are environmentally benign [26].

There are many studies have been conducted on the solar power tower system. Yagli et al. provided a computationally efficient approach for the purpose of concentrating sunlight onto the solar tower receiver [27]. They classed solar tower systems according to their intended application, and they investigated the electrical, thermal, energetic, and exergy performance of solar power tower thermal systems.

Bioenergy generation is one of the most promising solutions for minimizing carbon monoxide emissions and substituting fossil fuels. Although gasification-based bioenergy production has been thoroughly explored, it continues to have limitations in terms of energy efficiency, particularly in small-scale development. Concentrated solar thermochemical gasification of biomass (CSTGB) is a potential method for gasification efficiency by driving the endothermic processes of gasification using concentrated solar thermal energy. Fang et al. [28] revealed the principles of solar-assisted thermochemical gasification of biomass, their applications, and the shortcomings that can be improved. According to studies, such systems will become more prevalent in the future as their efficiency improves and they include a variety of renewable energy sources.

When it comes to global warming, environmental and sustainability aspects, the integration of geothermal energy into gasification systems where wastes are used is of great importance. This integration is promising because of the almost constant mass flow rates that geothermal energies provide throughout the day. Moreover, gasification systems offer sustainable energy compared to other renewable energy sources, thus achieving sustainable and environmentally benign systems. As a matter of fact, investigations on geothermal and gasification systems are rising slowly but surely, and the advancement of these systems continues. Zhang et al. [29] have developed a combined power and heating system that is powered with partial gasification of biomass in which geothermal energy is integrated. Consequently, they calculated the yearly cost savings ratio as 23.62% and the carbon dioxide emission reduction ratio as 66.52%, respectively. In this manner, emissions are reduced, and higher efficiency systems are obtained.

In the literature review, the composition of waste utilized in waste-to-energy systems and the gasification techniques that can be used based on this composition, as well as the integration of solar and geothermal energy into the combined gasification systems. In this regard, the literature review focuses mainly on the following critical areas:

- Manure powered integrated gasification systems
- Waste tire based integrated gasification systems
- Underground coal gasification systems
- Integrated solar energy systems

- Integrated geothermal energy systems

2.1 Manure Powered Integrated Gasification Systems

Renewable energy generation is a common issue when examining solutions to mitigate the environmental effect of cattle production. Gasification is one such method. It is a sequence of chemical processes that involve heating a suitable organic material to the point where it is heated by hydrocarbons in a controlled, low-oxygen environment (simple organic compounds containing only hydrogen and carbon). It is turned to syngas, namely syngas, as a consequence of chemical reactions by manure-controlled gasification. Syngas is composed mostly of carbon monoxide and hydrogen, with trace quantities of methane and carbon dioxide, all of which may be collected and utilized to generate heat and electricity. [30]. After the materials such as methane, mercury, and hydrogen sulfide are separated from the syngas, the remaining hydrogen and carbon monoxide are called "clean syngas." These high-temperature and pressure syngas are used to produce electricity, heat, and absorption cooling in combined cycles, before being used for hydrogen generation in a water gas shift reactor. Hydrogen is obtained by a water gas shift reaction from clean syngas with a decreasing temperature. Afterwards, the produced hydrogen can be used to obtain ethanol or be stored and transported due to the hydrogen liquefaction process.

Kahraman and Dincer [31] conducted a parametrical study to investigate the energy and exergy deficiencies of a solar-based manure-powered integrated gasification combined cycle, which objectives are producing multiple useful outputs, including power generation, ethanol, hydrogen, cooling, heating, and for a sustainable community. System outputs were examined depending on the changing input parameters, and the rise in energetic and exergetic efficiencies in the system depended on the increasing gasification temperature and steam supplying rate. The gasifier oxygen and manure feed rate were taken 0.7 kg/s and 10 kg/s, respectively, and the energetic and exergetic efficiencies were found as 61.1% and 56.4%, respectively.

In another similar study [32], a flowsheet model was developed for the steam gasification of animal manure. Depending on three different parameters, including energy and exergy efficiencies, as well as hydrogen production rate and, accordingly, production costs per kg of hydrogen, were analyzed. Furthermore, calcium oxide and carbon dioxide capture

process is provided in the system. Still, it was observed that there was an increase of 7.58% in the system's efficiency if calcium oxide was not used. Studies were simulated, and thermodynamic analyses were conducted in Aspen Plus. Parametric studies in the conclusion section were compared with experimental studies to ensure system validation.

Bamisile et al. [33] conducted parametric studies for chicken manure and maize silage mixture-powered gasification systems. They observed that although the increase in ambient temperature had an adverse impact on exergy efficiency, there was no significant change in exergy destruction. According to their research, in the combustion chamber, which generates the most heat, the highest destruction of exergy occurs. Moreover, the energy and exergy performance of the systems increases as more useful outputs are generated. In the study, energy and exergy efficiencies of the system were found to be 25.16% and 18.61%, respectively, in the case of power generation only. On the contrary, if multiple useful outputs are produced, the energy and exergy efficiencies of the system increase significantly to 73.15% and 27.27%, respectively. This research demonstrates the beneficial impact of using multiple production systems on overall system efficiency.

An experimental study [33] examined the applicability of waste biomass such as animal manure or sewage sludge as a gasification fuel using a fluidized bed steam gasifier. According to the test results, the gasifier temperature was 820 °C to 950 °C resulted in a more than 10% increase in overall energy efficiency. In another experimental study [34], pre-dried chicken manure and woody biomass mixture were used in various proportions. Therefore, the LHV of syngas decreased from 2.7 MJ/m3 to less than 2 MJ/m3. During the gasification process, reactor temperature profiles demonstrate a significant effect of the varying sizes of chicken manure and wood pellets, as well as variations in ash concentration, on the gasification process. The main component of the syngas produced as a result of using chicken manure is carbon monoxide, while hydrogen and methane have a lower share in the syngas.

2.2 Waste Tire Based Integrated Gasification Systems

As global vehicle usage rises, waste tires likewise increase significantly. As a consequence, many tires are discarded in landfills, allowed to deteriorate or even combust each year. Tire disposal poses detrimental environmental risks at the time. Numerous nations, including

the United States, have initiated initiatives to mitigate the ecological damage and space consumption caused by tires. Currently, around one-third of tires can be recycled, while about half of them are utilized to create Tire Derived Fuels (TDF), according to a report of CATRA (Canadian Association of Tire Recycling Agencies) [35].

Numerous studies have been conducted to determine the feasibility of employing waste products as feedstocks for integrated gasification combined systems. In order to examine the applicability of waste tires to waste to energy systems, Ongen et al. [35] undertook an experimental study using a fix bed reactor. The reactor's ash was sent to the gasifier to be regasified with a cyclone separator. In the study, in which dry air and pure oxygen were used as gasification agents, hydrogen and methane production volumetric rates were found as 35% and 40%, respectively.

Gungor and Dincer [36] proposed a waste powered and solar integrated multigeneration system that utilizes waste tires gasification to generate multiple useful outputs, including freshwater, cooling, heating, electricity generation, sulfuric acid and hydrogen production for a sustainable community. In this parametric study, the operating temperature and pressure of the fluidized base gasifier have been considered as 1227 °C 1600 kPa, respectively. Moreover, the waste tires were shredded and used as the gasification unit's feedstock. Aspen Plus software has been utilized to model, simulate and analyze the system thermodynamically. Furthermore, in order to conduct parametrical studies for the multi-effect desalination unit, Aspen HYSYS has been uitilized. While overall energetic efficiency was calculated 74%, overall exergetic efficiency was found as 73% of this IGCC system, in the selected operating conditions.

Hasan and Dincer [37] compared and evaluated waste tires as a feedstock against coal and coconut char. Aspen Plus simulation program was utilized to investigate system through energy and exergy approach as well as conducting parametrical to examine its competitiveness against high-quality coals. The hydrogen generation to feedstock rate of the system was found as 0.158. This production rate is very close to Illinois coal, which has a pretty high lower heating value, with a production rate of 0.161. Moreover, the system's energy and exergy efficiency was found to be as 55.01% and 52.31%,

respectively. Hence, this system is promising in terms of showing the competitiveness of waste tires as an alternative to high-rank coal gasification systems.

Machin et al. [38] demonstrated the energetic evaluation of waste tires in their study. For the gasification of waste tire-derived fuel, a large-scale updraft gasifier on an IGCC was proposed. This gasifier is capable of producing between 10 and 16 MJ electrical power per kilogramme of waste tyre-derived fuel supplied to the reactor. Implementing these technologies will enable the energetic re-use of discarded tyres in Brazil, resolve waste disposal issues, generate employment, minimize negative environmental consequences associated with landfill disposal, and expand distributed energy production.

According to the literature review, the gasification parameters to be examined were determined as:

- Gasifier temperature
- Steam feed rate
- Oxygen feed rate
- The waste type used in gasification
- Syngas utilization method

2.3 Underground Coal Gasification Systems

While coal was the primary raw material for energy production until the early twentieth century, oil has accounted for the majority of global energy consumption since the 1960s. Between 1973 and 1979, the international oil crises compelled nations with insufficient oil reserves to implement a number of policies to reduce their reliance on oil. While there is growing production of coal, which is abundant and has a large reserve base, tremendous emphasis has been placed on research and development of other energy sources including hydroelectric, nuclear, solar, hydrogen, the geothermal, wind, and tidal. Gasification is an effective technology for evaluating coal reserves with a low calorific value that traditional mining cannot economically appraise. In this perspective, gasification is seen as a potential alternative for the clean use of coal in the modern world [39].

Coal, which is abundant in many parts of the world, is a resource that can be utilized to produce energy and chemicals. Turkey's proven hard coal reserves are 1.6 tons, and lignite

reserves are 19.14 billion tons as of 2021, according to the International Energy Agency (IEA) Turkey 2021 energy policy review [40]. Since most of these deposits have low calorific value, they cannot be evaluated economically by classical methods.

Underground coal gasification is an alternative energy recovery process for bituminous, sub-bituminous, or lignite coal and bituminous coal reserves that cannot be economically evaluated by conventional mining methods. The process aims to convert the energy of coal into a combustible gas product without using traditional mining techniques and to eliminate health, safety, and environmental problems. During gasification, the coal bed itself acts as a reactor, where first the volatile matter of the coal is removed, and then it is combusted and gasified [41].

Bicer and Dincer [42] proposed an integrated underground multigeneration gasification system producing bitumen, syngas, electricity and bitumen for a sustainable community. In their research, they utilized solid oxide fuel cell and steam-assisted gravity drainage in addition to underground coal gasification. It is a very flexible system because it contains both oil and coal as feedstock. They proposed coal as an alternative fuel to natural gas. They conducted their studies and thermodynamic analysis under the energetic and exergetic approach. Consequently, they found the system's energy and exergy efficiencies as 19.3% and 17.3%, respectively.

Yilmaz et al. [43] proposed a multigeneration system that produces fresh water, cooling, heating, electricity as well as hydrogen production. In their work, they also made hydrogen liquefaction in order to transport hydrogen to other places. In addition, useful output changes such as hydrogen production, energy and exergy efficiencies depending on gasifier temperature, ambient temperature and coal feed rate were examined. The system's total irreversibility is calculated to be 65126 kW. Moreover, the proposed power generation system's energetic and exergetic efficiencies were calculated 58.47% and 55.72%, respectively.

Seyitoglu et al. [44] investigated coal-powered integrated gasification combine system for six different coal types including Soma, Yatagan, Can, Beypazari, Elbistan and Tuncbilek lignites. All of these coals are of lignite type, and because of their low LHV values, they are important in terms of leading these systems. They utilized Aspen Plus and EES

(Engineering equation solver) programs to conduct parametric studies in their studies. The entire system's energetic and exergetic efficiencies were found as 41% and 36.5%, respectively. Tuncbilek coal is the most prominent in terms of energy and exergy efficiency since Tuncbilek lignites have higher LHV as well as higher hydrogen content in their composition. For this reason, parametric studies are carried out using Tuncbilek lignites in the integrated underground coal gasification system, which is examined in this thesis.

2.4 Integrated Solar Energy Systems

Photovoltaics (PV) and concentrated solar power (CSP) technologies are the two primary methods of converting solar energy into electricity and heat. Studies on solar energy systems are increasing since solar energy can be utilized relatively more equally in the world than other types of power and the increasing efficiency of solar panels. Integration of solar energy systems with other renewable energy sources is also an important approach to establishing more environmentally friendly systems. Solar energy can support these energy needs in this regard. Moreover, solar energy is a natural renewable source of energy that can be utilized wherever on the planet and will continue to exist as long as the sun persists [45].

Tukenmez et al. [46] sugested an integrated solar energy based waste-to-energy innovative multigeneration system consisting of a PEM electrolyzer, biomass gasifier, parabolic dish collector and hydrogen compressor unit as well as an ammonia reactor and storage unit to generate many useful outputs such as ammonia, hydrogen, cooling, electricity and hot water. The power generation was obtained using the Brayton, Rankine and organic Rankine combine cycles. In addition, the total electricity generation of this innovative system was found as 20,125 kW. The developed system's overall energetic and exergetic effectiveness was calculated as 58.76% and 55.64%, respectively. According to the study, as the gasification feedstock feed rates increase, the energy losses will increase less than the energy gains. Therefore, the energetic and exergetic efficiencies of the system increased gradually.

A novel integrated biomass gasification combined cycle [47] utilized solar thermal power to supply electricity for the community as well as steam for the gasification system. The suggested technology improves the overall efficiency of renewable energy sources by using

novel waste heat recovery techniques. The gas turbine is discovered to have a partially high rate of exergy destruction of 26.1 MW. Depending on the changing parameters, the system's energetic and exergetic efficiencies were examined, and the highest was ccalculated as 69.2% and 52.9%, respectively. In the system, the biomass feed rate was determined as 2.2 kg/s. Additionally, wastewater brine is processed to generate freshwater by a combination of evaporation and membrane-based water treatment.

An important disadvantage of solar energy is that it cannot be used in the evening hours. This reduces the sustainability of solar systems. However, this can be avoided with storage systems. Additionally, thermal storage technologies maximize the use of renewable energy while minimizing system energy imbalances. Systems for storing energy in the short term generally have lower capacities and keep the heat for a limited period of time, ranging from a few hours to a few days. These types of systems can also be utilized for storing solar thermal energy throughout the day to be used throughout the colder hours of the day when warmth is required [47].

Temiz and Dincer [48] used a parabolic through collector with a storage option to supply electricity to the CUCL cycle for hydrogen production and many useful outputs for a community. Thanks to the solar thermal storage system, the proposed method can work all day long, and the sustainability of the system is increased. In another solar-powered multigeneration system was utilized many subsystems such as bifacial photovoltaic (BiPV), concentrated solar plant (CSP) as well as ocean thermal energy conversion (OTEC) with ammonia trilateral Rankine cycle, and cascaded heat pump to provide electricity and heating for arctic communities. In addition, hydrogen production was provided with an electrolyzer [49].

2.5 Integrated Geothermal Energy Systems

Subterranean heat energy can be utilized to generate many useful outputs, including, power and heating. By 2050, while concentrated solar energy will be providing 2%, geothermal energy sources will provide 1% of the main globally dispatchable renewable sources. Moreover, electricity generation from geothermal sources is increasing by more than 2% annually [50]. Ghazvini et al. [51] technically reviewed geothermal energy systems for hydrogen production. Moreover, They compared the cost of hydrogen production based on

geothermal energy economically compared to other renewable energy sources. Especially, geothermal energy has great advantages in terms of cost compared to hydrogen production techniques based on wind energy.

Figure 2.1 illustrates the direct use of geothermal energy by country. Although immediate use of geothermal energy is common in China and Turkey, very high temperatures of geothermal energy sources in countries such as the Us, Italy, and Japan allow them to be used for multigeneration systems. Indeed, a freshly developed supercritical geothermal and solar-based integrated energy system [52] was investigated thermodynamically for a community Kakkonda geothermal power plant in Shinozaki, Japan. According to the calculations, more than 2 tons of hydrogen can be generated yearly with the proposed system. In addition, the energy and exergy efficiencies of the system were calculated as 22.7% and 18.2%, respectively. According to calculations, the system's payback period is just over five years, which is a very promising result for a geothermal energy-based hydrogen production system.

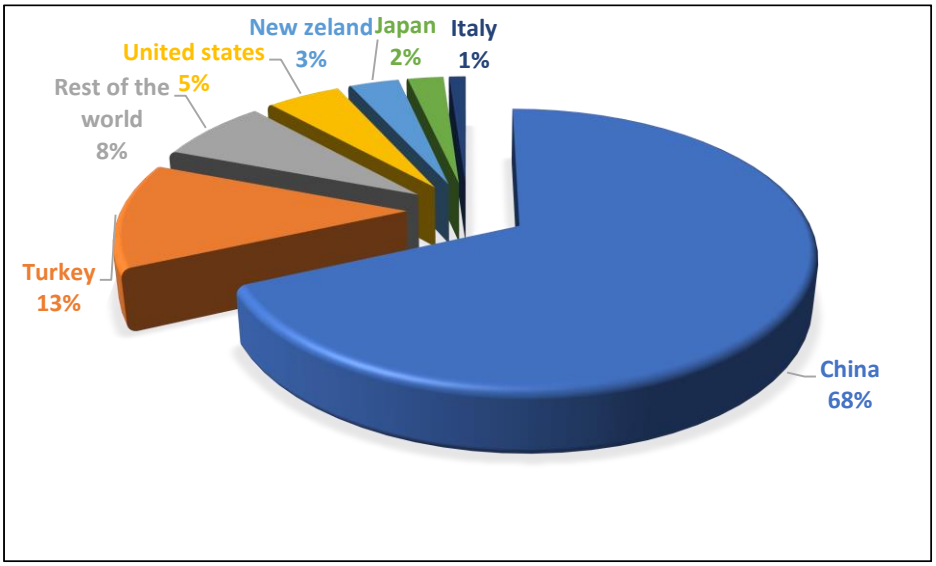

Figure 2.1: Geothermal direct use by countries, 2020 (data from [53])

One way of producing hydrogen from geothermal energy is the organic Rankine cycle. To generate electricity from pumped geothermal water, the Rankine cycle can be utilized, which can then be used to produce hydrogen with an electrolyzer. Another method is to provide steam from the geothermal energy to gasification systems for hydrogen production. Gungor and Dincer [54] proposed a geothermal energy-based integrated gasification

combined cycle to produce hydrogen sulfur, electricity, hydrogen for a circular economy and sustainable development. In the designed system, hot geothermal water is injected directly into the gasifier, and the need for steam for syngas production is met.

Three different systems were designed in a comprehensive study [55] that considered geothermal energy, solar PV, and biomass gasification as energy sources. These systems have been evaluated and analyzed depending on many thermodynamic parameters. In the study, the EES program was used together with the Aspen Plus simulation program. The energetic and exergetic efficiencies for the integrated gasification system were found to be 53.6% and 49.8%, in this respect.

2.6 Main Literature Gaps

Many researchers studied integrated gasification combine systems due to their higher efficiencies in comparison to other thermochemical multi-generation production systems. In spite of the fact that various studies investigating integrated waste-to-energy multi-generation systems aim to produce electricity and generate multiple useful outputs, very few of them conduct comparative research depending on various waste types and different system combinations.

Integrated multigeneration systems are gaining enormous momentum among worldwide energy generating systems due to their considerably higher energy efficiencies and multiple useful outputs. Many studies are available on multigeneration systems. However, a few of them designed waste and renewable energy-based technologies. This research aims to maximize useful outputs while minimizing input using entirely renewable energy sources such as waste, solar energy and geothermal energy.

Multigeneration systems working with renewable resources have been actively studied by many researchers. Especially with the increase in demand for environmentally friendly energy production techniques, the studies on these systems have increased even more. Unlike multigeneration systems based on renewable resources, waste-to-energy multigeneration systems have more commercial viability in terms of sustainability due to their constant energy and fuel production throughout the day. However, there are very few studies focusing on multigeneration systems working with renewable energy based on different wastes. In addition, there are very few comprehensive studies on the efficiencies

of multigeneration systems and their emission production depending on waste types and system combinations.

As previously stated, hydrogen and ethanol are environmentally friendly alternatives to fossil fuels, as they are high energy carriers and can be combusted without carbon emissions. This study focuses on integrated waste-to-energy multigeneration systems that produce many useful outputs including ethanol, power, cooling, heating and sulfuric acid working with waste, solar, hydrogen and renewable energy sources.

Chapter 3. Developments of Systems

In this chapter, three different waste-to-energy multigeneration systems are evaluated, similar and different aspects of the systems are defined. Each system is introduced and detailed with its subsystems. In addition, the approaches used, thermodynamic analysis methods, and various system details are mentioned. All three systems have gasification systems working with waste in common. However, there are differences in the type of organic fuel used and the methodology accordingly. In addition, depending on the waste used, the amount of hydrogen and ethanol produced together with the syngas compositions also varies. These are discussed in more detail in the next results section.

Systems have closed and open loops. While open loops also release high energy and increase the amount of electricity production, they bring system losses. Therefore, the positive and negative features of this technique are also mentioned in this section and examined in detail in the discussion section.

Parametric studies are simulated in the Aspen Plus program, and the EES (Engineering equation solver) program is also utilized. The methodologies used are discussed in further depth in the next section. The three proposed systems can be summarized as follows:

- System 1: Solar based waste to energy system
- System 2: Geothermal based waste to energy system
- System 3: Underground lignite gasification based system

In all three systems, the Rankine cycle is used for electricity generation. In the first system, some of the syngas is combusted, and electrical energy is produced with the open type Brayton Rankine combined cycle. In the second system, the rejected heat coming from the syngas is utilized with the closed type Brayton Rankine combine cycle. In the third system, the reheat and regenerative Rankine cycle are used for power generation.

The absorption refrigeration cycle and the water gas shift reactor are the two common system components in all three systems. The heat rejected from the steam or gas cycles is transferred through a heat exchanger to the absorption refrigeration cycle, which provides heating and cooling for the community.In the water gas shift reaction, carbon dioxide and

hydrogen are produced by reacting with syngas steam consisting of carbon monoxide and hydrogen.

In order to compare the systems, the same useful outputs are produced in all three systems. The systems produce six different useful outputs listed below:

- Electricity generation
- Heating
- Cooling
- Hydrogen production
- Ethanol production
- Sulfuric Acid production

3.1 System 1: Solar Based Waste to Energy System

The designed waste powered and solar assisted multigeneration combined system is illustrated in Figure 3.1. In solar power tower systems, a heliostat field collects and directs sun irradiation toward a central receiver, which heats a working fluid. The same fluid or another heated in a heat exchanger creates a thermodynamic cycle that generates mechanical power, which is converted to electrical energy through an electrical subsystem. In this proposed system, solar tower's rejected heat run the primary Rankine cycle through heat exchanger 1 and mechanical power is generated there. Solar receivers can achieve pretty high temperatures exceeding 700 C, ensuring a high cycle efficiency [56].

Since it is in liquid form at atmospheric pressure, molten salt is used in solar power tower systems. Moreover, these are a cost-effective medium for storing thermal energy. Furthermore, they also have operating temperatures suitable for today's high-pressure and high-temperature steam turbines. They are environmentally benign mediums because they are neither flammable nor non-toxic [57].

Throughout the day, a thermal storage subsystem which utilizes salten malt as a fluid is used to compensate for energy imbalances in the solar tower. The molten salt is composed of 60% sodium nitrate and 40% potassium nitrate, often known as saltpetre. The salt melts at 223.4 degrees Celsius and is maintained liquid at a temperature of 291.6 degrees Celsius in an isolated cold storage tank. The salt is then pumped to the tower's summit, where

intense sunlight warms it to 710 degrees Celsius in a receiver. The receiver consists of a series of stainless steel tubes with sidewalls. The heated salts are then returned to an isolated hot storage tank. The capacity of this tank is decided by the utility's needs. The tanks are configured to store enough energy to run the primary Rankine cycle in the ten-hour period between 8 pm, and 6 am.

3.1.1 Primary Rankine Cycle

The heat from the molten salt storage system, which comprises a LTTS and a HTTS operated between 390°C and 640 °C, is transferred to the primary Rankine cycle (PRC) via heat exchanger 1. The pump in the Rankine cycle pressurizes the water and directs it to the heat exchanger 1. Here, the water, which absorbs the heat from the molten salt storage system, turns into steam, expands in the turbine and produces work. Afterwards releases its heat in the heat exchanger 2. Rejected heat in heat exchanger 2 is used to obtain the steam to be used in this heat gasification.

3.1.2 Manure Based Pressurized Fluidized Bed Gasifier

Feedstock wastes are suspended by fluidized-bed gasifiers in an oxygen-rich gas, forming a bed that behaves as a fluid within the gasifier. These gasifiers use back-mixing to effectively combine input manure particles with manure particles that have previously been gasified. To maintain fluidization, or the suspension of manure particles inside the gasifier, manure with a particle size of fewer than six millimetres is often utilized. Waste stock enters the reactor from the side, while steam and oxygen enter towards the bottom at a considerable pace to entirely suspend or fluidize the reactor bed. The gasifier's extensive mixing ensures that the reactor bed maintains a consistent temperature. Gasifiers are typically operated at a relatively high temperature in order to obtain an adequate carbon conversion rate (90–95%) and break down the majority of the tar, oils, phenols, and other liquid pollutants. However, operating temperatures are typically lower than the ash fusion temperature to minimize the development of clinker and the likelihood of bed de-fluidization. This implies that fluidized-bed gasifiers are best suited for highly reactive carbon-rich wastes, lignites, and alternative fuels such as biomass [58].

Bubbling fluidized-bed (BFB) gasifiers, a subtype of fluidized bed gasifiers distinguished by a shorter height, a bigger cross-section, denser beds and lower fluidization velocities, is

the most proven of the biomass gasification methods studied [59]. The bubbling fluidized-bed gasifiers are capable of operating at a broad variety of temperatures, pressures, and throughputs, as well as with a large variety of biomass sources. In biomass bubbling fluidized-bed gasification, the temperature range between 1,200-1,300°C or more [60]. Since over 1200 °C almost no tar, methane or higher hydrocarbons, hydrogen production benefits from high temperatures. Therefore, clean syngas generation is enhanced [61].

Manure gasification process in a bubbling fluidized bed occurs at very high temperatures such as 1300 °C during gasification [62]. Therefore, tar formation is almost non-existent due to these high temperatures. For this reason, there is no tar cleaning unit in the proposed integrated gasification system. Moreover, due to high temperatures, methane production is also very low compared to the pyrolysis method. Basically, the raw gas composition consists of hydrogen, carbon dioxide, carbon monoxide and hydrogen sulfide.

This multigeneration system takes utilize of a manure-fueled high-pressure fluidized bed gasifier. The temperature of pressurized water from pump 2 increases to 240 °C as it goes through heat exchanger 2 owing to waste heat generated by the primary Rankine cycle has been determined that the gasifier's working temperatures and pressures are 1300 °C and 1600 kPa, respectively. The gasifier is fed with animal manures at reference points. Additionally, stages 8 and 9 provide the gasifier with pure oxygen, manure, and steam. The Aspen Plus model, seen in Figure 3.2, was utilized to investigate and analyze the gasification system. Thermochemical computations are solved by means of the The RK-SOAVE model. The R-YIELD reactor is utilized to mimic the phase of pyrolysis, and the mass yield of the separated products is determined using Fortran code. Animal dung is gasified in the presence of water vapor and a limited amount of oxygen in a pressurized gasifier. This leads in the creation of biomass at high temperatures and pressures, which is mostly consist of carbon monoxide and hydrogen. At state point 10, the raw syngas exiting the gasifier is delivered to the cyclone separator. Additionally, the ash and char gasifiers are reintroduced into the system to facilitate further gasification. Sulfuric acid is extracted for economic benefit from other clean syngas by utilizing gas cleaning operation.

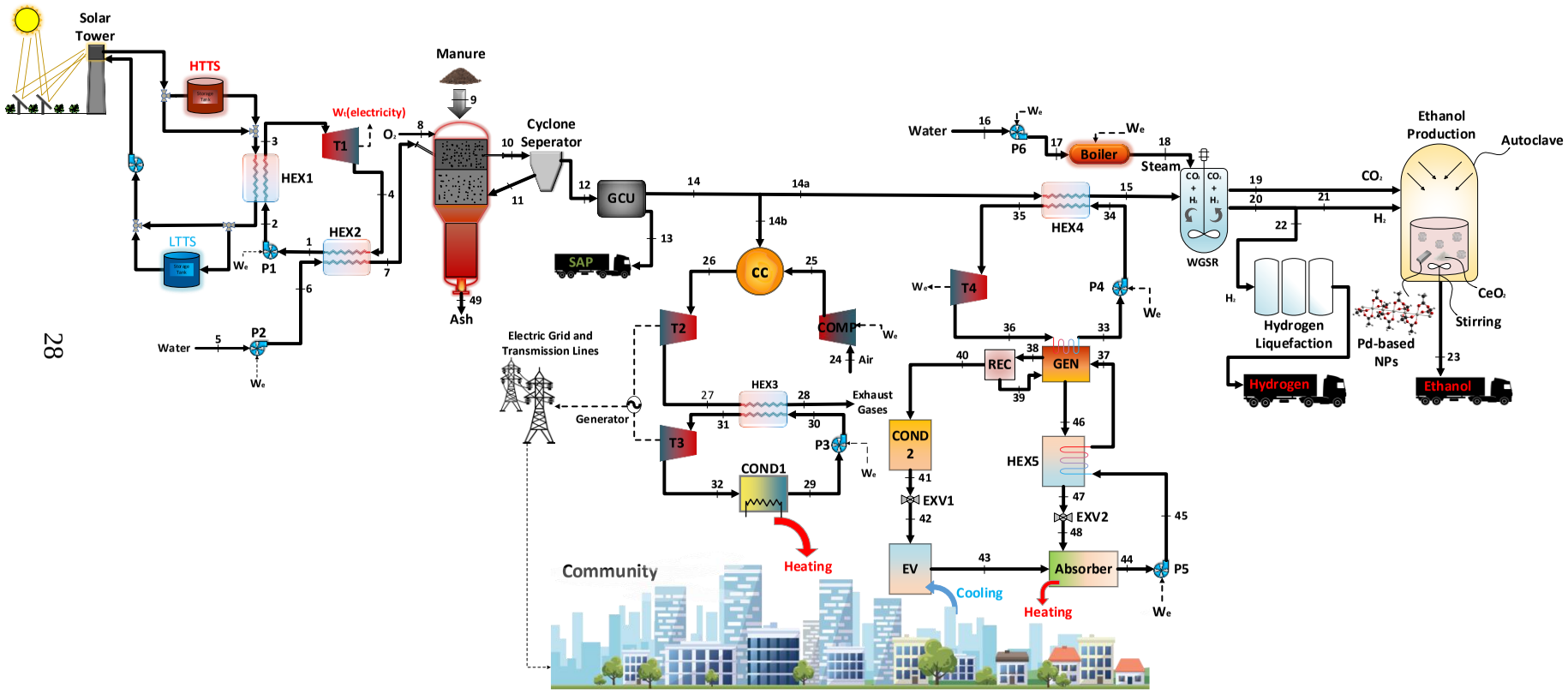

Figure 3.1 Schematic of System 1

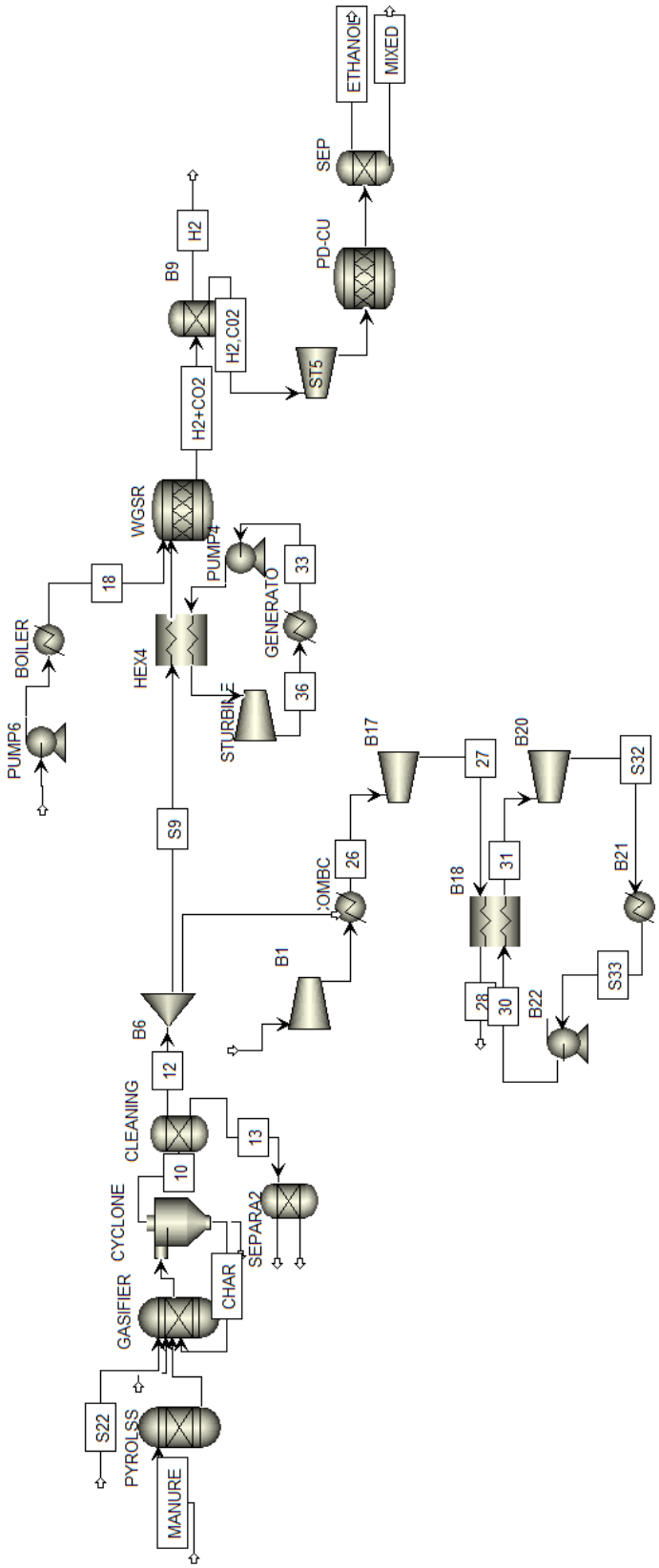

Figure 3.2 Aspen Plus model of system 1

The combustion chamber combusts 50% of the syngas generated at step 14 in preparation for use in the Rankine- Brayton combine cycle. The remaining portion is directed to a water gas shift reactor (WGSR) to generate ethanol and hydrogen.

3.1.3 Combined Gas-Steam Power Cycle

Air pressurized from 100 kPa to 450 kPa in the compressor with a 50 kg/s mass flow rate. Afterwards, half of the clean syngas containing mostly hydrogen and carbon monoxide are combusted in the combustion chamber. The released hot and pressurized exhaust gas expands in the turbine and rejects its heat in the heat exchanger, providing the rejected heat energy to be used in the Rankine cycle. During this operation, residual heat is transferred to an additional Rankine cycle through heat exchanger 3, and pressured water is transformed to steam at pump 3. Following the generation of power in Turbine 3, condenser 1 provides heating for the community.

Table 3.1 The main gasification reactions [63]

Heterogeneous reactions		
$C + O_2 \rightarrow CO_2 + 394\ kJ/mol$	Complete combustion	R1
$C + 0.5O_2 \rightarrow CO + 111\ kJ/mol$	Partial combustion	R2
$C + CO_2 \rightarrow 2CO - 172\ kJ/mol$	Boudouard	R3
$C + H_2O \rightarrow CO + H_2 - 131\ kJ/mol$	Water-gas	R4
$C + 2H_2 \rightarrow CH_4 + 75\ kJ/mol$	Methanation	R5
Homogeneous reactions		
$CO + 0.5O_2 \rightarrow CO_2 + 283\ kJ/mol$	CO partial combustion	R6
$H_2 + 0.5O_2 \rightarrow H_2O + 242\ kJ/mol$	H_2 combustion	R7
$CO + H_2O \rightarrow CO_2 + H_2 + 41\ kJ/mol$	Water-gas shift (WGS)	R8
$CH_4 + H_2O \rightarrow CO + H_2 - 206\ kJ/mol$	Reforming	R9
H_2S and NH_3 formation reactions		
$H_2 + S \rightarrow H_2S$	H_2S formation	R10
$3H_2 + N_2 \rightarrow 2NH_3$	NH_3 formation	R11

3.1.4 Third Rankine Cycle and Absorption Refrigeration System

The steam cycle's heat energy needs are provided by using waste heat produced by the gas cleaning unit's clean syngas via the heat exchanger 4. Compressed water absorbs heat and is converted to steam in heat exchanger 4, which generates energy in turbine 4. This system features a cooling absorption unit that utilizes an ammonia-water combination to provide cooling. The gas turbine 4's output stream is used to create the heat required by the generator for cooling production in the absorption refrigeration system (ARS). The generator evaporates the ammonia-water mixture and sends it to the rectifier, where it is

largely separated from the ammonia. While the mixture is mostly ammonia, which is rejected by the condenser at state point 40, the majority of the water is returned to the generator through stage 39. In the derived model, the ammonia mass fraction rate at state point 40 is 0.9996. It passes via expansion valve 1 between state points 41 and 42, where its temperature and pressure drop significantly before entering the evaporator. The chilly ammonia-water mixture absorbs heat and cools the surrounding environment as it passes through the evaporator. The absorber combines the liquid water from condition 48 with the ammonia water mixture from state 43 and transports it to the generator through pump 5.

3.1.5 Water Shift Gas Reactor

The water-gas shift reaction (WGSR), which takes place in the gas conditioning step, is used to enrich the hydrogen in the gas by reacting the carbon monoxide in the syngas with the steam. In the reaction realized according to Equation R8 in Table 3.1 by the fed water vapor, the amount of CO in the syngas formed after gasification decreases, while the amount of hydrogen and CO2 increases. Water-gas shift reactions take place in reactors containing catalysts. Water-gas shift reaction works with various catalysts between 150 °C and 650 °C. Since the reaction's molar totals do not change, the pressure effect on the reaction is negligible.

Water vapor is evaporated in the boiler after pressure application through pump 6, and then mixes and reacts with clean syngas, which contains carbon monoxide and hydrogen, from the gasifier in this subsystem. Hydrogen and carbon dioxide are produced in a water gas shift reactor. Afterwards, half of the hydrogen liquefied to -252,6 °C since hydrogen is usually not used where it is produced and transported to other locations. In the following sub-system, the other half of the hydrogen produced in the designed system is utilized for electricity production and ethanol generation.

3.1.6 Carbon Dioxide Hydrogenation

After the hot pressurized carbon dioxide and hydrogen produced in the water gas shift reaction expand in a turbine, the pressure drops, hydrogenation is used to produce ethanol from carbon dioxide. Here, half of the produced hydrogen is utilized for ethanol generation. Because ordered Pd Cu Nanoparticles are very selective, active, and stable catalysts for

the hydrogenation of carbon dioxide to ethanol [64], they were selected as the catalyst for the designed system.

3.2 System 2: Geothermal Energy and Waste Tires Based System

The utilization of the rich geothermal energy resources in some regions allows the production of environmentally benign and renewable energy. At the same time, the presence of significant amounts of waste tires potential in these regions also creates a source for the production of hydrogen gas, which is an energy carrier. High purity hydrogen can be produced by using syngas obtained as a result of the gasification of waste tires. Within the scope of this study, it is aimed to evaluate geothermal and waste tires energy resources together.

A power generation system integrated into hydrogen production from waste tire sourced synthesis gas, which can be established in the Larderello field in the Tuscany region of Italy, which has geothermal resources, is modelled. For this, the waste tire feed rate is determined as 20 kg/s. On this basis, the proposed system is simulated using the Aspen Plus simulation program, and the system's feasibility is investigated. As a result of simulation and analysis studies, 3.046 kg/s hydrogens can be produced for the determined capacity.

In Italy, about 350,000 tons of tires reach the end of their life each year [60]. This amount is the equivalent of almost 40 million tires, from cars, two-wheelers and trucks to large industrial and agricultural vehicles. Tires with a high carbon ratio of about 75% are also very suitable for gasification due to their high LHV. Since they have lower moisture content than organic wastes, the amount of gasification steam feed rate that should be given to the system is higher.

The hydrogen production process from waste tire sourced synthesis gas compose of gasification, gas cleaning, water gas shift reaction and hydrogen liquefaction steps. Gasification technology is the process of formation of syngas as a result of the reaction of solid wastes with oxygen, steam, air or their various mixtures. The syngas generated is a mixture of carbon dioxide, carbon monoxide, hydrogen, methane as well as other gases, and light hydrocarbons and heavy hydrocarbons such as tar. Tar is an especially undesirable compound in the syngas formed due to gasification. Tar conversion is generally carried out

by cold and hot gas cleaning systems. In the reaction that occurs according to Equation R8 by means of the fed water vapor, the amount of CO in the syngas formed after gasification decreases, while the amount of hydrogen and CO2 increases. Water-gas shift reactions take place in reactors containing catalysts.

The system layout is illustrated in Figure 3.3 Geothermal energy transfers its energy to the water utilizing a heat exchanger, and the required steam for gasification is supplied. Although geothermal energy has high temperatures, it should not be used directly in gasifiers due to having intense minerals because these minerals corrode the gasifier in the long run and reduce the system efficiency.

Water has a 25 °C temperature and 32.62 kg/s mass flow rate in state point 2. It turns into steam with the heat rejected from heat exchanger 1, at 203.1 degrees. In addition, less oxygen is sent to the system that cannot combust the waste tires completely. A compressor pressurizes this oxygen and sends it to the system at 1600 kPa. The main reason oxygen is chosen instead of air directly is that the nitrogen in the air turns into NOx, which is very toxic at high temperatures.

After the tires have been shrunk, they can be gasified better by means of a shredder gasifier. Because a fluidized bed gasifier is used, wastes are sent to the system from a point relatively above the gasifier. Ash that does not combust in gasification is sent back to the gasifier through a cyclone separator. The raw synthesis gas components obtained at the outlet of the gasifier are as follows:

- Hydrogen
- Carbon dioxide
- Carbon monoxide
- Methane
- Hydrogen sulfide

Since waste tires have high LHV like coals, they can reach very high temperatures such as 1300 °C during gasification. Therefore, tar formation is almost non-existent due to these high temperatures. For this reason, there is no tar cleaning unit in the designed system. In addition, due to high temperatures, methane production is also very low compared to the

pyrolysis method. Basically, the raw gas composition consists of hydrogen, carbon dioxide, carbon monoxide and hydrogen sulfide.

The carbon dioxide found in raw syngas is removed by scrubbing. According to environmental regulations, the sulfur content in syngas should be less than 30 parts per million [65]. Therefore, hydrogen sulfide is separated from syngas with an acid gas removal system and clean syngas containing carbon monoxide and hydrogen remains. As the hot clean syngas passes through the heat exchanger, it rejects energy to the Rankine cycle.

The Rankine cycle produces mechanical work as the water expands in the turbine with increasing temperature and pressure. It transfers heat to the following Rankine cycle as it passes through the water heat exchanger 4, which expands and has a relatively low temperature and pressure. Heat exchanger 4 provides energy to the reheat and regenerative Rankine cycle. The energy of the water pressurized at pump 1 and pump 2 increases with the heat rejected by the heat exchanger 4, then it expands to turbine 2 and generates work.

However, the pressure at the exit to turbine 2 is still at a level that can be utilized in another turbine. The water vapor, the temperature of which drops a little, passes through the heat exchanger 3, draws heat from the syngas again, increases its energy and expands to turbine 3 again. The partially cooled water vapor coming out of turbine 3 transfers the heat from the generator to the absorption refrigeration system before it is included in the Rankine cycle. The generator evaporates the ammonia-water combination, sending it to the rectifier, where the ammonia is significantly separated. While the mixture is mostly ammonia, which goes through the condenser's state point 37 reject heat, most of the water returns to the generator through stage 39. The ammonia mass fraction rate at state point 40 is 0.998 in the developed model. It flows via expansion valve 1 between state points 39 and 40, where its temperature and pressure drop before entering the evaporator. As the cold ammonia-water combination goes through the evaporator, it absorbs heat and cools the surrounding environment. In the absorber, liquid water from state point 46 is combined with the ammonia water mixture from state point 41 and delivered to the generator via pump 5.

The water-gas shift reaction (WGS) occurs during the gas conditioning process and is used to enhance the hydrogen content of the gas by reacting the syngas' carbon monoxide with

steam. The quantity of carbon monoxide in the syngas created after gasification reduces due to the reaction described in Equation R8 in Table 3.1, while the amount of hydrogen and carbon dioxide rises. Water-gas shift reactions occur in reactors equipped with catalysts. The water-gas shift reaction is carried out at temperatures ranging from 150 to 650 degrees Celsius using a variety of catalysts. Because the molar totals of the reaction remain constant, the pressure impact on the reaction is insignificant.

The geothermal heat source produces the required water vapor via heat exchange 1. Then, in this steam water gas shift reaction mixes and reacts with the clean synthesis gas containing carbon monoxide and hydrogen from the gasifier. The water-gas reaction produces hydrogen and carbon dioxide with high calorific value. Hydrogens are then liquefied to -252.6 °C because hydrogen is usually not used where it is produced and transported elsewhere. Half of the hydrogen produced in the designed system is used for electricity production and ethanol generation in the following subsystem. The carbon monoxide separated from the hydrogen is directed to an electrochemical synthesis reactor. The conversion is carried out in an electrochemical synthesis reactor in a sodium bicarbonate electrolyte solution. Cu-Zn was used as the cathode, and carbon was used as the anode. Ethanol is synthesized directly from carbon dioxide with a yield of 10.44% [66]. Hence, there is no need for hydrogen usage for ethanol production.

3.3 System 3: Underground Lignite Gasification Based System

Carbon dioxide, carbon monoxide, methane, hydrogen, water vapor, ethane, higher molecular hydrocarbon blends, and trace quantities of hydrogen sulphide are produced during the coal gasification process. Syngas that a combustible gas is produced. This gas can be used to produce electricity, liquid hydrocarbon fuels such as hydrogen and ethanol, as well as valuable chemicals.

3.3.1 Basic Principles of The Underground Coal Gasification Process

The process of coal gasification is split into two broad categories. The gaseous product is produced from coal using surface gasifiers in the first commercially applied technology. Coal is mined from the resource using traditional mining methods, pre-treated, and gasified in gasification facilities throughout this process.

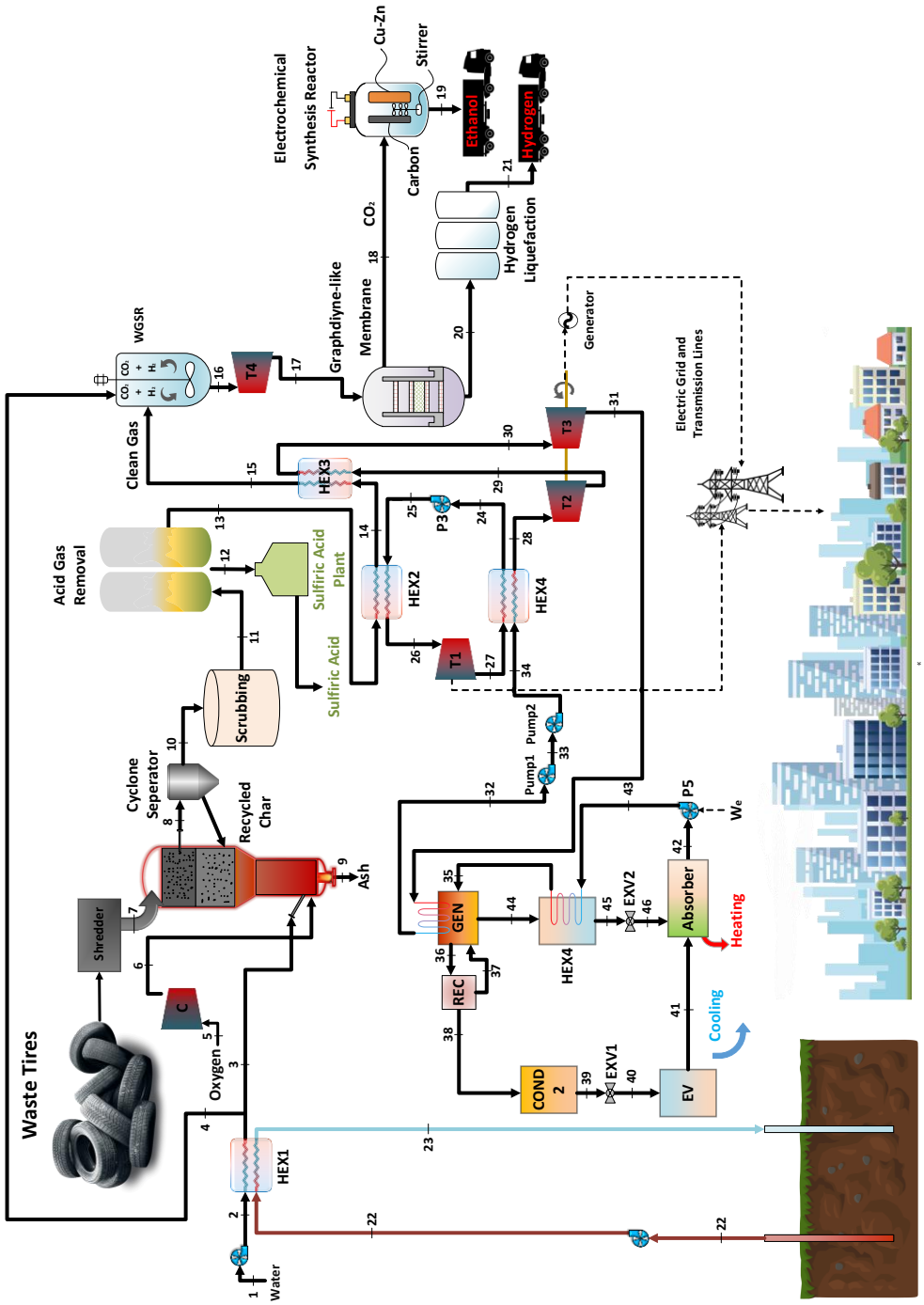

Figure 3.3 Schematic of System

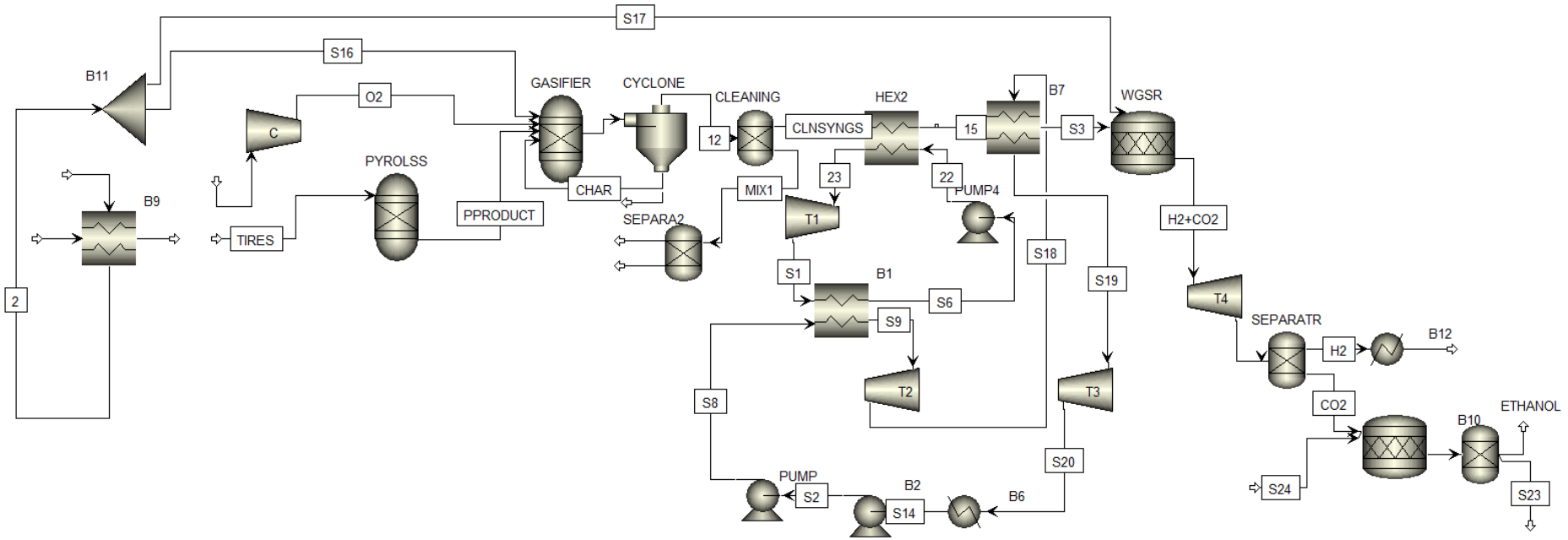

Figure 3.4 Aspen Plus model of system 2

This technology usually requires the construction of special facilities with gasifiers and warehouses for large-scale coal storage. For this reason, this technology requires a significant financial commitment.

An alternative method is a technique where the coal is gasified without transporting it to the ground, called "underground coal gasification." In this method, injection and production wells are drilled from the coal mine surface, and these wells are connected. It is ignited in a controlled manner with coal, propane type or another type of burner by the injection of air or oxygen. The hot gases formed are forced to move towards the production wells in the coal layer. In the gasification process, groundwater flowing into the cavity formed as a result of combustion in the coal mine is utilized. The produced synthetic gas is brought to the surface through production wells. The gas passed through the pre-cleaning stage is treated according to its purpose [67, 68].

The composition of the gas production to be obtained from the underground coal gasification process, therefore its calorific value and production amount vary depending on the following variables:

- Coal bed depth, the type of coal, seam thickness, permeability, foreign matter and crevices in the coal
- Water inlet
- Steam and oxygen injection mass flow rate
- Injection gas composition (air, pure oxygen, or vapor-oxygen mixture)

3.3.2 Advantages of the Underground Coal Gasification Process

The thickness of the coal seam is another aspect that affects the heating value of the fuel gas. As the seam thickness decreases, the thermal value of the gas produced may decrease due to the increase in heat losses to the environment.

Very deep coal reserves, especially if they have low calorific value and consist of thin veins, are considered uneconomical deposits and cannot be evaluated by conventional mining methods. In addition, high ash, sulfur and moisture contents prevent these coals from being used as an energy source. Underground coal gasification is a method that can be used to economically unfeasible coal beds. It is easier to remove sulfur from the syngas

produced by this method since the majority of the sulfur in the gas product that rises to the surface is in the form of H_2S rather than SO_2. It is cheaper and easier to remove H_2S gas before the gas product is burned. For this reason, this method has a much less negative impact on air pollution when compared to the direct burning of coal [69].

The underground coal gasification process has many advantages over the surface coal gasification process. Since gasifiers are not used in underground coal gasification techniques, the investment cost is reasonable. In this process, coal is not subjected to pretreatment and does not require solid waste management because the ash remains underground. There is no need for investment, and the workforce for underground coal mining's environmental impact is negligible. There are no expenses related to the transportation of coal. It is possible to use raw materials and water directly underground, and therefore the water consumption in this process is much less than the surface gasification method. In addition, it can be used for the sequestration of hollow carbon dioxide formed during the process. However, the most crucial advantage is that when the UCG technique is used, the thermal efficiency ranges between 75-90% [70]; the efficiency is around 70% in the surface gasification technique [71].

Furthermore, since the synthetic gas generated by this technique has a low calorific value; It can not be economical to transport this gas over long distances. For this reason, it is more economical to consume gas in areas close to the place where it is produced.

3.3.3 Assessment of Lignite Characteristics for Underground Coal Gasification

Since a large part of Turkey's roughly 19 billion tons of coal reserves has low calorific value, it cannot be economically appraised using conventional techniques [40]. Gasification technology is a suitable option for evaluating coal reserves with low calorific value, which cannot be assessed economically with conventional mining. At this stage, suitable lignite is determined for thermodynamic analyzes and real case scenarios for considering its real-life applicability.

Element contents of coal such as hydrogen, sulfur , ash, volatile matter, carbon, moisture, oxygen, nitrogen, fixed carbon, the heating value of coal and trace elements in coal content are important factors for gasification reaction. Trace elements in coal gain importance because they act as catalysts.

Low calorific value coals contain high volatile matter. These coals with high permeability are more suitable for underground coal gasification. In addition, low calorific value coal beds have a higher gasification rate at low temperatures. Low-temperature gasification reduces heat losses [72].

The bed depth of the coal where the underground coal gasification method will be applied should be between 50-1500 m, the cover thickness should be at most 900 m, and the coal bed thickness should be at least two meters. There are no restrictions on coal bed slope. The appropriate gasification method can be selected among various gasification methods depending on the bed slope. The area of the gasification blocks depends on the bed depth and the gasification method. This area must be larger than 1 square kilometre. In addition to these; Shale or similar foreign bands in the coal layer are undesirable [70].

LHV of Tuncbilek lignite is higher than other lignite types in Turkey. While the hydrogen ratio in its structure is higher, the sulfur ratio is lower [73]. In addition to these, it provides the bearing mentioned above features. For these reasons, Tuncbilek coal deposits in Kütahya, Turkey, were chosen to implement underground coal gasification.

3.3.4 System Design

The water vapor and oxygen sent to the underground coal beds cause partial combustion of the coal here first, but the reaction continues as gasification due to insufficient oxygen. While heavy materials such as tar, mercury and ash continue to remain underground, the syngas formed is directed to the scrubber from state point 4 to be separated its carbon dioxide. Unlike other gasification methods, syngas does not contain ash. The char remains underground and is regasified during the gasification period. After hydrogen sulfide removal from syngas in the acid gas removal unit, syngas passes through heat exchangers 1 and 2, leaving some of their energy to Rankine and Brayton cycle. The partially cooled syngas water is directed to the gas shift reactor, where it is converted to hydrogen and carbon monoxide. Later, the syngas that expands in turbine 3 and half of the produced hydrogen is utilized for ethanol generation under CO_2C catalyst, while the other half of the syngas is used for hydrogen production. After the carbon dioxide removal process is carried out, the liquefied hydrogen is kept in liquid form at -252.6 °C.

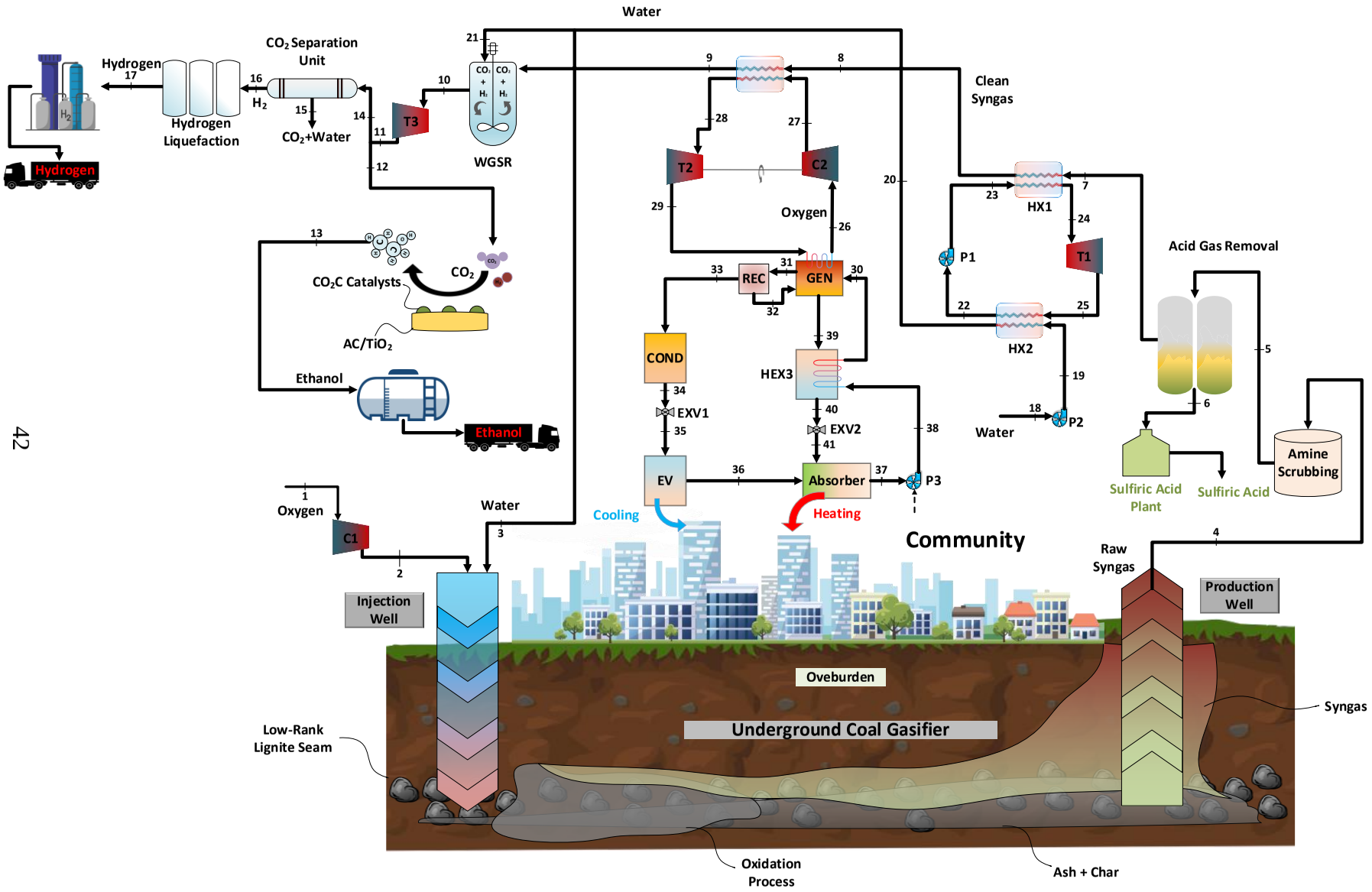

Figure 3.5 Schematic of System 3

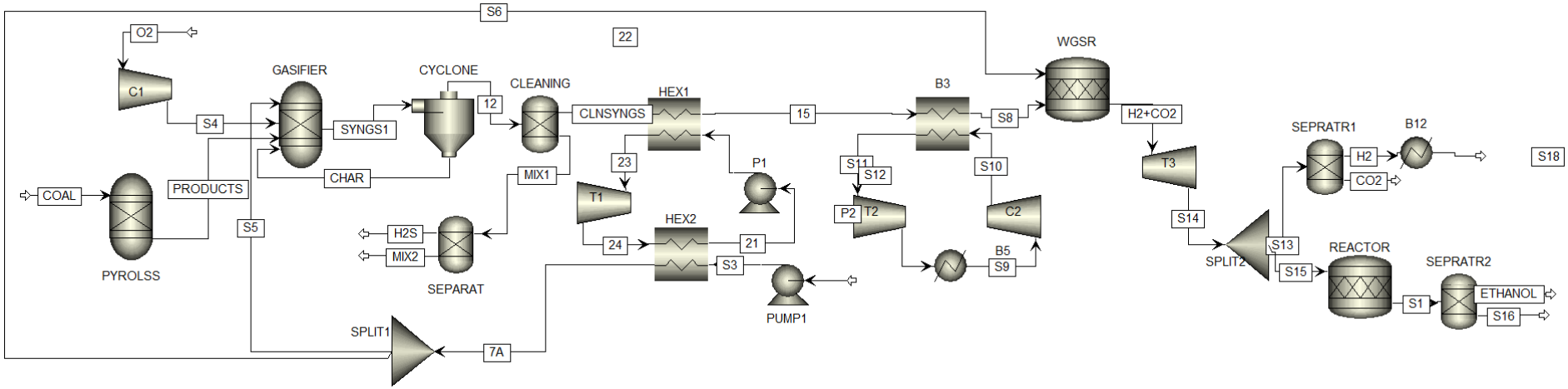

Figure 3.6 Aspen Plus model of system 3

Required steam for both the water gas shift reaction and underground coal gasification is supplied through the rejected heat by the heat exchanger 2 in the steam Rankine cycle. With the heat rejected from the closed Brayton cycle, the absorption refrigeration cycle is run, and heating and cooling are generated for the community by this cycle.

Chapter 4. Modelling and Analysis

Various parametric studies on all subsystems and subcomponents of multigeneration systems are carried out. To develop multigeneration systems, subsystems are modelled, examined, and interconnected with each other. While energy and exergy approaches are utilized in these parametric studies, the simulations of the systems are conducted in the Aspen Plus software. In addition, thermodynamic analyzes of absorption refrigeration cycles are carried out using the EES (engineering equation solver) program. In addition to the overall energy and exergy efficiencies of the systems, the exergy destructions of each component are calculated, and the subsystems with the most energy loss are examined.

4.1 Thermodynamic Analysis

To perform parametric studies in this work, Aspen Plus [74] and EES [75] are utilized in conjunction. EES version 11.183 is utilized in the analyses. All computations in Aspen Plus use the RK-SOAVE property technique. To perform the analysis, the following assumptions are made:

- The ambient temperature and pressure are considered as 25 °C and 101.325 kPa, respectively.
- The heat exchangers are isobaric, and the pressure drops throughout are negligible.
- Both the air and the combustion gases are considered ideal gas mixes.
- The changes in kinetic and potential energy, as well as exergy, are negligible.
- The gas turbine and steam turbine working fluids are air and steam, respectively.
- The animal dung that is utilized in the gasification process is dried and does not contain moisture in the proximate analysis.
- The combustion chamber is regarded to be highly insulated, with a heat loss of zero.
- Turbines and pumps used in the systems have 80% and 90% isentropic efficiency, respectively.
- The vapor power cycle and all subsystems of gasification run as a steady-state process.
- In the absorption refrigeration cycle, no chemical reactions between ammonia and water occur.

- Chemical exergy values for subsystems with chemical reactions such as combustion and gasification are also included in the calculations.
- The valves, pumps, as well as turbines, are all adiabatic.

The following equations represent the for each of the multigeneration systems, general equations for mass, energy, entropy, and exergy balance are given:

For each system, a general mass balance equation can be expressed as follows:

$$\sum_i \dot{m}_i = \sum_j \dot{m}_j \tag{4.1}$$

According to the first law of thermodynamics, heat is a form of energy, and so thermodynamic operations are consistent with the principle of energy conservation. This implies that neither heat energy nor cold energy can be generated or destroyed [76].

In this context, if the first law of thermodynamics is formulated, the overall energy efficiency for all systems can be written as:

$$\sum_{net} \dot{Q}_{net} + \sum_{net} \dot{W}_{net} + \sum_i \dot{m}_i \left(h_i + \frac{V_i^2}{2} + gZ_i\right) = \sum_j \dot{m}_j \left(h_j + \frac{V_j^2}{2} + gZ_j\right) \tag{4.2}$$

For each of the multigeneration systems, the following equations and rates of entropy production can be denoted as follows:

$$\sum_i \dot{m}_i s_i + \sum_{net} \frac{\dot{Q}_{net}}{T_s} + \dot{S}_{gen} = + \sum_j \dot{m}_j s_j \tag{4.3}$$

The general exergy balance equation for the first system is calculated as follows:

$$\sum_i \dot{E}x_{\dot{Q}_i} + \dot{W}_i + \dot{E}x^Q + \sum_i \dot{m}_i ex_i = \sum_j \dot{E}x_{\dot{Q}_j} + \dot{W}_j + \sum_j \dot{m}_j ex_j + \dot{E}x_d \tag{4.4}$$

The mass, energy, entropy, and exergy balance equations for the heat exchanger 1 in the first multigeneration system can be denoted, respectively, as follows:

$$\dot{m}_2 = \dot{m}_3 \text{ and } \dot{m}_{st_h} = \dot{m}_{st_l} \tag{4.5}$$

$$\dot{m}_2 h_2 + \dot{m}_{st_h} h_{st_h} = \dot{m}_3 h_3 + \dot{m}_{st_l} h_{st_l} \tag{4.6}$$

$$\dot{m}_2 s_2 + \dot{m}_{st_h} s_{st_h} + \dot{S}_{gen,HEX1} = \dot{m}_3 s_3 + \dot{m}_{st_l} s_{st_l} \tag{4.7}$$

$$\dot{m}_2 ex_2 + \dot{m}_{st_h} ex_{st_h} = \dot{m}_3 ex_3 + \dot{m}_{st_l} ex_{st_l} + \dot{E}x_{d,HEX1} \tag{4.8}$$

The following equations for mass, energy, entropy, and exergy balance for each turbine in the first waste to energy multigeneration system can be denoted, respectively, as:

$$\dot{m}_i = \dot{m}_j \tag{4.9}$$

$$\dot{m}_i h_i = \dot{W}_t + \dot{m}_j h_j \tag{4.10}$$

$$\dot{m}_i s_i + \dot{S}_{gen,t} = \dot{m}_j s_j \tag{4.11}$$

$$\dot{m}_i ex_i = \dot{W}_t + \dot{m}_j ex_j + \dot{E}x_{d,t} \tag{4.12}$$

The following equations for mass, energy, entropy, and exergy balance for the heat exchanger 2 in the first waste to energy multigeneration system can be denoted, respectively, as:

$$\dot{m}_4 = \dot{m}_1 \text{ and } \dot{m}_6 = \dot{m}_7 \tag{4.13}$$

$$\dot{m}_4 h_4 + \dot{m}_6 h_6 = \dot{m}_1 h_1 + \dot{m}_7 h_7 \tag{4.14}$$

$$\dot{m}_4 s_4 + \dot{m}_6 s_6 + \dot{S}_{gen,HEX2} = \dot{m}_1 s_1 + \dot{m}_7 s_7 \tag{4.15}$$

$$\dot{m}_4 ex_4 + \dot{m}_6 ex_6 = \dot{m}_1 ex_1 + \dot{m}_7 ex_7 + \dot{E}x_{d,HEX2} \tag{4.16}$$

The following equations for mass, energy, entropy, and exergy balance for each pump in the first waste to energy multigeneration system can be denoted, respectively, as:

$$\dot{m}_i = \dot{m}_j \tag{4.17}$$

$$\dot{m}_i h_i + \dot{W}_p = \dot{m}_j h_j \tag{4.18}$$

$$\dot{m}_i s_i + \dot{S}_{gen,p} = \dot{m}_j s_j \tag{4.19}$$

$$\dot{m}_i ex_i + \dot{W}_p = \dot{m}_j ex_j + \dot{E}x_{d,p} \tag{4.20}$$

The mass, energy, entropy, and exergy balance equations for the gasifier in the first multigeneration system can be analyzed, respectively, as follows:

$$\dot{m}_7 + \dot{m}_8 + \dot{m}_9 + \dot{m}_{11} = \dot{m}_{10} + \dot{m}_{49} \tag{4.21}$$

$$\dot{m}_7 h_7 + \dot{m}_8 h_8 + \dot{m}_9 h_9 + \dot{m}_{11} h_{11} + \dot{Q}_G = \dot{m}_{10} h_{10} + \dot{m}_{49} h_{49} \tag{4.22}$$

$$\dot{m}_7 s_7 + \dot{m}_8 s_8 + \dot{m}_9 s_9 + \dot{m}_{11} s_{11} + \frac{\dot{Q}_G}{T_S} + \dot{S}_{gen,G} = \dot{m}_{10} s_{10} + \dot{m}_{49} s_{49} \quad (4.23)$$

$$\dot{m}_7 ex_7 + \dot{m}_8 ex_8 + \dot{m}_9 ex_9 + \dot{m}_{11} ex_{11} + \dot{E}x_{d,\dot{Q}_G} = \dot{m}_{10} ex_{10} + \dot{m}_{49} ex_{49} + \dot{E}x_{d,G} \quad (4.24)$$

A fluidized bed gasifier is used to produce hydrogen, a form of energy. As stated in the research [77] on biomass gasification under different operating parameters, syngas generated using pure oxygen have the most significant carbon monoxide concentration compared to air and oxygen-enriched air. As a result, pure oxygen is utilized in the gasification unit rather than air. To avoid total combustion, the steam and manure ratios were set at 1:4, and the oxygen/manure ratio of the gasifier was set to 0.7:10 to prevent complete combustion. Additionally, the pressure and temperature of the gasifier are set to 1600 kPa and 1300 °C. The ultimate and proximate analyses needed to model the system in the Aspen Plus are listed in Table 3.1. While preparing this chart, Konya was picked because it has the highest level of livestock farming in Turkey [78]. Previous research data on chicken and cow dung are connected with data from a Turkish statistics organization on the number of animals in Konya. Thus, the feedstock data for the gasification subsystem were gathered in the most realistic manner possible.

Table 4.1 Ultimate and proximate analyses of animal manure [79].

Ultimate Analysis	(weight %)
C	43.76
N	2.08
O	44.37
H	5.46
S	0.22
Ash	4.12
Proximate Analysis	
VM	83.56
FC	12.32
Moisture	0.00
Ash	4.12

The lower calorific value of dried animal dunk was found as 17.12 MJ/kg. Utilizing the data in Table 3.1, the composition of the animal dunk used in this research was formulated

mathematically as follows, taking into account the sulfur, nitrogen, oxygen, carbon and sulfur hydrogen content:

The mass, energy, entropy, and exergy balance equations for the cyclone separator in the first multigeneration system can be denoted, respectively, as follows:

$$\dot{m}_{10} = \dot{m}_{11} + \dot{m}_{12} \tag{4.25}$$

$$\dot{m}_{10}h_{10} = \dot{m}_{11}h_{11} + \dot{m}_{12}h_{12} \tag{4.26}$$

$$\dot{m}_{10}s_{10} + \dot{S}_{gen,cs} = \dot{m}_{11}s_{11} + \dot{m}_{12}s_{12} \tag{4.27}$$

$$\dot{m}_{10}ex_{10} = \dot{m}_{11}ex_{11} + \dot{m}_{12}ex_{12} + \dot{E}x_{d,cs} \tag{4.28}$$

The following equations for mass, energy, entropy, and exergy balance equations for the scrubber in the first waste to energy multigeneration system can be denoted, respectively, as:

$$\dot{m}_{12} = \dot{m}_{13} + \dot{m}_{13a} \tag{4.29}$$

$$\dot{m}_{12}h_{12} = \dot{m}_{13}h_{13} + \dot{m}_{13a}h_{13a} \tag{4.30}$$

$$\dot{m}_{12}s_{12} + \dot{S}_{gen,sc} = \dot{m}_{13}s_{13} + \dot{m}_{13a}s_{13a} \tag{4.31}$$

$$\dot{m}_{12}ex_{12} = \dot{m}_{13}ex_{13} + \dot{m}_{13a}ex_{13a} + \dot{E}x_{d,sc} \tag{4.32}$$

The mass, energy, entropy, and exergy balance equations for the acid gas removal unit in the first multigeneration system can be denoted, respectively, as follows:

$$\dot{m}_{13} = \dot{m}_{14} + \dot{m}_{50} \tag{4.33}$$

$$\dot{m}_{13}h_{13} = \dot{m}_{14}h_{14} + \dot{m}_{50}h_{50} \tag{4.34}$$

$$\dot{m}_{13}s_{13} + \dot{S}_{gen,agr} = \dot{m}_{14}s_{14} + \dot{m}_{50}s_{50} \tag{4.35}$$

$$\dot{m}_{13}ex_{13} = \dot{m}_{15}ex_{15} + \dot{m}_{50}ex_{50} + \dot{E}x_{d,agr} \tag{4.36}$$

The mass, energy, entropy, and exergy balance equations for the heat exchanger 4 in the first multigeneration system can be denoted, respectively, as follows:

$$\dot{m}_{14a} = \dot{m}_{15} \text{ and } \dot{m}_{34} = \dot{m}_{35} \tag{4.37}$$

$$\dot{m}_{14a}h_{14a} + \dot{m}_{34}h_{34} = \dot{m}_{15}h_{15} + \dot{m}_{35}h_{35} \quad (4.38)$$

$$\dot{m}_{14a}s_{14a} + \dot{m}_{34}s_{34} + \dot{S}_{gen,HEX4} = \dot{m}_{15}s_{15} + \dot{m}_{35}s_{35} \quad (4.39)$$

$$\dot{m}_{14a}ex_{14a} + \dot{m}_{34}ex_{34} = \dot{m}_{15}ex_{15} + \dot{m}_{35}ex_{35} + \dot{E}x_{d,HEX4} \quad (4.40)$$

Augustine et al. [80] determined that the operating temperature should be 450 °C.

The following equation explains the reaction between syngas and boiler steam in the water gas shift reaction:

$$CO + H_2O \leftrightarrow CO_2 + H_2 \quad (4.41)$$

The mass, energy, entropy, and exergy balance equations for the water gas shift reaction in the first multigeneration system can be denoted, respectively, as follows:

$$\dot{m}_{15} + \dot{m}_{18} = \dot{m}_{19} + \dot{m}_{20} \quad (4.42)$$

$$\dot{m}_{15}h_{15} + \dot{m}_{18}h_{18} = \dot{m}_{19}h_{19} + \dot{m}_{20}h_{20} \quad (4.43)$$

$$\dot{m}_{15}s_{15} + \dot{m}_{18}s_{18} + \dot{S}_{gen,wgsr} = \dot{m}_{19}s_{19} + \dot{m}_{20}h_{20} \quad (4.44)$$

$$\dot{m}_{15}ex_{15} + \dot{m}_{18}ex_{18} = \dot{m}_{19}ex_{19} + \dot{m}_{20}ex_{20} + \dot{E}x_{d,wgsr} \quad (4.45)$$

The mass, energy, entropy, and exergy balance equations for the boiler in the first multigeneration system can be analyzed as follows:

$$\dot{m}_{17} = \dot{m}_{18} \quad (4.46)$$

$$\dot{m}_{17}h_{17} + \dot{W}_b = \dot{m}_{18}h_{18} \quad (4.47)$$

$$\dot{m}_{17}s_{17} + \dot{S}_{gen,b} = \dot{m}_{18}s_{18} \quad (4.48)$$

$$\dot{m}_{17}ex_{17} + \dot{W}_b = \dot{m}_{18}ex_{18} + \dot{E}x_{d,b} \quad (4.49)$$

Rather than converting carbon dioxide directly to ethanol, the majority of carbon dioxide hydrogenation processes documented in the literature entail first converting it to methanol and subsequently to ethanol. [64]. The present research synthesizes ethanol from hydrogen and carbon dioxide by direct hydrogenation of carbon dioxide in the presence of an ordered Pd-Cu nanoparticle catalyst. When ordered Pd-Cu nanoparticles are used in carbon dioxide

hydrogenation, the catalyst's ethanol selectivity can reach up to 92%.The hydrogenation of carbon dioxide follows the following chemical equation:

$$2CO_2 + 6H_2 \rightarrow C_2H_5OH + 3H_2O \quad (4.50)$$

The mass, energy, entropy, and exergy balance equations for the ethanol production unit in the first multigeneration system can be analyzed as follows:

$$\dot{m}_{19} = \dot{m}_{23} \quad (4.51)$$

$$\dot{m}_{19}h_{19} + \dot{W}_{epu} = \dot{m}_{23}h_{23} \quad (4.52)$$

$$\dot{m}_{19}s_{19} + \dot{S}_{gen,epu} = \dot{m}_{23}s_{23} \quad (4.53)$$

$$\dot{m}_{19}ex_{19} + \dot{W}_{epu} = \dot{m}_{23}ex_{23} + \dot{E}x_{d,epu} \quad (4.54)$$

The mass, energy, entropy, and exergy balance equations for carbon dioxide separation unit membrane in the first multigeneration system can be denoted, respectively, as follows:

$$\dot{m}_{21} = \dot{m}_{22} + \dot{m}_{51} \quad (4.55)$$

$$\dot{m}_{21}h_{21} = \dot{m}_{22}h_{22} + \dot{m}_{51}h_{51} \quad (4.56)$$

$$\dot{m}_{21}s_{21} + \dot{S}_{gen,csu} = \dot{m}_{22}s_{22} + \dot{m}_{51}s_{51} \quad (4.57)$$

$$\dot{m}_{21}ex_{21} = \dot{m}_{22}ex_{22} + \dot{m}_{51}ex_{51} + \dot{E}x_{d,csu} \quad (4.58)$$

At stage number four, half of the clean syngas is divided in half and sent to the combustion chamber for use in the Brayton cycle. The compressor raises the air pressure to 450 kPa. The clean syngas combusts in the following way after the gasification unit:

$$C_6H_6 + 7.5O_2 \rightarrow 6CO_2 + 3H_2O \quad (4.59)$$

$$H_2 + 0.5O_2 \rightarrow H_2O \quad (4.60)$$

$$CO + 0.5O_2 \rightarrow CO_2 \quad (4.61)$$

$$CH_4 + 2O_2 \rightarrow CO_2 + 2H_2O \quad (4.62)$$

The mass, energy, entropy, and exergy balance equations for the combustion chamber in the first multigeneration system can be analyzed, respectively, as follows:

$$\dot{m}_{14b} + \dot{m}_{25} = \dot{m}_{26} \quad (4.63)$$

$$\dot{m}_{14b}h_{14b} + \dot{m}_{25}h_{25} + \dot{Q}_{cc} = \dot{m}_{26}h_{26} \quad (4.64)$$

$$\dot{m}_{14b}s_{14b} + \dot{m}_{25}s_{25} + \frac{\dot{Q}_{cc}}{T_S} + \dot{S}_{gen,cc} = \dot{m}_{26}s_{26} \quad (4.65)$$

$$\dot{m}_{14b}ex_{14b} + \dot{m}_{25}ex_{25} + \dot{E}x_{d,\dot{Q}_{cc}} = \dot{m}_{26}ex_{26} + \dot{E}x_{d,G} \quad (4.66)$$

The following equations for mass, energy, entropy, and exergy balance equations for the compressor in the first waste to energy multigeneration system can be analyzed as:

$$\dot{m}_{24} = \dot{m}_{25} \quad (4.67)$$

$$\dot{m}_{24}h_{24} + \dot{W}_c = \dot{m}_{25}h_{25} \quad (4.68)$$

$$\dot{m}_{24}s_{24} + \dot{S}_{gen,c} = \dot{m}_{25}s_{25} \quad (4.69)$$

$$\dot{m}_{24}ex_{24} + \dot{W}_c = \dot{m}_{25}ex_{25} + \dot{E}x_{d,c} \quad (4.70)$$

The mass, energy, entropy, and exergy balance equations for the heat exchanger 3 in the first multigeneration system can be denoted, respectively, as follows:

$$\dot{m}_{27} = \dot{m}_{28} \text{ and } \dot{m}_{30} = \dot{m}_{31} \quad (4.71)$$

$$\dot{m}_{27}h_{27} + \dot{m}_{30}h_{30} = \dot{m}_{28}h_{28} + \dot{m}_{31}h_{31} \quad (4.72)$$

$$\dot{m}_{27}s_{27} + \dot{m}_{30}s_{30} + \dot{S}_{gen,HEX3} = \dot{m}_{28}s_{28} + \dot{m}_{31}s_{31} \quad (4.73)$$

$$\dot{m}_{27}ex_{27} + \dot{m}_{30}ex_{30} = \dot{m}_{28}ex_{28} + \dot{m}_{31}ex_{31} + \dot{E}x_{d,HEX3} \quad (4.74)$$

The mass, energy, entropy, and exergy balance equations for the condenser 1 in the first multigeneration system can be denoted, respectively, as follows:

$$\dot{m}_{32} = \dot{m}_{29} \quad (4.75)$$

$$\dot{m}_{32}h_{32} = \dot{m}_{29}h_{29} + \dot{Q}_{cond1} \quad (4.76)$$

$$\dot{m}_{32}s_{32} + \dot{S}_{gen,cond1} = \dot{m}_{29}s_{29} + \frac{\dot{Q}_{cond1}}{T_{surr_{cond1}}} \quad (4.77)$$

$$\dot{m}_{32}ex_{32} = \dot{m}_{29}ex_{29} + \dot{E}x_{\dot{Q}_{cond1}} + \dot{E}x_{d,cond1} \quad (4.78)$$

The following equations for mass, energy, entropy, and exergy balance equations for the generator in the first waste to energy multigeneration system can be analyzed as:

$$\dot{m}_{37} + \dot{m}_{39} = \dot{m}_{38} + \dot{m}_{46} \tag{4.79}$$

$$\dot{m}_{37}h_{37} + \dot{m}_{39}h_{39} + \dot{Q}_{gen} = \dot{m}_{38}h_{38} + \dot{m}_{46}h_{46} \tag{4.80}$$

$$\dot{m}_{37}s_{37} + \dot{m}_{39}s_{39} + \frac{\dot{Q}_{gen}}{T_{s_{gen}}} + \dot{S}_{\mathrm{gen,gen}} = \dot{m}_{38}s_{38} + \dot{m}_{46}s_{46} \tag{4.81}$$

$$\dot{m}_{37}ex_{37} + \dot{m}_{39}ex_{39} + \dot{E}x_{\dot{Q}_{\mathrm{gen}}} = \dot{m}_{38}ex_{38} + \dot{m}_{46}ex_{46} + \dot{E}x_{\mathrm{d,gen}} \tag{4.82}$$

The mass, energy, entropy, and exergy balance equations for the condenser in the first multigeneration system can be denoted, respectively, as follows:

$$\dot{m}_{40} = \dot{m}_{41} \tag{4.83}$$

$$\dot{m}_{40}h_{40} = \dot{m}_{41}h_{41} + \dot{Q}_{cond} \tag{4.84}$$

$$\dot{m}_{40}s_{40} + \dot{S}_{\mathrm{gen,cond}} = \dot{m}_{41}s_{41} + \frac{\dot{Q}_{cond}}{T_{surr_{cond}}} \tag{4.85}$$

$$\dot{m}_{40}ex_{40} = \dot{m}_{41}ex_{41} + \dot{E}x_{\dot{Q}_{\mathrm{cond}}} + \dot{E}x_{\mathrm{d,cond}} \tag{4.86}$$

The mass, energy, entropy, and exergy balance equations for the expansion valve 1 in the first multigeneration system can be denoted, respectively, as follows:

$$\dot{m}_{41} = \dot{m}_{42} \tag{4.87}$$

$$\dot{m}_{41}h_{41} = \dot{m}_{42}h_{42} \tag{4.88}$$

$$\dot{m}_{41}s_{41} + \dot{S}_{\mathrm{gen,exv1}} = \dot{m}_{42}s_{42} \tag{4.89}$$

$$\dot{m}_{41}ex_{41} = \dot{m}_{42}ex_{42} + \dot{E}x_{\mathrm{d,exv1}} \tag{4.90}$$

The following equations for mass, energy, entropy, and exergy balance equations for the evaporator in the first waste to energy multigeneration system can be analyzed as:

$$\dot{m}_{42} = \dot{m}_{43} \tag{4.91}$$

$$\dot{m}_{42}h_{42} + \frac{\dot{Q}_{ev}}{T_{s_{ev}}} = \dot{m}_{43}h_{43} \quad (4.92)$$

$$\dot{m}_{42}s_{42} + \dot{S}_{\text{gen,ev}} = \dot{m}_{43}s_{43} \quad (4.93)$$

$$\dot{m}_{42}ex_{42} + \dot{E}x_{\dot{Q}_{\text{ev}}} = \dot{m}_{43}ex_{43} + \dot{E}x_{\text{d,ev}} \quad (4.94)$$

The mass, energy, entropy, and exergy balance equations for the absorber in the first multigeneration system can be denoted, respectively, as follows:

$$\dot{m}_{43} + \dot{m}_{48} = \dot{m}_{44} \quad (4.95)$$

$$\dot{m}_{43}h_{43} + \dot{m}_{48}h_{48} = \dot{m}_{44}h_{44} + \dot{Q}_{abs} \quad (4.96)$$

$$\dot{m}_{43}s_{43} + \dot{m}_{48}s_{48} + \dot{S}_{\text{gen,abs}} = \dot{m}_{44}s_{44} + \frac{\dot{Q}_{abs}}{T_{surr_{abs}}} \quad (4.97)$$

$$\dot{m}_{43}ex_{43} + \dot{m}_{48}ex_{48} = \dot{m}_{44}ex_{44} + \dot{E}x_{\dot{Q}_{\text{abs}}} + \dot{E}x_{\text{d,abs}} \quad (4.98)$$

The mass, energy, entropy, and exergy balance equations for the heat exchanger 5 in the first multigeneration system can be denoted, respectively, as follows:

$$\dot{m}_{45} = \dot{m}_{37} \text{ and } \dot{m}_{46} = \dot{m}_{47} \quad (4.99)$$

$$\dot{m}_{45}h_{45} + \dot{m}_{46}h_{46} = \dot{m}_{37}h_{37} + \dot{m}_{47}h_{47} \quad (4.100)$$

$$\dot{m}_{45}s_{45} + \dot{m}_{46}s_{46} + \dot{S}_{\text{gen,HEX5}} = \dot{m}_{37}s_{37} + \dot{m}_{47}s_{47} \quad (4.101)$$

$$\dot{m}_{45}ex_{45} + \dot{m}_{46}ex_{46} = \dot{m}_{37}ex_{37} + \dot{m}_{47}ex_{47} + \dot{E}x_{\text{d,HEX5}} \quad (4.102)$$

The mass, energy, entropy, and exergy balance equations for the expansion valve 2 in the first multigeneration system can be denoted, respectively, as follows:

$$\dot{m}_{47} = \dot{m}_{48} \quad (4.103)$$

$$\dot{m}_{47}h_{47} = \dot{m}_{48}h_{48} \quad (4.104)$$

$$\dot{m}_{47}s_{47} + \dot{S}_{\text{gen,exv2}} = \dot{m}_{48}s_{48} \quad (4.105)$$

$$\dot{m}_{47}ex_{47} = \dot{m}_{48}ex_{48} + \dot{E}x_{\text{d,exv2}} \quad (4.106)$$

Most carbon dioxide hydrogenation procedures described in the literature include first converting carbon dioxide to methanol and then converting it to ethanol, rather than a direct conversion of carbon dioxide to ethanol [64]. The present work utilizes direct hydrogenation of carbon dioxide to produce ethanol in the presence of an ordered Pd-Cu Nanoparticles catalyst. When ordered Pd-Cu nanoparticles are utilized in carbon dioxide hydrogenation, the catalyst exhibits up to 92% ethanol selectivity. The following chemical equation describes the hydrogenation of carbon dioxide:

$$2CO_2 + 6H_2 \rightarrow C_2H_5OH + 3H_2O \quad (4.107)$$

Sulfuric acid, cooling, methane, electric power, hydrogen, heating, and ethanol are all useful outputs of the whole system. Although the suggested system produces very little methane, it is included in the calculations. In addition to the general system's heat and work equations, the energy and exergy equations are expressed as follows:

$$\Sigma\dot{Q}_{in} = \dot{Q}_{Solar} + \dot{Q}_B + \dot{Q}_G \quad (4.108)$$

$$\Sigma\dot{W}_{in} = \dot{W}_{p_1} + \dot{W}_{p_2} + \dot{W}_{p_3} + \dot{W}_{p_4} + \dot{W}_{P_5} + \dot{W}_{p_6} + \dot{W}_c \quad (4.109)$$

$$\Sigma\dot{Q}_{out} = \dot{Q}_{cond} + \dot{Q}_{cond} + \dot{Q}_{ab} + \dot{Q}_{ev} + \dot{m}_{H_2}LHV_{H_2} + \dot{m}_{C_2H_5OH}LHV_{C_2H_5OH} + \dot{m}_{H_2S}LHV_{H_2S} + \dot{m}_{CH_4}LHV_{CH_4} \quad (4.110)$$

$$\Sigma\dot{W}_{out} = \dot{W}_{T_1} + \dot{W}_{T_2} + \dot{W}_{T_3} + \dot{W}_{T_4} + \dot{W}_{T_5} \quad (4.111)$$

$$\Sigma\dot{W}_{net} = \Sigma\dot{W}_{out} - \Sigma\dot{W}_{in} \quad (4.112)$$

$$\Sigma\dot{E}x_{in} = \dot{Q}_{Solar}\left(1 - \frac{T_0}{T_{sun}}\right) + \dot{Q}_B\left(1 - \frac{T_0}{T_B}\right) + \dot{Q}_G\left(1 - \frac{T_0}{T_G}\right) \quad (4.113)$$

$$\Sigma\dot{E}x_{out,1} = \dot{Q}_{cond1}\left(1 - \frac{T_0}{T_{cond1}}\right) + \dot{Q}_{cond2}\left(1 - \frac{T_0}{T_{cond2}}\right) + \dot{Q}_{ab}\left(1 - \frac{T_0}{T_{ab}}\right) + \dot{Q}_{ev}\left(\frac{T_0}{T_{ev}} - 1\right) + \dot{m}_{H_2}ex_{H_2} + \dot{m}_{C_2H_5OH}ex_{C_2H_5OH} + \dot{m}_{H_2}ex_{H_2} + \dot{m}_{H_2S}ex_{H_2S} + \dot{m}_{CH_4}ex_{CH_4} \quad (4.114)$$

The overall system energy efficiency is determined as:

$$\eta_{overall} = \frac{\Sigma\dot{Q}_{out} + \Sigma\dot{W}_{net}}{\Sigma\dot{Q}_{in}} \quad (4.115)$$

The overall system energy efficiency is calculated as:

$$\psi_{overall} = \frac{\Sigma\dot{E}x_{out,1} + \Sigma\dot{W}_{net}}{\Sigma\dot{E}x_{in}} \quad (4.116)$$

The mass, energy, entropy, and exergy balance equations for each pump in the second multigeneration system can be denoted, respectively, as follows:

$$\dot{m}_i = \dot{m}_j \tag{4.117}$$

$$\dot{m}_i h_i + \dot{W}_p = \dot{m}_j h_j \tag{4.118}$$

$$\dot{m}_i s_i + \dot{S}_{gen,p} = \dot{m}_j s_j \tag{4.119}$$

$$\dot{m}_i ex_i + \dot{W}_p = \dot{m}_j ex_j + \dot{E}x_{d,p} \tag{4.120}$$

The mass, energy, entropy, and exergy balance equations for the heat exchanger 1 in the second multigeneration system can be denoted, respectively, as follows:

$$\dot{m}_2 = \dot{m}_3 \text{ and } \dot{m}_{22} = \dot{m}_{23} \tag{4.121}$$

$$\dot{m}_2 h_2 + \dot{m}_{24} h_{24} = \dot{m}_3 h_3 + \dot{m}_{25} h_{25} \tag{4.122}$$

$$\dot{m}_2 s_2 + \dot{m}_{24} s_{24} + \dot{S}_{gen,HEX1} = \dot{m}_3 s_3 + \dot{m}_{25} s_{25} \tag{4.123}$$

$$\dot{m}_2 ex_2 + \dot{m}_{24} ex_{24} = \dot{m}_3 ex_3 + \dot{m}_{25} ex_{25} + \dot{E}x_{d,HEX1} \tag{4.124}$$

The mass, energy, entropy, and exergy balance equations for the compressor in the second multigeneration system can be analyzed as follows:

$$\dot{m}_6 = \dot{m}_7 \tag{4.125}$$

$$\dot{m}_6 h_6 + \dot{W}_c = \dot{m}_7 h_7 \tag{4.126}$$

$$\dot{m}_6 s_6 + \dot{S}_{gen,c} = \dot{m}_7 s_7 \tag{4.127}$$

$$\dot{m}_6 ex_6 + \dot{W}_c = \dot{m}_7 ex_7 + \dot{E}x_{d,c} \tag{4.128}$$

Table 4.2: Ultimate and proximate analyses of waste tires [81].

Ultimate Analysis	(weight %)
C	75
N	0.3
O	2.7
H	7
S	1.5
CI	0
Ash	4.12
Proximate Analysis	
VM	55

FC	30
Moisture	1.5
Ash	13.5

The mass, energy, entropy, and exergy balance equations for the gasifier in the second multigeneration system can be analyzed, respectively, as follows:

$$\dot{m}_4 + \dot{m}_7 + \dot{m}_8 + \dot{m}_{10} = \dot{m}_9 + \dot{m}_{11} \quad (4.129)$$

$$\dot{m}_4 h_4 + \dot{m}_7 h_7 + \dot{m}_8 h_8 + \dot{m}_{10} h_{10} + \dot{Q}_G = \dot{m}_9 h_9 + \dot{m}_{11} h_{11} \quad (4.130)$$

$$\dot{m}_4 s_4 + \dot{m}_7 s_7 + \dot{m}_8 s_8 + \dot{m}_{10} s_{10} + \frac{\dot{Q}_G}{T_S} + \dot{S}_{gen,G} = \dot{m}_9 s_9 + \dot{m}_{11} s_{11} \quad (4.131)$$

$$\dot{m}_4 ex_4 + \dot{m}_7 ex_7 + \dot{m}_8 ex_8 + \dot{m}_{10} ex_{10} + \dot{E}x_{d,G} = \dot{m}_9 ex_9 + \dot{m}_{11} ex_{11} + \dot{E}x_{d,G} \quad (4.132)$$

The mass, energy, entropy, and exergy balance equations for the cyclone separator in the second multigeneration system can be denoted, respectively, as follows:

$$\dot{m}_9 = \dot{m}_{10} + \dot{m}_{12} \quad (4.133)$$

$$\dot{m}_9 h_9 = \dot{m}_{10} h_{10} + \dot{m}_{12} h_{12} \quad (4.134)$$

$$\dot{m}_9 s_9 + \dot{S}_{gen,cs} = \dot{m}_{10} s_{10} + \dot{m}_{12} s_{12} \quad (4.135)$$

$$\dot{m}_9 ex_9 = \dot{m}_{10} ex_{10} + \dot{m}_{12} ex_{12} + \dot{E}x_{d,cs} \quad (4.136)$$

The following equations for mass, energy, entropy, and exergy balance equations for the scrubber in the second waste to energy multigeneration system can be analyzed as:

$$\dot{m}_{12} = \dot{m}_{13} + \dot{m}_{13a} \quad (4.137)$$

$$\dot{m}_{12} h_{12} = \dot{m}_{13} h_{13} + \dot{m}_{13a} h_{13a} \quad (4.138)$$

$$\dot{m}_{12} s_{12} + \dot{S}_{gen,sc} = \dot{m}_{13} s_{13} + \dot{m}_{13a} s_{13a} \quad (4.139)$$

$$\dot{m}_{12} ex_{12} = \dot{m}_{13} ex_{13} + \dot{m}_{13a} ex_{13a} + \dot{E}x_{d,sc} \quad (4.140)$$

The mass, energy, entropy, and exergy balance equations for the acid gas removal unit in the second multigeneration system can be denoted, respectively, as follows:

$$\dot{m}_{13} = \dot{m}_{14} + \dot{m}_{15} \tag{4.141}$$

$$\dot{m}_{13}h_{13} = \dot{m}_{14}h_{14} + \dot{m}_{15}h_{15} \tag{4.142}$$

$$\dot{m}_{13}s_{13} + \dot{S}_{gen,agr} = \dot{m}_{14}s_{14} + \dot{m}_{15}s_{15} \tag{4.143}$$

$$\dot{m}_{13}ex_{13} = \dot{m}_{15}ex_{15} + \dot{m}_{15}ex_{15} + \dot{E}x_{d,agr} \tag{4.144}$$

The mass, energy, entropy, and exergy balance equations for the heat exchanger 2 in the second multigeneration system can be denoted, respectively, as follows:

$$\dot{m}_{15} = \dot{m}_{16} \text{ and } \dot{m}_{27} = \dot{m}_{28} \tag{4.145}$$

$$\dot{m}_{15}h_{15} + \dot{m}_{27}h_{27} = \dot{m}_{16}h_{16} + \dot{m}_{28}h_{28} \tag{4.146}$$

$$\dot{m}_{15}s_{15} + \dot{m}_{27}s_{27} + \dot{S}_{gen,HEX2} = \dot{m}_{16}s_{16} + \dot{m}_{28}s_{28} \tag{4.147}$$

$$\dot{m}_{15}ex_{15} + \dot{m}_{27}ex_{27} = \dot{m}_{16}ex_{16} + \dot{m}_{28}ex_{28} + \dot{E}x_{d,HEX2} \tag{4.148}$$

The mass, energy, entropy, and exergy balance equations for the heat exchanger 3 in the second multigeneration system can be analyzed, respectively, as follows:

$$\dot{m}_{16} = \dot{m}_{17} \text{ and } \dot{m}_{31} = \dot{m}_{32} \tag{4.149}$$

$$\dot{m}_{16}h_{16} + \dot{m}_{17}h_{17} = \dot{m}_{31}h_{31} + \dot{m}_{32}h_{32} \tag{4.150}$$

$$\dot{m}_{16}s_{16} + \dot{m}_{17}s_{17} + \dot{S}_{gen,HEX3} = \dot{m}_{31}s_{31} + \dot{m}_{32}s_{32} \tag{4.151}$$

$$\dot{m}_{16}ex_{16} + \dot{m}_{17}ex_{17} = \dot{m}_{31}ex_{31} + \dot{m}_{32}ex_{32} + \dot{E}x_{d,HEX3} \tag{4.152}$$

The mass, energy, entropy, and exergy balance equations for the water gas shift reaction in the second multigeneration system can be denoted, respectively, as follows:

$$\dot{m}_5 + \dot{m}_{17} = \dot{m}_{18} \tag{4.153}$$

$$\dot{m}_5h_5 + \dot{m}_{17}h_{17} = \dot{m}_{18}h_{18} \tag{4.154}$$

$$\dot{m}_5s_5 + \dot{m}_{17}s_{17} + \dot{S}_{gen,wgsr} = \dot{m}_{18}s_{18} \tag{4.155}$$

$$\dot{m}_5ex_5 + \dot{m}_{17}ex_{17} = \dot{m}_{18}ex_{18} + \dot{E}x_{d,wgsr} \tag{4.156}$$

The following equations for mass, energy, entropy, and exergy balance equations for each turbine in the second waste to energy multigeneration system can be denoted as:

$$\dot{m}_i = \dot{m}_j \tag{4.157}$$

$$\dot{m}_i h_i = \dot{W}_t + \dot{m}_j h_j \tag{4.158}$$

$$\dot{m}_i s_i + \dot{S}_{gen,t} = \dot{m}_j s_j \tag{4.159}$$

$$\dot{m}_i ex_i = \dot{W}_t + \dot{m}_j ex_j + \dot{E}x_{d,t} \tag{4.160}$$

The mass, energy, entropy, and exergy balance equations for the graphdiyne membrane in the second multigeneration system can be denoted, respectively, as follows:

$$\dot{m}_{19} = \dot{m}_{20} + \dot{m}_{22} \tag{4.161}$$

$$\dot{m}_{19} h_{19} = \dot{m}_{20} h_{20} + \dot{m}_{22} h_{22} \tag{4.162}$$

$$\dot{m}_{19} s_{19} + \dot{S}_{gen,cs} = \dot{m}_{20} s_{20} + \dot{m}_{22} s_{22} \tag{4.163}$$

$$\dot{m}_{19} ex_{19} = \dot{m}_{20} ex_{20} + \dot{m}_{22} ex_{22} + \dot{E}x_{d,glm} \tag{4.164}$$

The mass, energy, entropy, and exergy balance equations for electrochemical synthesis reactor in the second multigeneration system can be denoted, respectively, as follows:

$$\dot{m}_{20} + \dot{m}_w = \dot{m}_{21} \tag{4.165}$$

$$\dot{m}_{20} h_{20} + \dot{m}_w h_w + \dot{W}_{esr} = \dot{m}_{21} h_{21} \tag{4.166}$$

$$\dot{m}_{20} s_{20} + \dot{m}_w s_w + \dot{S}_{gen,esr} = \dot{m}_{21} s_{21} \tag{4.167}$$

$$\dot{m}_{20} ex_{20} + \dot{m}_w ex_w + \dot{W}_{esr} = \dot{m}_{21} ex_{21} + \dot{E}x_{d,esr} \tag{4.168}$$

The mass, energy, entropy, and exergy balance equations for hydrogen liquefaction reactor in the second multigeneration system can be denoted, respectively, as follows:

$$\dot{m}_{22} = \dot{m}_{23} \tag{4.169}$$

$$\dot{m}_{22} h_{22} + \dot{W}_{hl} = \dot{m}_{23} h_{23} \tag{4.170}$$

$$\dot{m}_{22} s_{22} + \dot{m}_{hl} s_{hl} + \dot{S}_{gen,hl} = \dot{m}_{23} s_{23} \tag{4.171}$$

$$\dot{m}_{22}ex_{22} + \dot{W}_{hl} = \dot{m}_{23}ex_{23} + \dot{E}x_{d,hl} \quad (4.172)$$

The mass, energy, entropy, and exergy balance equations for the heat exchanger 4 in the second multigeneration system can be denoted, respectively, as follows:

$$\dot{m}_{29} = \dot{m}_{26} \text{ and } \dot{m}_{36} = \dot{m}_{30} \quad (4.173)$$

$$\dot{m}_{29}h_{29} + \dot{m}_{26}h_{26} = \dot{m}_{36}h_{36} + \dot{m}_{30}h_{30} \quad (4.174)$$

$$\dot{m}_{29}s_{29} + \dot{m}_{26}s_{26} + \dot{S}_{gen,HEX4} = \dot{m}_{36}s_{36} + \dot{m}_{30}s_{30} \quad (4.175)$$

$$\dot{m}_{29}ex_{29} + \dot{m}_{26}ex_{26} = \dot{m}_{36}ex_{36} + \dot{m}_{30}ex_{30} + \dot{E}x_{d,HEX4} \quad (4.176)$$

The following equations for mass, energy, entropy, and exergy balance equations for the generator in the second waste to energy multigeneration system can be analyzed as:

$$\dot{m}_{37} + \dot{m}_{39} = \dot{m}_{38} + \dot{m}_{46} \quad (4.177)$$

$$\dot{m}_{37}h_{37} + \dot{m}_{39}h_{39} + \dot{Q}_{gen} = \dot{m}_{38}h_{38} + \dot{m}_{46}h_{46} \quad (4.178)$$

$$\dot{m}_{37}s_{37} + \dot{m}_{39}s_{39} + \frac{\dot{Q}_{gen}}{T_{s_{gen}}} + \dot{S}_{gen,gen} = \dot{m}_{38}s_{38} + \dot{m}_{46}s_{46} \quad (4.179)$$

$$\dot{m}_{37}ex_{37} + \dot{m}_{39}ex_{39} + \dot{E}x_{\dot{Q}_{gen}} = \dot{m}_{38}ex_{38} + \dot{m}_{46}ex_{46} + \dot{E}x_{d,gen} \quad (4.180)$$

The following equations for mass, energy, entropy, and exergy balance equations for the condenser in the second waste to energy multigeneration system can be analyzed as:

$$\dot{m}_{40} = \dot{m}_{41} \quad (4.181)$$

$$\dot{m}_{40}h_{40} = \dot{m}_{41}h_{41} + \dot{Q}_{cond} \quad (4.182)$$

$$\dot{m}_{40}s_{40} + \dot{S}_{gen,cond} = \dot{m}_{41}s_{41} + \frac{\dot{Q}_{cond}}{T_{surr_{cond}}} \quad (4.183)$$

$$\dot{m}_{40}ex_{40} = \dot{m}_{41}ex_{41} + \dot{E}x_{\dot{Q}_{cond}} + \dot{E}x_{d,cond} \quad (4.184)$$

The mass, energy, entropy, and exergy balance equations for the expansion valve 1 in the second multigeneration system can be denoted, respectively, as follows:

$$\dot{m}_{41} = \dot{m}_{42} \quad (4.185)$$

$$\dot{m}_{41}h_{41} = \dot{m}_{42}h_{42} \quad (4.186)$$

$$\dot{m}_{41}s_{41} + \dot{S}_{gen,exv1} = \dot{m}_{42}s_{42} \quad (4.187)$$

$$\dot{m}_{41}ex_{41} = \dot{m}_{42}ex_{42} + \dot{E}x_{d,exv1} \quad (4.188)$$

The following equations for mass, energy, entropy, and exergy balance equations for the evaporator in the second waste to energy multigeneration system can be analyzed as:

$$\dot{m}_{42} = \dot{m}_{43} \quad (4.189)$$

$$\dot{m}_{42}h_{42} + \frac{\dot{Q}_{ev}}{T_{s_{ev}}} = \dot{m}_{43}h_{43} \quad (4.190)$$

$$\dot{m}_{42}s_{42} + \dot{S}_{gen,ev} = \dot{m}_{43}s_{43} \quad (4.191)$$

$$\dot{m}_{42}ex_{42} + \dot{E}x_{\dot{Q}_{ev}} = \dot{m}_{43}ex_{43} + \dot{E}x_{d,ev} \quad (4.192)$$

The following equations for mass, energy, entropy, and exergy balance equations for the absorber in the second waste to energy multigeneration system can be analyzed as:

$$\dot{m}_{43} + \dot{m}_{48} = \dot{m}_{44} \quad (4.193)$$

$$\dot{m}_{43}h_{43} + \dot{m}_{48}h_{48} = \dot{m}_{44}h_{44} + \dot{Q}_{abs} \quad (4.194)$$

$$\dot{m}_{43}s_{43} + \dot{m}_{48}s_{48} + \dot{S}_{gen,abs} = \dot{m}_{44}s_{44} + \frac{\dot{Q}_{abs}}{T_{surr_{abs}}} \quad (4.195)$$

$$\dot{m}_{43}ex_{43} + \dot{m}_{48}ex_{48} = \dot{m}_{44}ex_{44} + \dot{E}x_{\dot{Q}_{abs}} + \dot{E}x_{d,abs} \quad (4.196)$$

The mass, energy, entropy, and exergy balance equations for the heat exchanger 5 in the second multigeneration system can be denoted, respectively, as follows:

$$\dot{m}_{45} = \dot{m}_{37} \text{ and } \dot{m}_{46} = \dot{m}_{47} \quad (4.197)$$

$$\dot{m}_{45}h_{45} + \dot{m}_{46}h_{46} = \dot{m}_{37}h_{37} + \dot{m}_{47}h_{47} \quad (4.198)$$

$$\dot{m}_{45}s_{45} + \dot{m}_{46}s_{46} + \dot{S}_{gen,HEX5} = \dot{m}_{37}s_{37} + \dot{m}_{47}s_{47} \quad (4.199)$$

$$\dot{m}_{45}ex_{45} + \dot{m}_{46}ex_{46} = \dot{m}_{37}ex_{37} + \dot{m}_{47}ex_{47} + \dot{E}x_{d,HEX5} \quad (4.200)$$

The mass, energy, entropy, and exergy balance equations for the expansion valve 2 in the second multigeneration system can be denoted, respectively, as follows:

$$\dot{m}_{47} = \dot{m}_{48} \tag{4.201}$$

$$\dot{m}_{47} h_{47} = \dot{m}_{48} h_{48} \tag{4.202}$$

$$\dot{m}_{47} s_{47} + \dot{S}_{gen,exv2} = \dot{m}_{48} s_{48} \tag{4.203}$$

$$\dot{m}_{47} ex_{47} = \dot{m}_{48} ex_{48} + \dot{E}x_{d,exv2} \tag{4.204}$$

The mass, energy, entropy, and exergy balance equations for compressor 1 in the third multigeneration system can be analyzed as follows:

$$\dot{m}_1 = \dot{m}_2 \tag{4.205}$$

$$\dot{m}_1 h_1 + \dot{W}_{c1} = \dot{m}_2 h_2 \tag{4.206}$$

$$\dot{m}_1 s_1 + \dot{S}_{gen,c1} = \dot{m}_2 s_2 \tag{4.207}$$

$$\dot{m}_1 ex_1 + \dot{W}_{c1} = \dot{m}_2 ex_2 + \dot{E}x_{d,c1} \tag{4.208}$$

Table 4.3 Ultimate and proximate analyses of Tuncbilek lignite [73].

Ultimate Analysis	(weight %)
C	62.24
N	2.24
O	10.87
H	4.42
S	0.43
CI	0
Ash	18.7
Proximate Analysis	
VM	34.18
FC	47.11
Moisture	14.06
Ash	16.07

The mass, energy, entropy, and exergy balance equations for the gasifier in the third multigeneration system can be analyzed, respectively, as follows:

$$\dot{m}_2 + \dot{m}_3 + \dot{m}_{coal} = \dot{m}_4 + \dot{m}_{ash} + \dot{m}_{char} \tag{4.209}$$

$$\dot{m}_2 h_2 + \dot{m}_3 h_3 + \dot{m}_{coal} h_{coal} + \dot{Q}_G = \dot{m}_4 h_4 + \dot{m}_{ash} h_{ash} + \dot{m}_{char} h_{char} \quad (4.210)$$

$$\dot{m}_2 s_2 + \dot{m}_3 s_3 + \dot{m}_{coal} s_{coal} + \frac{\dot{Q}_G}{T_S} + \dot{S}_{gen,G} = \dot{m}_4 s_4 + \dot{m}_{ash} s_{ash} + \dot{m}_{char} s_{char} \quad (4.211)$$

$$\dot{m}_2 ex_2 + \dot{m}_3 ex_3 + \dot{m}_{coal} ex_{coal} + \dot{E}x_{d,G} = \dot{m}_4 ex_4 + \dot{m}_{ash} ex_{ash} + \dot{m}_{char} ex_{char}$$

$$+\dot{E}x_{d,G} \quad (4.212)$$

The following equations for mass, energy, entropy, and exergy balance equations for the scrubber in the third waste to energy multigeneration system can be denoted, as:

$$\dot{m}_4 = \dot{m}_5 + \dot{m}_{5a} \quad (4.213)$$

$$\dot{m}_4 h_4 = \dot{m}_5 h_5 + \dot{m}_{5a} h_{5a} \quad (4.214)$$

$$\dot{m}_4 s_4 + \dot{S}_{gen,sc} = \dot{m}_5 s_5 + \dot{m}_{5a} s_{5a} \quad (4.215)$$

$$\dot{m}_4 ex_4 = \dot{m}_5 ex_5 + \dot{m}_{5a} ex_{5a} + \dot{E}x_{d,sc} \quad (4.216)$$

The mass, energy, entropy, and exergy balance equations for the acid gas removal unit in the third multigeneration system can be denoted, respectively, as follows:

$$\dot{m}_5 = \dot{m}_6 + \dot{m}_7 \quad (4.217)$$

$$\dot{m}_5 h_5 = \dot{m}_6 h_6 + \dot{m}_7 h_7 \quad (4.218)$$

$$\dot{m}_5 s_5 + \dot{S}_{gen,agr} = \dot{m}_6 s_6 + \dot{m}_7 s_7 \quad (4.219)$$

$$\dot{m}_5 ex_5 = \dot{m}_6 ex_6 + \dot{m}_7 ex_7 + \dot{E}x_{d,agr} \quad (4.220)$$

The mass, energy, entropy, and exergy balance equations for the heat exchanger 1 in the third multigeneration system can be denoted, respectively, as follows:

$$\dot{m}_7 = \dot{m}_8 \text{ and } \dot{m}_{23} = \dot{m}_{24} \quad (4.221)$$

$$\dot{m}_7 h_7 + \dot{m}_{23} h_{23} = \dot{m}_8 h_8 + \dot{m}_{24} h_{24} \quad (4.222)$$

$$\dot{m}_7 s_7 + \dot{m}_{23} s_{23} + \dot{S}_{gen,HEX1} = \dot{m}_8 s_8 + \dot{m}_{24} s_{24} \quad (4.223)$$

$$\dot{m}_7 ex_7 + \dot{m}_{23} ex_{23} = \dot{m}_8 ex_8 + \dot{m}_{24} ex_{24} + \dot{E}x_{d,HEX1} \quad (4.224)$$

The mass, energy, entropy, and exergy balance equations for the heat exchanger 3 in the third multigeneration system can be denoted, respectively, as follows:

$$\dot{m}_8 = \dot{m}_9 \text{ and } \dot{m}_{27} = \dot{m}_{28} \tag{4.225}$$

$$\dot{m}_8 h_8 + \dot{m}_{27} h_{27} = \dot{m}_9 h_9 + \dot{m}_{28} h_{28} \tag{4.226}$$

$$\dot{m}_8 s_8 + \dot{m}_{27} s_{27} + \dot{S}_{gen,HEX3} = \dot{m}_9 s_9 + \dot{m}_{28} s_{28} \tag{4.227}$$

$$\dot{m}_8 ex_8 + \dot{m}_{27} ex_{27} = \dot{m}_9 ex_9 + \dot{m}_{28} ex_{28} + \dot{E}x_{d,HEX3} \tag{4.228}$$

The mass, energy, entropy, and exergy balance equations for the water gas shift reaction in the third multigeneration system can be denoted, respectively, as follows:

$$\dot{m}_9 + \dot{m}_{21} = \dot{m}_{10} \tag{4.229}$$

$$\dot{m}_9 h_9 + \dot{m}_{21} h_{21} = \dot{m}_{10} h_{10} \tag{4.230}$$

$$\dot{m}_9 s_9 + \dot{m}_{21} s_{21} + \dot{S}_{gen,wgsr} = \dot{m}_{10} s_{10} \tag{4.231}$$

$$\dot{m}_9 ex_9 + \dot{m}_{21} ex_{21} = \dot{m}_{10} ex_{10} + \dot{E}x_{d,wgsr} \tag{4.232}$$

The following equations for mass, energy, entropy, and exergy balance equations for each turbine in the third waste to energy multigeneration system can be denoted as:

$$\dot{m}_i = \dot{m}_j \tag{4.233}$$

$$\dot{m}_i h_i = \dot{W}_t + \dot{m}_j h_j \tag{4.234}$$

$$\dot{m}_i s_i + \dot{S}_{gen,t} = \dot{m}_j s_j \tag{4.235}$$

$$\dot{m}_i ex_i = \dot{W}_t + \dot{m}_j ex_j + \dot{E}x_{d,t} \tag{4.236}$$

The mass, energy, entropy, and exergy balance equations for carbon dioxide separation unit membrane in the third multigeneration system can be denoted, respectively, as follows:

$$\dot{m}_{14} = \dot{m}_{15} + \dot{m}_{16} \tag{4.237}$$

$$\dot{m}_{14} h_{14} = \dot{m}_{15} h_{15} + \dot{m}_{16} h_{16} \tag{4.238}$$

$$\dot{m}_{14} s_{14} + \dot{S}_{gen,csu} = \dot{m}_{15} s_{15} + \dot{m}_{16} s_{16} \tag{4.239}$$

$$\dot{m}_{14}ex_{14} = \dot{m}_{15}ex_{15} + \dot{m}_{16}ex_{16} + \dot{E}x_{d,csu} \quad (4.240)$$

The mass, energy, entropy, and exergy balance equations for hydrogen liquefaction reactor in the third multigeneration system can be denoted, respectively, as follows:

$$\dot{m}_{16} = \dot{m}_{17} \quad (4.241)$$

$$\dot{m}_{16}h_{16} + \dot{W}_{hl} = \dot{m}_{17}h_{17} \quad (4.242)$$

$$\dot{m}_{16}s_{16} + \dot{m}_{hl}s_{hl} + \dot{S}_{gen,hl} = \dot{m}_{17}s_{17} \quad (4.243)$$

$$\dot{m}_{16}ex_{16} + \dot{W}_{hl} = \dot{m}_{17}ex_{17} + \dot{E}x_{d,hl} \quad (4.244)$$

The mass, energy, entropy, and exergy balance equations for the carbon hydrogenation unit in the third multigeneration system can be denoted, respectively, as follows:

$$\dot{m}_{12} = \dot{m}_{13} \quad (4.245)$$

$$\dot{m}_{12}h_{12} = \dot{m}_{13}h_{13} \quad (4.246)$$

$$\dot{m}_{12}s_{12} + \dot{S}_{gen,chu} = \dot{m}_{13}s_{13} \quad (4.247)$$

$$\dot{m}_{12}ex_{12} = \dot{m}_{13}ex_{13} + \dot{E}x_{d,chu} \quad (4.248)$$

The following equations for mass, energy, entropy, and exergy balance equations for each pump in the second waste to energy multigeneration system can be denoted as:

$$\dot{m}_i = \dot{m}_j \quad (4.249)$$

$$\dot{m}_i h_i + \dot{W}_p = \dot{m}_j h_j \quad (4.250)$$

$$\dot{m}_i s_i + \dot{S}_{gen,p} = \dot{m}_j s_j \quad (4.251)$$

$$\dot{m}_i ex_i + \dot{W}_p = \dot{m}_j ex_j + \dot{E}x_{d,p} \quad (4.252)$$

The mass, energy, entropy, and exergy balance equations for the heat exchanger 2 in the third multigeneration system can be denoted, respectively, as follows:

$$\dot{m}_{19} = \dot{m}_{20} \text{ and } \dot{m}_{25} = \dot{m}_{22} \quad (4.253)$$

$$\dot{m}_{19}h_{19} + \dot{m}_{25}h_{25} = \dot{m}_{20}h_{20} + \dot{m}_{22}h_{22} \quad (4.254)$$

$$\dot{m}_{19}s_{19} + \dot{m}_{25}s_{25} + \dot{S}_{gen,HEX2} = \dot{m}_{20}s_{20} + \dot{m}_{22}s_{22} \quad (4.255)$$

$$\dot{m}_{19}ex_{19} + \dot{m}_{25}ex_{25} = \dot{m}_{20}ex_{20} + \dot{m}_{22}ex_{22} + \dot{E}x_{d,HEX2} \quad (4.256)$$

The mass, energy, entropy, and exergy balance equations for the compressor 2 in the third multigeneration system can be analyzed, as follows:

$$\dot{m}_{26} = \dot{m}_{27} \quad (4.257)$$

$$\dot{m}_{26}h_{26} + \dot{W}_{c2} = \dot{m}_{27}h_{27} \quad (4.258)$$

$$\dot{m}_{26}s_{26} + \dot{S}_{gen,c2} = \dot{m}_{27}s_{27} \quad (4.259)$$

$$\dot{m}_{26}ex_{26} + \dot{W}_{c2} = \dot{m}_{27}ex_{27} + \dot{E}x_{d,c2} \quad (4.260)$$

The mass, energy, entropy, and exergy balance equations for the generator in the third multigeneration system can be denoted, respectively, as follows:

$$\dot{m}_{30} + \dot{m}_{32} = \dot{m}_{31} + \dot{m}_{39} \quad (4.261)$$

$$\dot{m}_{30}h_{30} + \dot{m}_{32}h_{32} + \dot{Q}_{gen} = \dot{m}_{31}h_{31} + \dot{m}_{39}h_{39} \quad (4.262)$$

$$\dot{m}_{30}s_{30} + \dot{m}_{32}s_{32} + \frac{\dot{Q}_{gen}}{T_{s_{gen}}} + \dot{S}_{gen,gen} = \dot{m}_{31}s_{31} + \dot{m}_{39}s_{39} \quad (4.263)$$

$$\dot{m}_{30}ex_{30} + \dot{m}_{32}ex_{32} + \dot{E}x_{\dot{Q}_{gen}} = \dot{m}_{31}ex_{31} + \dot{m}_{39}ex_{39} + \dot{E}x_{d,gen} \quad (4.264)$$

The mass, energy, entropy, and exergy balance equations for the condenser in the third multigeneration system can be denoted, respectively, as follows:

$$\dot{m}_{33} = \dot{m}_{34} \quad (4.265)$$

$$\dot{m}_{33}h_{33} = \dot{m}_{34}h_{34} + \dot{Q}_{cond} \quad (4.266)$$

$$\dot{m}_{33}s_{33} + \dot{S}_{gen,cond} = \dot{m}_{34}s_{34} + \frac{\dot{Q}_{cond}}{T_{surr_{cond}}} \quad (4.267)$$

$$\dot{m}_{33}ex_{33} = \dot{m}_{34}ex_{34} + \dot{E}x_{\dot{Q}_{cond}} + \dot{E}x_{d,cond} \quad (4.268)$$

The mass, energy, entropy, and exergy balance equations for the expansion valve 1 in the third multigeneration system can be denoted, respectively, as follows:

$$\dot{m}_{34} = \dot{m}_{35} \tag{4.269}$$

$$\dot{m}_{34} h_{34} = \dot{m}_{35} h_{35} \tag{4.270}$$

$$\dot{m}_{34} s_{34} + \dot{S}_{\text{gen,exv1}} = \dot{m}_{35} s_{35} \tag{4.271}$$

$$\dot{m}_{34} ex_{34} = \dot{m}_{35} ex_{35} + \dot{E}x_{\text{d,exv1}} \tag{4.272}$$

The mass, energy, entropy, and exergy balance equations for the evaporator in the third multigeneration system can be denoted, respectively, as follows:

$$\dot{m}_{35} = \dot{m}_{36} \tag{4.273}$$

$$\dot{m}_{35} h_{35} + \frac{\dot{Q}_{ev}}{T_{s_{ev}}} = \dot{m}_{36} h_{36} \tag{4.274}$$

$$\dot{m}_{35} s_{35} + \dot{S}_{\text{gen,ev}} = \dot{m}_{36} s_{36} \tag{4.275}$$

$$\dot{m}_{35} ex_{35} + \dot{E}x_{\dot{Q}_{\text{ev}}} = \dot{m}_{36} ex_{36} + \dot{E}x_{\text{d,ev}} \tag{4.276}$$

The mass, energy, entropy, and exergy balance equations for the absorber in the third multigeneration system can be denoted, respectively, as follows:

$$\dot{m}_{36} + \dot{m}_{41} = \dot{m}_{37} \tag{4.277}$$

$$\dot{m}_{36} h_{36} + \dot{m}_{41} h_{41} = \dot{m}_{37} h_{37} + \dot{Q}_{abs} \tag{4.278}$$

$$\dot{m}_{36} s_{36} + \dot{m}_{41} s_{41} + \dot{S}_{\text{gen,abs}} = \dot{m}_{37} s_{37} + \frac{\dot{Q}_{abs}}{T_{surr_{abs}}} \tag{4.279}$$

$$\dot{m}_{36} ex_{36} + \dot{m}_{41} ex_{41} = \dot{m}_{37} ex_{37} + \dot{E}x_{\dot{Q}_{\text{abs}}} + \dot{E}x_{\text{d,abs}} \tag{4.280}$$

The mass, energy, entropy, and exergy balance equations for the heat exchanger 4 in the third multigeneration system can be denoted, respectively, as follows:

$$\dot{m}_{38} = \dot{m}_{30} \text{ and } \dot{m}_{39} = \dot{m}_{40} \tag{4.281}$$

$$\dot{m}_{38} h_{38} + \dot{m}_{39} h_{39} = \dot{m}_{30} h_{30} + \dot{m}_{40} h_{40} \tag{4.282}$$

$$\dot{m}_{38} s_{38} + \dot{m}_{39} s_{39} + \dot{S}_{\text{gen,HEX4}} = \dot{m}_{30} s_{30} + \dot{m}_{40} s_{40} \tag{4.283}$$

$$\dot{m}_{38} ex_{38} + \dot{m}_{39} ex_{39} = \dot{m}_{30} ex_{30} + \dot{m}_{40} ex_{40} + \dot{E}x_{\text{d,HEX4}} \tag{4.284}$$

The mass, energy, entropy, and exergy balance equations for the expansion valve 2 in the third multigeneration system can be denoted, respectively, as follows:

$$\dot{m}_{40} = \dot{m}_{41} \tag{4.285}$$

$$\dot{m}_{40} h_{40} = \dot{m}_{41} h_{41} \tag{4.286}$$

$$\dot{m}_{40} s_{40} + \dot{S}_{gen,exv2} = \dot{m}_{41} s_{41} \tag{4.287}$$

$$\dot{m}_{40} ex_{40} = \dot{m}_{41} ex_{41} + \dot{E}x_{d,exv2} \tag{4.288}$$

4.2 Cost Assessment

To establish the economic feasibility of multigeneration systems, cost comparison methodologies such as the pay-back period (PBP), internal rate of return (IRR), and net present value (NPV) is calculated. The bank loan from Royal bank of Canada (RBC) is assumed to have a 4.14 % interest rate [91] CAD dollars are considered as the currency in the calculations. Sales charges for electricity, heating, and cooling are assumed to be 11 ¢/kWh, 3 ¢/kWh, and 4 ¢/kWh, respectively. While net present values have been calculated, the investment period has been considered to be 30 years [82]. The capital cost estimations of multigeneration systems are performed using the parameters presented in Table 4.4. Moreover, annual maintenance costs are calculated according to the data in Table 4.5 and included in the cost calculations. In the calculations, the prices of hydrogen and ethanol are considered as 2.7 $/kg and 1.2 $/kg, respectively [83]. The scaling exponent is found by proportioning the capacities of each multigeneration system and its subcomponents, reference system and subcomponents. The scaling exponent provides the assessment of multigeneration systems in relation to the reference system

The net present value method is used to determine the current value of a sequence of cash flows that occur at different points in time. A cash flow's present value is proportional to the time interval between now and the cash flow. Additionally, the discount rate is taken into account. NPV is a measure of money's time value. According to Xin-gang et al. [92], the net present value can be calculated according to the following equation:

$$\mathrm{NPV} = \frac{R_t}{(1+r)^t} \tag{4.289}$$

In this equation, R represents net cash flow at time t. While t represents time of the cash flow, r is the discount rate. The discount rate is considered as 4.14% [91] for each system. R_t represents annual total revenues from electricity, ethanol, hydrogen, space heating, cooling and sulfuric acid production and can be calculated according to the following equation:

$$R_t = 0.96 \times \left(R_{hydrogen} + R_{ethanol} + R_{heating} + R_{cooling} + R_{sulfuric\ acid} + R_{electricity}\right) - (R_{oc} + R_{mc}) \quad (4.290)$$

This total income is multiplied by a coefficient of 0.96 considering that the systems cannot be utilized for some reasons, such as maintenance and repair, in the 2-week part of the annual working period.

The internal rate of return is another economic evaluation parameter for systems. It can be helpful to understand whether a system is economically viable. Here, the CF_0value indicates the initial investment amount. Service life of 30 years is considered for all three systems in this study, and N is accepted as 30 [82]. According to Xin-gang et al. [92], the general rate of return equation can be denoted as follows:

$$\sum_{n=0}^{N} \frac{R_n}{(1+IRR)^n} \quad (4.291)$$

When a company has financial constraints, the payback time is preferred since it indicates how long the money invested in the project should take to return. In this regard, it is important to compare the payback period of systems. The payback period can be calculated as follows:

$$\sum_{n=0}^{PBP} R(n) = COC \quad (4.292)$$

Here, NCF stands for annual net cash flow, and COC denotes the cost of capital. On the other hand, PBP indicates the payback period and specifies the payment period of the capital cost back.

A cost assessment is used to determine the economic viability and cost effectiveness of proposed multigeneration systems. The goal of this cost evaluation is to approximately estimate which system would be more feasible from an economic point of view.

Table 4.4: Reference costs, capacities, and scaling exponents for all three systems [82]

Equipment	Scaling Parameter	Reference Cost (M$)	Reference Capacity	Scaling Exponent	Scaling Exponent	Scaling Exponent
ASU	Oxygen produced [kg/s]	70.93	26.54	0.026	0.024	0.024
Ash handling	Ash flowrate [kg/s]	17.60	4.65	0.09	0.31	0.79
HRSG	ST gross power [MW]	39.01	182.36	0.11	0.09	0.1
Gas turbine	Net power output [MW]	97.46	254.42	0.11	0.09	0.1
Steam turbine	ST gross power [MW]	60.50	182.36	0.11	0.09	0.1
Condenser	ST gross power [MW]	44.62	182.36	0.26	0.29	0.24
Gasifier	Feedstock thermal input [MW]	178.20	828.02	0.2	0.21	0.41
Gas clean-up	Syngas flowrate [kg/s]	63.83	75.26	0.15	0.34	0.27
WGSR	Syngas flowrate [kg/s]	23.23	89.21	0.15	0.34	0.27
Hot gas clean-up	Syngas flowrate [kg/s]	50.73	89.21	1712.5	1712.5	1712.5

Table 4.5: Operating and maintenance costs for all three systems [82, 83]

Fixed O&M Costs		
Operating labour	Included in maintenance	
Maintenance and administrative cost	56	$/kW year
Cost of ash disposal	9.73	$/GJ LHV
Variable O&M Costs		
Process water costs	6	$/t
Cooling water make up costs	0.325	$/t
CO_2 Costs		
Transport and storage	10	$/t
Chemicals		
WGSR Catalyst	45,000	$/month

Chapter 5. Results and Discussion

Three renewable energy-based waste to energy multigeneration system working with different waste types are designed for Turkey and Italy. In addition to examining the systems in detail with energetic and exergetic approaches, the system parameters affecting the system and their diverse effects on the systems are also investigated. The first multigeneration system, animal manure, feeds gasifier as waste in dried form. The gasifier's steam is produced by a solar power tower supported by a molten salt storage system. EES and the Aspen Plus simulation program is used together to conduct the thermodynamics analysis, state points and the energy and exergy efficiencies accordingly.

In this section, the effects of the operational condition changes on the system efficiencies and the amount of hydrogen and ethanol produced by the system are examined. Furthermore, the graphs illustrate how hydrogen and ethanol production ratios compare to other products. In addition, the hydrogen amounts produced in the system depending on the gasifier temperature and steam feed rate changes are compared with the experimental data, and the results are validated.

5.1 System 1 Thermodynamic Analysis Results

In Table 5.2, the state point properties for the first integrated multigeneration system are illustrated. While creating the table, the chemical exergy values are not written to the state point table. While the calculations are being made, the chemical exergy for the section where the chemically reacting substances reacted is included. When calculating specific exergy and exergy destruction, physical exergy is considered for each component since physical exergy is created by temperature and pressure deviations from ambient conditions. Additionally, chemical exergy is calculated because the chemical compositions of animal manure are altered during partially combustion and gasification in the gasifier. Chemical energy is the energy contained in the bonds of chemical molecules [84]. Likewise, chemical exergy is considered when hydrogen is combusted in the combustion chamber by reaction with air. Chemical exergy is also included in the calculations for sections such as gasification, combustion chamber and water gas shift reactor where chemical reactions occur because the energy changes that occur during the breaking of chemical bonds as a result of the reactions taking place in these sections should also be evaluated. Exergy

destruction rates increase in units where chemical reactions take place. According to Figure 5.1, exergy destruction occurred mostly in gasifier and combustion chambers. The main reason for this is that they have high temperatures, so irreversibility increases in the combustion chamber and gasifier, resulting in more significant physical exergy destruction. In addition, the amount of exergy destruction is high due to physical exergy changes as well as exergy destruction.

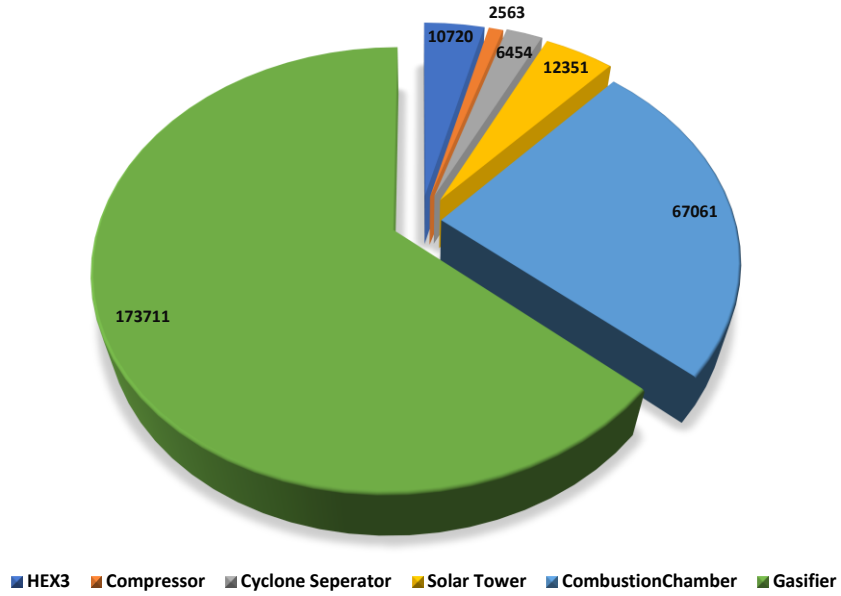

Figure 5.1 Exergy destruction rates of main system components of system 1

Since exergy destruction is the result of irreversibility, we should minimize losses to reduce exergy destruction. For this, we can replace the equipment used in the system with equipment with higher efficiency. The efficiency of solar thermal towers, especially in systems using solar energy, as well as gasifier and combustion chamber energy conversation efficiencies, is directly reflected in the exergy efficiency of the system and, therefore, in exergy destruction.

Exergy refers to the second law of thermodynamics. It is associated with the quality of energy itself. Therefore, an increase in exergy destruction indicates a loss of energy quality. The energy at high temperatures is of higher quality than at low temperatures. Therefore, the places where exergy destruction should be expected the most will be places with high temperatures. For these reasons, we should design the system to minimize losses by isolating the components with the highest temperature, especially when using high-quality energy in our systems. Moreover, the more irreversibilities the gas cycle affects, the higher

the pressure ratio is compared to its design ratio. By maintaining low pressures within a certain range, we can minimize the exergy destruction rate. Furthermore, exergy destruction reduction can be achieved by preheating the reactants and reducing the amount of excess or waste heat in the system and subsystems.

The first multigeneration system consists of three main subsystems: the primary Rankine cycle, the Brayton Rankine combined cycle, and the Rankine absorption refrigeration cycle. Their energy efficiency is 16.6%, 56.75%, and 58.2%, respectively, while their exergy efficiencies are 11.2%, 28.9, and 38.3%, respectively. On the other hand, the first multigeneration system's overall energy and exergy efficiencies are 61.1% and 56.4%, respectively. These results show us that the use of integrated systems with multiple useful outputs, rather than systems with only one useful output with single subsystems, improves energy and exergy efficiency and reduces the amount of waste energy. All this supports sustainability and can create an alternative for these high-energy systems to systems with relatively high energy conversion rates, such as fossil fuels. In Figure 5.2, the energy and exergy efficiency of subsystems in multigeneration system 1. The overall energy and exergy efficiencies for multigeneration system 1 are 61.1% and 56.6%, respectively, while the efficiencies of the individual subsystems are lower. Results show the advantage of multigeneration systems, in which subsystems are used together in terms of efficiency.

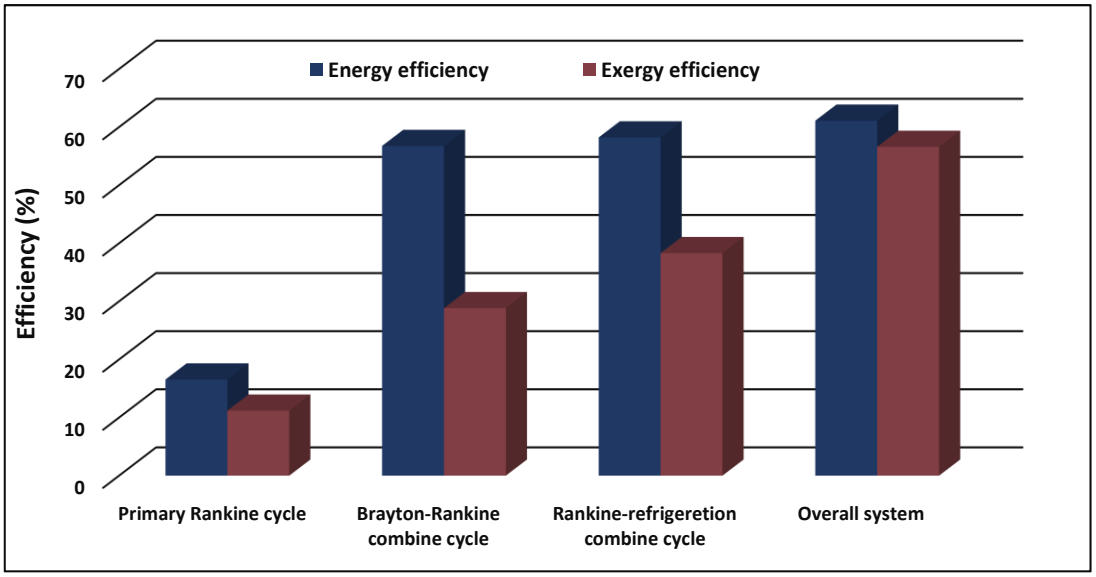

Figure 5.2 Energy and exergy efficiencies of sub-systems in system 1

The thermal energy supplied to the system by the solar power tower is calculated using the balance equations of the heat exchanger 1. The steam feed rate of the gasifier is selected as 2.5 kg per second, while the oxygen feed rate is accepted as 0.7 kg/s. The energy transmitted from the solar tower to the system is 8350.3731 kW to supply this steam at 240 °C. Table 5.1 summarizes the proposed system's primary heat and power inputs and outputs. According to the calculations, the total net power generation of the system is 21179.63 kW.

Table 5.1: Power and heat outputs and inputs of major system components

Parameter	**Unit (kW)**
$\dot{W}_{P_1}$	3.03
$\dot{W}_{P_2}$	3.75
$\dot{W}_{P_3}$	15.00
$\dot{W}_{P_4}$	5.67
$\dot{W}_{P_5}$	46.46
$\dot{W}_{P_6}$	3.63
$\dot{Q}_{Solar}$	8,350.37
$\dot{Q}_{Gasifier}$	219,571.67
$\dot{Q}_{Boiler}$	7,025.60
$\dot{W}_{C}$	12,243.93
$\dot{W}_{T_1}$	2179.62
$\dot{W}_{T_2}$	20,546.50
$\dot{W}_{T_3}$	6,344.00
$\dot{W}_{T_4}$	1,416.87
$\dot{W}_{T_5}$	3,814.74
$\dot{Q}_{CON_1}$	33,126.00
$\dot{Q}_{CON_2}$	4,134.12
$\dot{Q}_{EV}$	3,999.34
$\dot{Q}_{AB}$	5,874.77
$\dot{m}_{H_2} LHV_{H_2}$	40,959.00
$\dot{m}_{C_2H_5OH} LHV_{C_2H_5OH}$	31,933.20
$\dot{m}_{H_2S} LHV_{H_2S}$	362.32

Figure 5.3 illustrates the changes in overall energy and exergy efficiencies depending on the reference temperature for the multigeneration system 1. According to the calculations made, a slight decrease is observed in the exergy efficiency of the system depending on the increase in the accepted reference temperature. The exergy efficiency, about 58% at 1°C ambient temperature, decreased to 56.5% at 33°C reference temperature. No significant effect on the energy efficiency of the reference temperature is observed. This can be explained by the fact that the reference temperature does not have a decisive effect on the overall energy efficiency expression. The main reason is that the exergy efficiency formula includes the reference temperature. However, the energy efficiency formula does not contain the reference temperature.

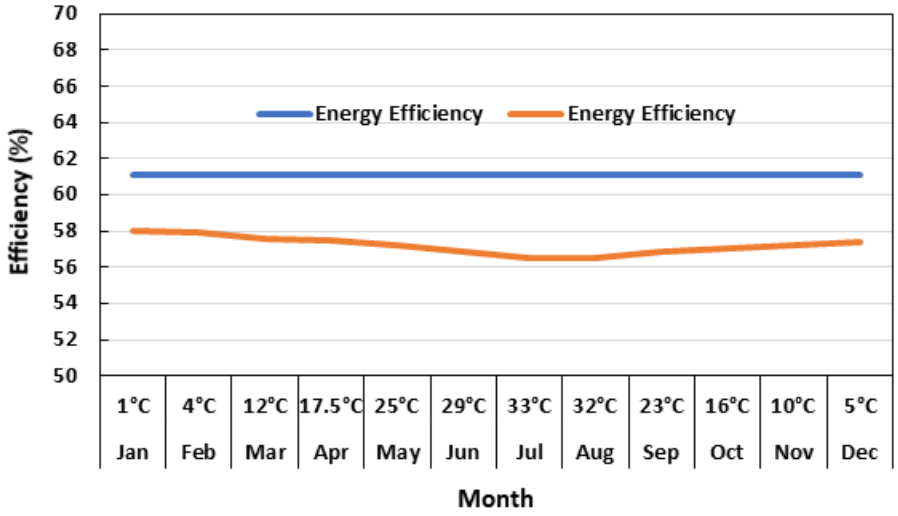

Figure 5.3 Overall energy and exergy efficiencies of system 1 depending on average reference temperature

5.2 System 1 Parametric Study Results

Pure oxygen is used as a gasification agent to increase efficiency in the gasifier. Various studies have been conducted on designing and analyzing systems. In order to evaluate system efficiencies, syngas compositions and system useful outputs, including hydrogen and ethanol, depending on system inputs, many parametric studies are performed, such as altering steam feed rate, gasification temperature and oxygen feed rate within the gasifier component—moreover, the effect of the manure feed rate on the overall system performances is examined.

In order to understand the outputs and efficiencies of systems in detail, syngas composition should be examined. Since syngas directly coming from the gasifier consists of hydrogen, methane, hydrogen sulfide, carbon monoxide, and carbon monoxide dioxide, it is crucial to understand its composition because it is impossible to calculate its content after cleaning operations. Thus, it can be understood whether the change of system outputs depends on syngas or other parameters in the next section. Although the analysis of syngas compositions depending on system parameters is only examined for system 1, the results are similar because the same methodology and carbon-based feedstocks are used in other systems.

One of the system's operating parameters is the variation in the composition of the syngas generated in the gasifier as a function of the gasifier's operating temperature and the total quantity of hydrogen and ethanol produced by the system. Volumetric analysis of the syngas at the gasifier outlet is performed by changing the gasifier operating temperature between 600 and 1300 °C for 0.7 kg/s oxygen feeding rate and 2.5 kg/s steam feed rate as well as 1600 kPa gasifier pressure, and it is shown in Figure 5.4.

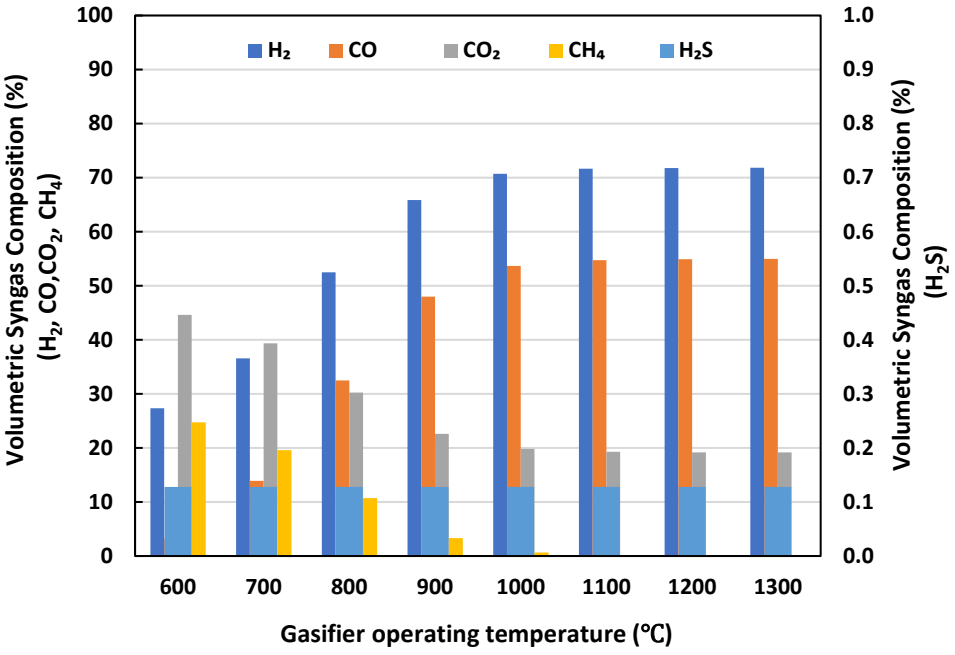

Figure 5.4 Variation in syngas composition as a function of gasifier operating temperature in system 1

The syngas composition leaving the gasifier at 600 °C gasification temperature consists of 27% hydrogen, 3% carbon monoxide, 45% carbon dioxide and 25% methane. The place of

hydrogen sulfide in the mixture is only 0.13%. At temperatures up to 1000 °C, the volume fraction of hydrogen and carbon monoxide in the mixture increases dramatically, while the amount of carbon dioxide and methane suddenly decrease.

These situations can be explained by considering the Boudouard reaction, which is one of the endothermic reactions involved in the gasification process with the increase of the gasification temperature. Carbon dioxide combines with the carbon element by taking heat and forms carbon monoxide with increasing gasification temperatures. Therefore, an increase occurs in the carbon monoxide composition in the syngas while the carbon dioxide ratio decreases exponentially.

Figure 5.5 shows the steam feed rate/dry manure mass values ranging from 0.1-1 for 10kg/s manure feeding rate, 1300 kPa pressure, 1300 °C temperature and 0.7 kg/s oxygen feed rate. As the amount of steam injected into the gasifier increases, more hydrogen and oxygen are released due to the splitting of more water molecules. The oxygen produced reacts with the carbon monoxide present in the gasifier to generate carbon dioxide. Therefore, with the increasing steam feed rate, the syngas' hydrogen and carbon dioxide ratio increases while the carbon monoxide ratio decreases.

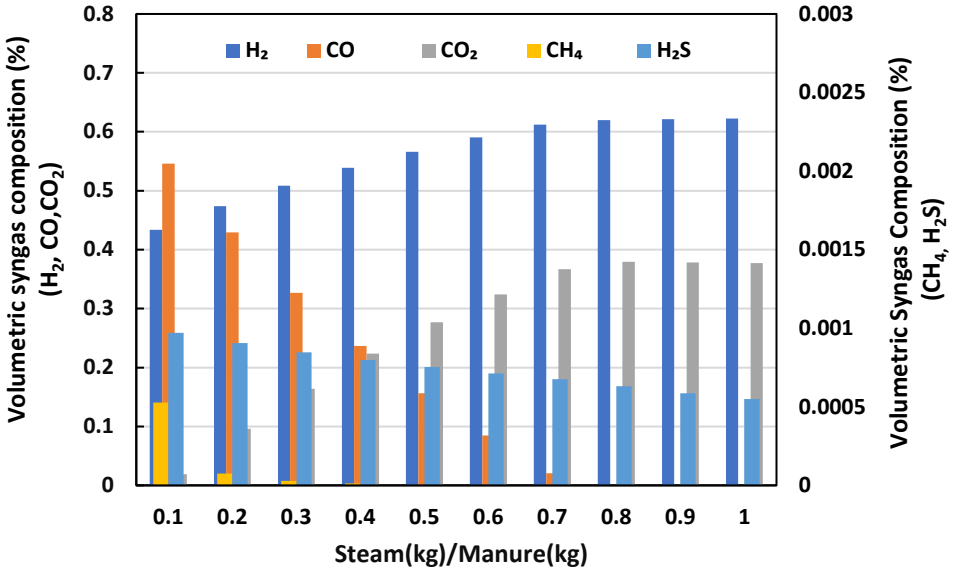

Figure 5.5 Variation in syngas composition as a function of gasifier steam feed ratio in system 1

Figure 5.6 illustrates the oxygen feed rate/dry manure mass values ranging from 0.1-1 for 10 kg/s manure feeding rate, 1300 kPa pressure, 1300 °C temperature and 2.5 kg/s steam

feed rate. Since the reaction reverts to complete combustion depending on the increased oxygen feed rate, the carbon monoxide molecules in the environment combust with oxygen and turn into carbon dioxide. As a result, the carbon monoxide ratio in the syngas composition decreases while the carbon dioxide ratio increases. Increasing oxygen feed rate does not affect the hydrogen composition in syngas.

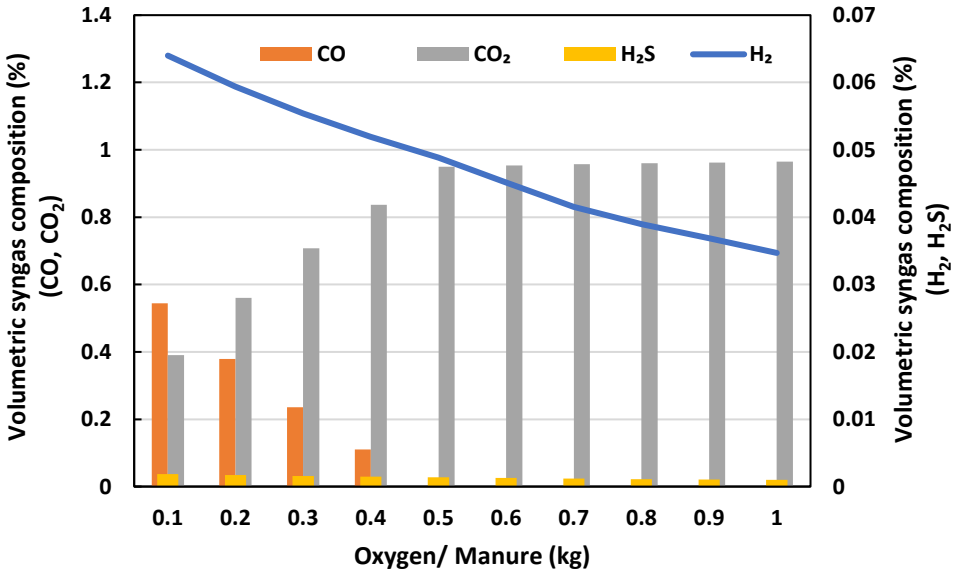

Figure 5.6 Variation in syngas composition as a function of gasifier oxygen feed ratio in system 1

As shown in Figure 5.7, rising gasification operating temperatures increase the amount of hydrogen and ethanol produced. The reason for the increase in hydrogen can be explained by the water-gas reaction in Table 3.1. Consequently, the steam is injected into the gasifier gradients in this endothermic process and reacts with the carbon, generating carbon monoxide and water. The increase in ethanol production is dependent on hydrogen. Since carbon hydrogenation is conducted with half of the hydrogen produced in the proposed first multigeneration system, the amount of ethanol also increases depending on the increased hydrogen production. Because half of the hydrogen is made into ethanol, the amount of hydrogen in the first system doesn't rise exponentially but instead grows at a slower pace.

The findings indicate that the operating temperature of gasification is directly related to the amount of hydrogen and carbon monoxide in syngas compounds. As a result, a richer syngas composition is formed, and energy and exergy efficiencies increase. In addition, the carbon dioxide ratio in syngas also decreased depending on the gasifier operating

temperature. Figure 5.7 shows the gasification operation temperature-dependent ethanol production ratio and comparison of ethanol production amount to other produced gases.

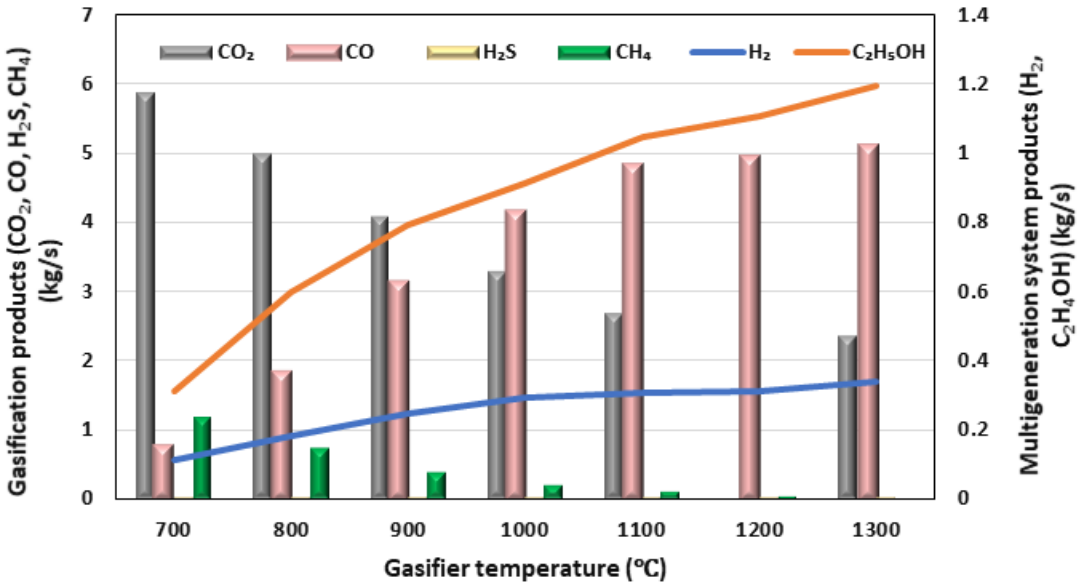

Figure 5.7 Effects of gasifier temperature on system products in system 1

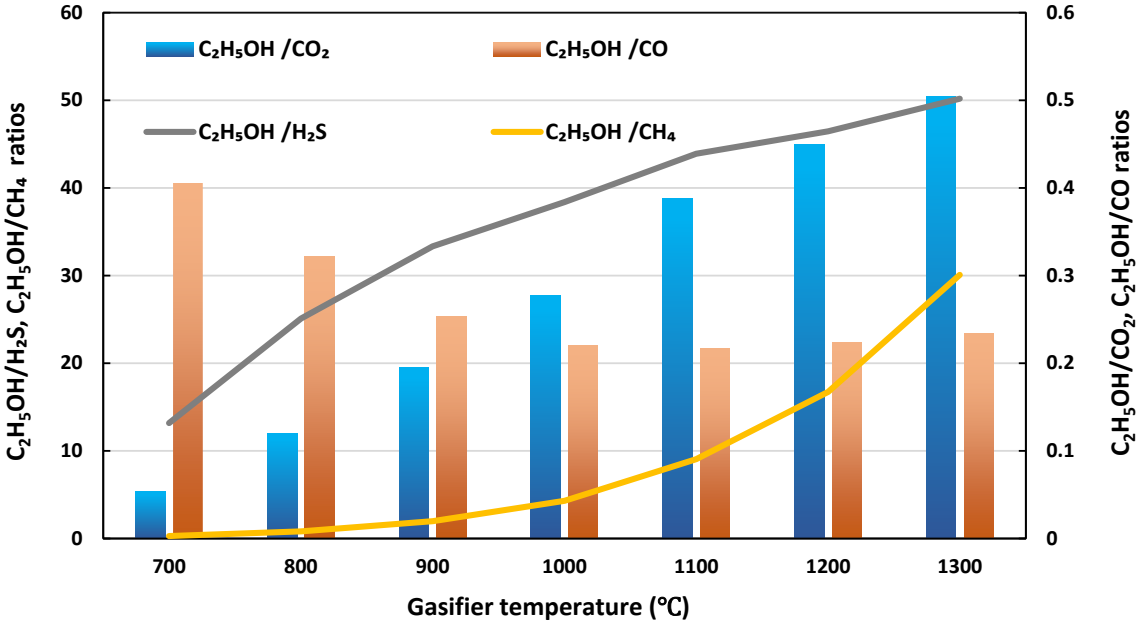

Figure 5.8 Effects of gasifier temperature on ethanol production ratio in system 1

In Figure 5.8, similar to the previous figure, the temperature-dependent increase in hydrogen production is compared to other produced gases. The changes in Figures 5.8 and 5.9 reveal that the carbon dioxide generation rate is much less than hydrogen and ethanol generation, depending on the temperature. This thereby enhances the H/C ratio of the

syngas by increasing the hydrogen ratio in the syngas much more than the carbon dioxide in the gasification temperature increases and reduces the green gas emissions that will be emitted to the environment in case the syngas is combusted.

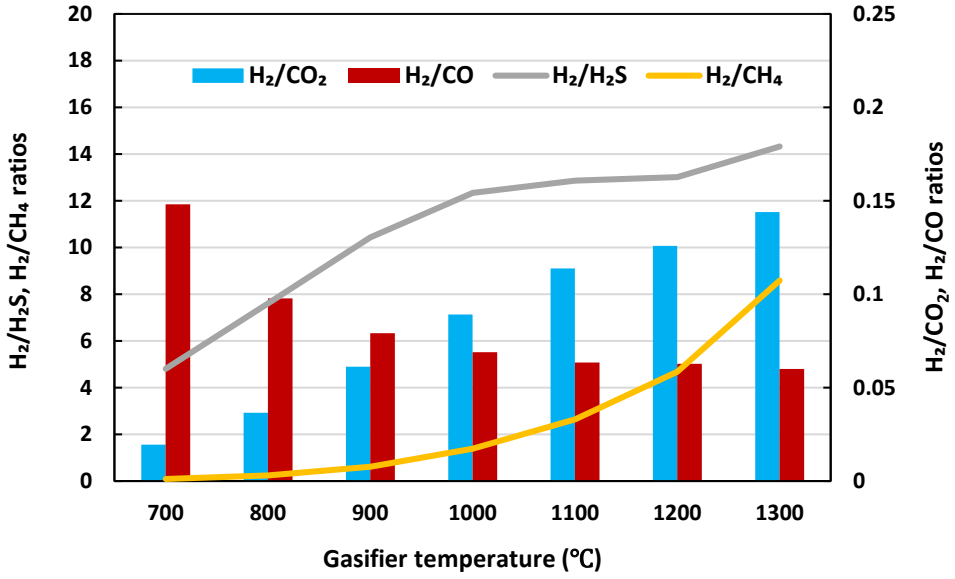

Figure 5.9 Effects of gasifier temperature on hydrogen production ratio in system 1

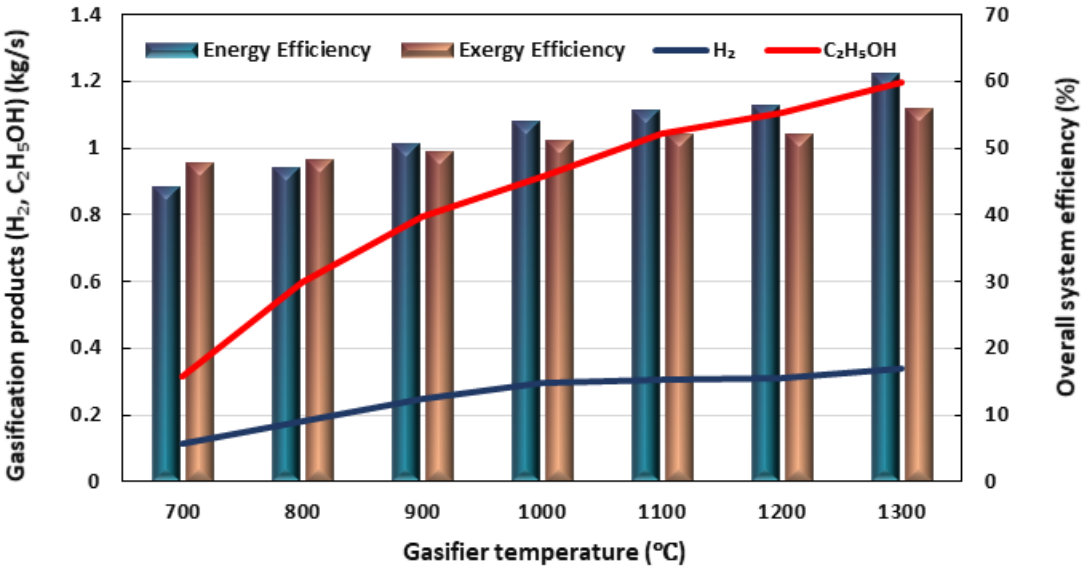

Figure 5.10 Effects of ethanol and hydrogen production rates, and gasifier temperature on system 1 efficiencies

Furthermore, as shown in Figure 5.10, the amounts of hydrogen and ethanol generated enhances as the gasifier temperature rises, benefiting system efficiency by increasing syngas temperature, which can be utilized in the turbine. Additionally, increased ethanol and hydrogen generation has a beneficial effect on efficiency. Therefore, increasing the

temperature of the gasifier has a substantial impact on system efficiency, ethanol, and hydrogen generation, as well as on carbon dioxide emissions reduction.

Figure 5.11 shows the effect of steam feed rate on the gasification and exergy efficiency of the system. As the steam feed rate increases, the efficiency improves as the hydrogen synthesis rate increases due to the water-gas reaction shown in table 3.1. However, as a result of this reaction, the oxygen released together with the hydrogen reacts with carbon monoxide and leads to the formation of carbon dioxide. As a result, the amount of carbon monoxide in the syngas decreases while carbon dioxide increases. Therefore, the amount of hydrogen produced in the water gas shift reaction decreases, but since more steam is injected into the gasifier, the reason for the hydrogen increase is not the reduction of carbon monoxide by reacting with water in the water gas shift reaction, but the rise in the number of water molecules decomposed in the gasifier. Despite the increase in the amount of carbon dioxide in the syngas composition, since these carbon dioxide molecules will be captured by the scrubber, clean syngas is deprived of carbon dioxide and monoxide. Although the amount of hydrogen increases with the steam feed rate, the amount of carbon dioxide is insufficient in the carbon hydrogenation reactor, so ethanol production declines in the first multigeneration system designed.

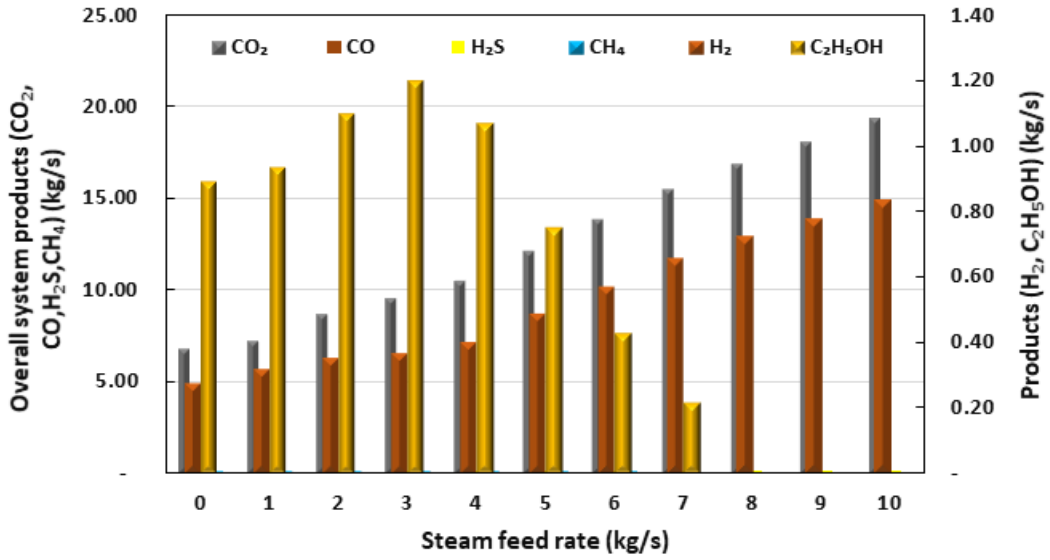

Figure 5.11 Effects of steam feed rate on outputs for system 1

Table 5.2: System 1 state point values

State No	Substance	T (°C)	P (kPa)	ṁ (kg/s)	h (kJ/kg)	s (kJ/kgK)	ex (kJ/kg)
1	Water	65.0	101.3	2.52	272.1	0.9	55.9
2	Water	65.0	1500.0	2.52	273.3	0.9	57.3
3	Water	550.0	1500.0	2.52	3583	7.7	1813.8
4	Water	280.0	101.3	2.52	3034	8.1	1136.7
5	Water	25.0	101.3	2.50	104.8	0.4	50.0
6	Water	25.0	1600.0	2.50	106.3	0.4	52.0
7	Water	240.0	1600.0	2.50	2894	6.6	1447.5
8	Oxygen	25.0	1600.0	0.70	4.08	0.7	337.2
9	Animal Manure	25.0	101.3	10.00	1547.15	1.1	1179.4
10	Raw Syngas 1	1300.0	1600.0	13.20	2315.44	4.4	1622.3
12	Raw Syngas 2	1300.0	1600.0	12.79	2734.32	4.4	1787.5
13	Hydrogen Sulfide	1300.0	1600.0	0.02	1045.84	2.6	767.3
14	Syngas	1300.0	1600.0	8.35	5328.84	6.4	4319.0
14a	Syngas	1300.0	1600.0	4.17	5328.84	5.6	4319.0
14b	Syngas	1300.0	1600.0	4.18	5328.84	5.7	4319.0
15	Syngas	450.0	1600.0	4.17	2535.8	0.9	1409.4
16	Water	25.0	101.3	2.42	104.9	0.4	0.2
17	Water	25.0	1600.0	2.42	106.4	0.4	2.1
18	Water	196.7	1600.0	2.42	842.2	2.4	257.3
19	Carbon dioxide	450.0	1600.0	5.91	913.02	0.4	803.2
20	Hydrogen	450.0	1600.0	0.68	6182.15	1.9	3668.0
20a	Hydrogen	450.0	1600.0	0.34	6182.15	1.9	3668.0
20b	Hydrogen	450.0	1600.0	0.34	6182.15	1.9	3668.0
21	Carbon dioxide + Hydrogen	450.0	1600.0	6.25	6990	0.9	7729.1
22	Carbon dioxide + Hydrogen	200.0	167.8	6.25	7600	1.2	7038.9
23	Ethanol	200.0	101.3	1.20	4800.03	1.0	2658.9
24	Air	25.0	101.3	50.00	0.06	0.0	43.6
25	Air	266.7	450.0	50.00	244.82	0.2	237.2
26	Air	1764.7	450.0	50.00	1994.65	1.7	1534.1
27	Exhaust Gases	1433.2	180.0	50.00	1583.72	1.7	1517.7
28	Exhaust Gases	770.5	180.0	50.00	794.63	1.2	902.6
29	Water	25.0	101.3	10.00	104.9	0.4	0.2
30	Water	25.0	1500.0	10.00	106.4	0.4	2.1
31	Water	680.0	1500.0	10.00	3875	8.0	2055.1
32	Water	381.4	180.0	10.00	3238	8.2	1367.4
33	Water	109.0	180.0	3.15	457.2	1.4	98.6
34	Water	109.1	1650.0	3.15	458.3	1.4	100.7

35	Water	402.6	1650.0	3.15	3260.85	7.2	1681.2
36	Water	166.9	180.0	3.15	2805	7.4	1174.9
37	Ammonia+Water	111.0	1547.0	27.49	308.5	1.5	18.7
38	Ammonia+Water	108.3	1547.0	4.11	1550	4.9	93.1
39	Ammonia+Water	108.3	1547.0	0.37	266.1	1.4	16.5
40	Ammonia+Water	43.9	1547.0	3.74	1294	4.2	72.0
41	Ammonia+Water	39.8	1547.0	3.74	189.8	0.7	14.1
42	Ammonia+Water	-15.3	234.8	3.74	189.8	0.8	14.1
43	Ammonia+Water	-11.0	234.8	3.74	1258	4.9	71.7
44	Ammonia+Water	39.8	234.8	27.49	0.32	0.5	0.0
45	Ammonia+Water	39.9	1547.0	27.49	2.17	0.5	0.1
46	Ammonia+Water	131.4	1547.0	23.75	404.2	1.7	25.2
47	Ammonia+Water	39.9	1547.0	23.75	41.04	0.5	2.4
48	Ammonia+Water	40.2	234.8	23.75	41.04	0.5	2.4

Figure 5.12 illustrates the effect of steam feed rate on the energetic and exergy efficiency of the overall system. As the steam feed rate increases, the efficiency improves as the hydrogen synthesis rate increases due to the water-gas reaction shown in Table 3.1. Even though the amount of hydrogen increases with the steam feed rate, carbon dioxide is insufficient in the carbon hydrogenation reactor, so ethanol production declines in the first multigeneration system. Although there is a slight decrease in the increase in the energy and exergy efficiency of the system due to the reduced ethanol production, more hydrogen to be produced due to more steam supplied to the system increases the system's efficiency.

Figure 5.13 illustrates the effects of oxygen feed rate on carbon monoxide, hydrogen, ethanol, hydrogen sulfide and methane production in Multigeneration system 1. In gasification, unlike pyrolysis, there is oxygen injection. However, the use of oxygen is limited, and complete combustion should not be achieved. At low rates, oxygen emits heat to the environment by entering into exothermic reactions in the R1 and R2 equations. In addition, the partial combustion reaction in the R2 equation increases the amount of carbon monoxide composition in the syngas. Since oxygen at low rates increases both carbon dioxide and carbon monoxide, the production of hydrogen and ethanol increases. However, if the oxygen addition continues and the reaction evolves into complete combustion, the amount of hydrogen obtained in the water gas shift reactor decreases as carbon monoxide in the syngas falls. Still, this decrease is not very sharp because the gasification temperatures increase. After all, the oxygen addition will increase the exothermic reactions.

Therefore, the amount of hydrogen produced in gasification increases. However, since the increased carbon dioxide will be separated from the syngas by the scrubbing process, ethanol production in multigeneration system 1 decreases.

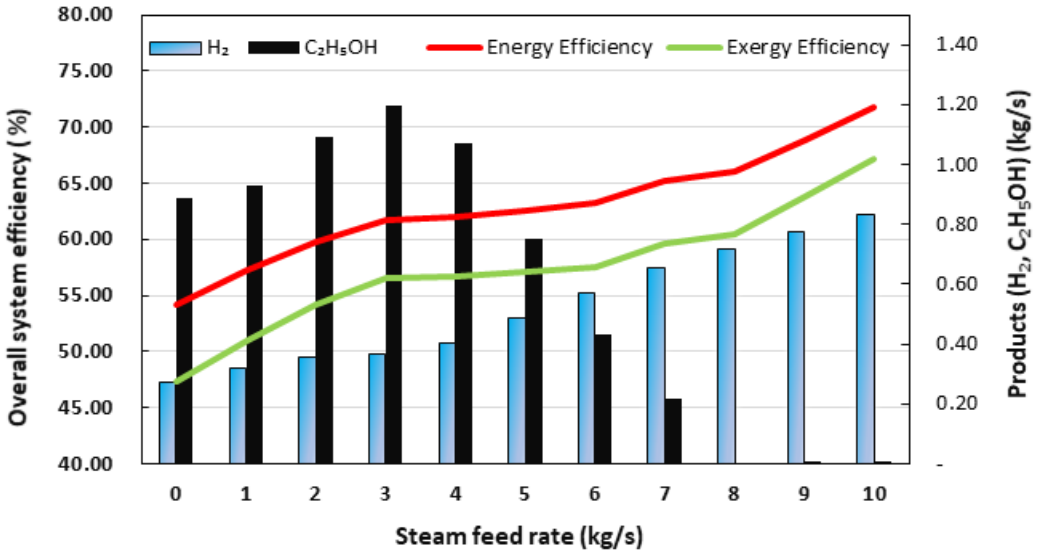

Figure 5.12 Effects of hydrogen and ethanol production rate and steam feed rate on overall system efficiencies for the multigeneration system 1

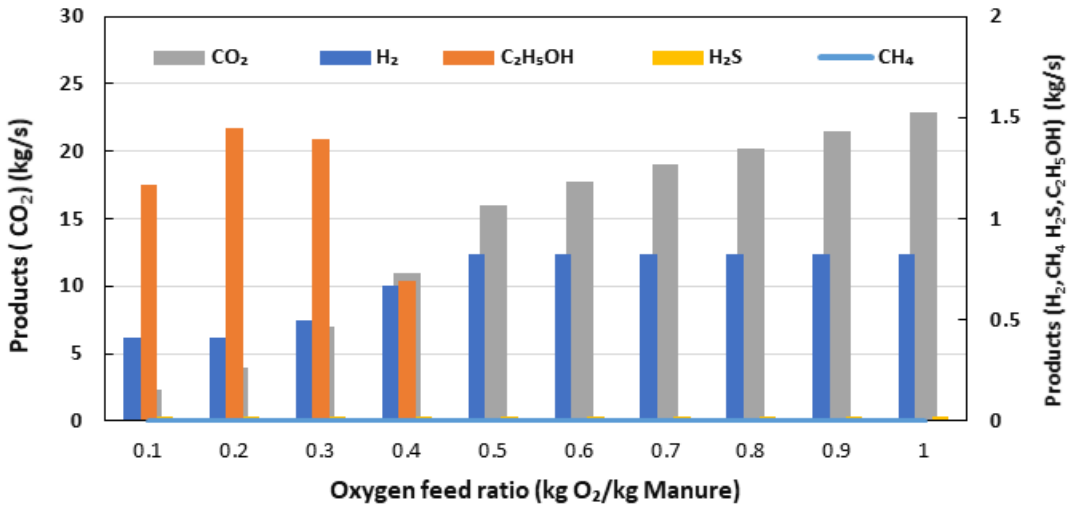

Figure 5.13 Effects of oxygen feed ratio on outputs for multigeneration system 1

The effects of oxygen feed rate on hydrogen and ethanol production rate as well as on overall system efficiencies are illustrated in Figure 5.14. Since partial combustion occurs at low oxygen feed rates, sufficient carbon monoxide production increases and this carbon monoxide is converted into hydrogen and oxygen with the water gas shift reaction. At this point, ethanol production for multigeneration system 1 is maximum. However, with increasing oxygen feed rates, partial combustion returns to complete combustion and

carbon monoxide production is reduced. Since carbon dioxide cannot be produced in the water gas shift reaction, ethanol production decreases for the designed system. With the decrease in ethanol production, the hydrogen used for ethanol production is not converted to ethanol and the number of hydrogen increases.

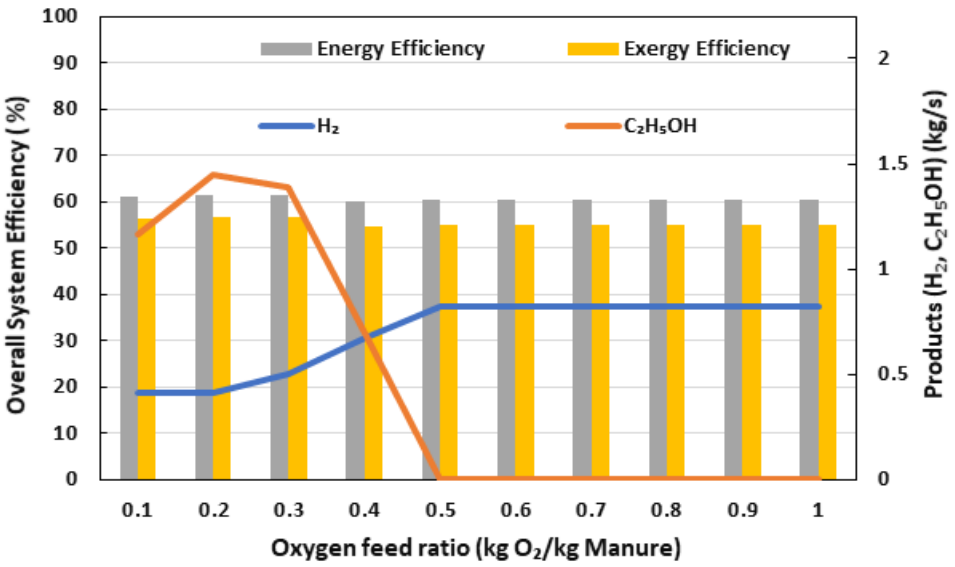

Figure 5.14 Effects of hydrogen and ethanol production rates and oxygen feed rates on overall system efficiencies for the multigeneration system 1

According to the chemical balance equations, the increase in the manure feed rate, which is the fuel used in the system, increases the hydrogen and ethanol productions at the same rate. Figure 5.15 shows the effect of the manure feed rate provided to the system on the energy and exergy efficiencies of the system. In the study, calculations are made by increasing other gasification agents such as steam and oxygen in the same proportion with the increased manure feed rate. Other useful output amounts such as ethanol, hydrogen and electricity produced due to the increase in manure are raised at the same ratio. Since the consumption of energy-consuming units such as compressors and pumps does not increase at this rate of increase, the efficiency also improves.

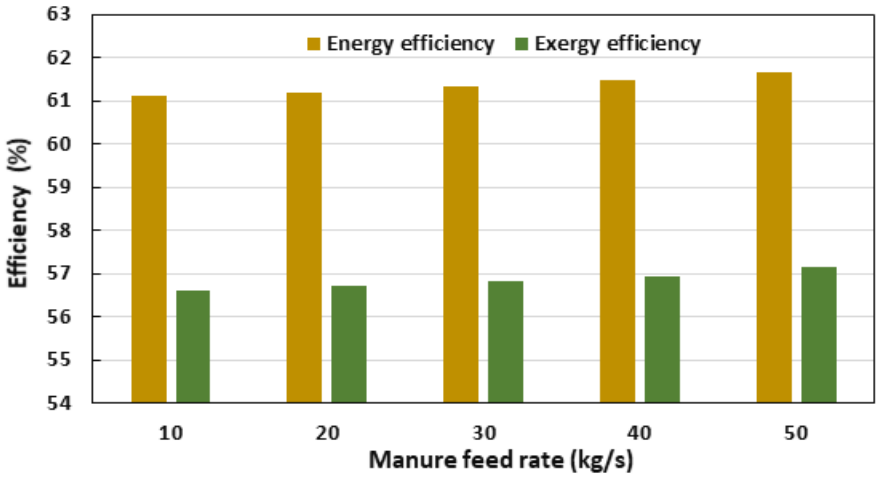

Figure 5.15 Overall energy and exergy efficiencies of system 1 depending on manure feed rate

Table 5.3: System 2 state point values

State No	Substance	T (°C)	P (kPa)	ṁ (kg/s)	h (kJ/kg)	s (kJ/kgK)	ex (kJ/kg)
1	Water	25.0	101.3	32.62	104.9	0.4	0.2
2	Water	25.0	1700.0	32.62	106.4	0.4	2.1
3	Water	203.1	1700.0	32.62	886.3	2.4	2756.1
4	Water	203.1	1700.0	20.00	886.3	2.4	2756.1
5	Water	203.1	1700.0	12.62	886.3	2.4	2756.1
6	Oxygen	25.0	101.3	0.65	0.0	0.0	0.0
7	Oxygen	437.1	1600.0	0.65	401.2	0.1	365.7
8	Tires	25.0	101.3	10.00	1725.2	1.1	263.1
9	Syngas	1250.0	1600.0	30.65	2585.3	3.1	2410.8
11	Ash	1250.0	1600.0	1.33	577.4	0.1	432.1
12	Syngas	1250.0	1600.0	29.32	2365.5	3.1	2393.4
13	Syngas	1250.0	1600.0	4.62	10245.3	10.5	9542.4
13a	Carbon Dioxide	1250.0	1600.0	24.70	972.4	1.1	9542.4
14	Hydrogen Sulfide	1250.0	1600.0	0.16	969.7	2.6	1179.5
15	Syngas	1250.0	1600.0	4.46	11240.3	10.6	9897.7
16	Syngas	684.0	1600.0	4.46	5237.8	5.4	5442.7
17	Syngas	450.0	1600.0	4.46	2876.8	2.5	3924.6
18	Hydrogen+ Carbon Dioxide	450.0	1600.0	17.08	3652.2	0.2	1712.5
19	Hydrogen+ Carbon Dioxide	113.7	101.3	17.08	2139.8	0.1	210.8
20	Carbon Dioxide	113.7	101.3	14.03	77.5	0.2	417.0
21	Ethanol	25.0	101.3	0.13	258.7	1.2	19.2
22	Hydrogen	113.7	101.3	3.05	5210.0	57.1	159.4

23	Hydrogen	-252.6	101.3	3.05	450.9	22.4	367.1
24	Water	382.0	6200.0	14.70	3127.2	6.5	1493.6
25	Water	169.5	6200.0	14.70	719.9	2.0	139.7
26	Water	60.0	120.0	5.83	251.3	0.8	9.2
27	Water	60.0	1320.0	5.83	252.3	0.8	10.8
28	Water	1019.5	1320.0	5.83	4688.0	8.8	2106.0
29	Water	579.0	120.0	5.83	3659.0	9.0	1037.0
30	Water	262.5	5000.0	9.12	1150.0	2.9	774.3
31	Water	55.9	2300.0	9.12	236.4	0.8	238.1
32	Water	531.9	2300.0	9.12	3536.0	7.5	1361.0
33	Water	148.1	90.0	9.12	2773.0	7.7	978.6
34	Water	59.0	90.0	9.12	247.1	0.8	8.7
35	Water	59.1	2650.0	9.12	249.2	0.8	12.1
36	Water	59.2	5000.0	9.12	251.2	0.8	15.3
37	Ammonia+ Water	111.0	1547.0	91.11	308.5	1.5	18.7
38	Ammonia+ Water	108.3	1547.0	13.62	1550.0	4.9	93.1
39	Ammonia+ Water	108.3	1547.0	1.21	266.1	1.4	16.5
40	Ammonia+ Water	43.9	1547.0	12.41	1294.0	4.2	72.0
41	Ammonia+ Water	39.8	1547.0	12.41	189.8	0.7	14.1
42	Ammonia+ Water	-15.3	234.8	12.41	189.8	0.8	14.1
43	Ammonia+ Water	-11.0	234.8	12.41	1258.0	4.9	71.7
44	Ammonia+ Water	39.8	234.8	91.11	0.3	0.5	0.0
45	Ammonia+ Water	39.9	1547.0	91.11	2.2	0.5	0.1
46	Ammonia+ Water	131.4	1547.0	78.70	404.2	1.7	25.2
47	Ammonia+ Water	39.9	1547.0	78.70	41.0	0.5	2.4
48	Ammonia+ Water	40.2	234.8	78.70	41.0	0.5	2.4

5.3 System 1 Validation

To validate the created simulation model, the syngas compositions as a function of gasifier temperature derived from the Aspen Plus simulations are compared to the experimental findings of Liu et al. [85]. A two-stage fluidized bed supplied with rice straw and oxygen-enriched air are used in their study at temperatures ranging from 600 to 800 °C. Even though the feedstock utilized in this experiment is slightly different, its organic nature makes it a useful reference for comparing the influence of gasification temperature on the generated gas components. Similar to the experimental data, the Aspen Plus results indicate that the quantity of hydrogen and carbon monoxide generated increases as the gasification temperature increases; on the other hand, the amount of carbon dioxide and methane produced decreases.

According to Le Chatelier's principle, higher temperatures favour the reactants in exothermic reactions and the products in endothermic reactions. Consequently, increased temperature tended to hydrocarbon endothermic reforming (equations R4 and R9), resulting in a substantial increase in H_2 concentration and a significant decrease in CH_4 and C_2 hydrocarbon concentrations. Carbon monoxide was primarily used to generate carbon dioxide via water gas shift reaction (equation R8), and greater temperatures enhanced the rate of carbon dioxide creation. In Figure 5.16, the experimental findings of Liu et al. [85] and parametrical analysis in the Aspen Plus are compared the syngas composition depending on gasifier temperature to validate the constructed simulation model.

Consequently, the hydrogen-to-carbon dioxide ratio increases as the temperature rises, whereas carbon monoxide drops. However, since part of the hydrogen created is combustible in the combustion chamber, the enhanced hydrogen generation rate is lower than carbon monoxide in this research. Although hydrogen production rises as the gasification temperature increases, the rate of production decreases as hydrogen is combusted. Since ethanol is created by carbon dioxide hydrogenation (equation 80) in the last stage of the planned system, an increase in hydrogen and carbon dioxide has a beneficial effect on ethanol production. In other words, since the increase in gasification temperature resulted in an increase in hydrogen generation, it also resulted in an increase in ethanol production implicitly.

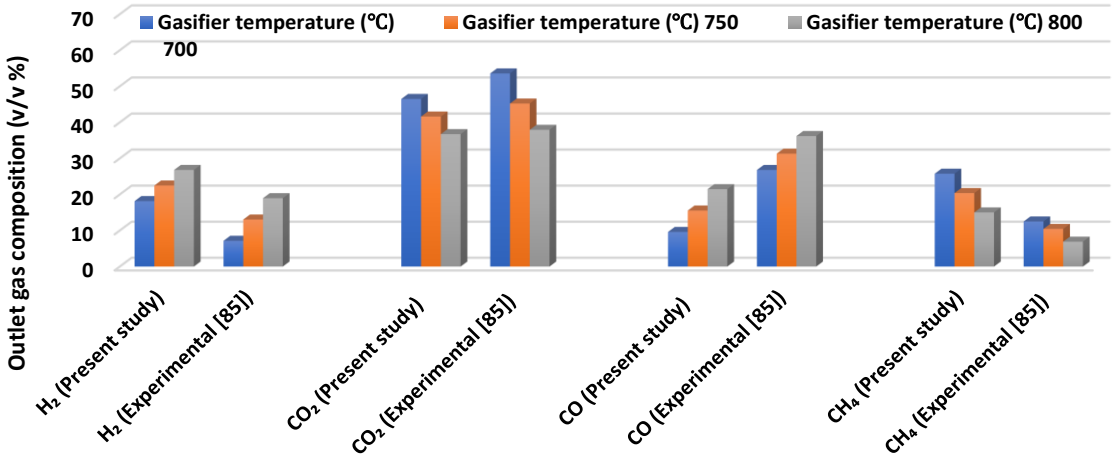

Figure 5.16 Comparison of H_2, CO_2, CO, CH_4 concentrations of syngas between the present study and the experimental for system 1

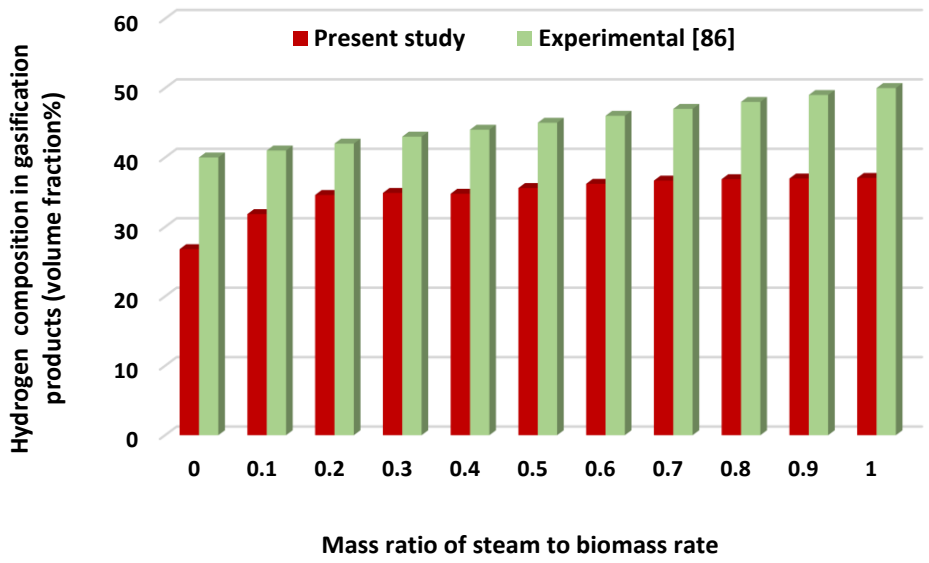

Figure 5.17 Comparison of steam to biomass ratio effects on hydrogen production rate between the present study and the experimental for system 1

The steam to biomass conversion rate is a critical measure for determining the hydrogen content of gasification outputs. In Figure 5.17, the experimental results of Li et al. [86] and the parametrical analysis in the Aspen Plus are compared in relation to steam to biomass ratio changes in order to verify the simulation model developed. In the experimental investigation, a combined fixed bed reactor is supplied with steam from municipal solid waste at different steam to biomass ratios ranging from 0 to 2.66. Due to the fact that the gasifier temperature is set at 800 °C in this experimental investigation, the precise temperature values determined using the Aspen Plus model are utilized in Figure 5.11.

The findings reveal that the steam input ratio favourably influences hydrogen generation in both tests. There is a mismatch of less than 20% between the experimental investigation and the proposed model. This disparity is attributable to numerous variables, including the waste composition employed, the gasifier model utilized in the experiment, the margin of error in the inquiry and the simulation model.

5.4 System 2 Thermodynamic Analysis Results

Figure 5.18 illustrates the main system components's destruction of exergy rates in multigeneration system 2. The highest exergy destruction occurs in the gasifier with 137238 kW. The main reason for this is that they have high temperatures, so irreversibility increases in the gasifier, resulting in more significant physical destruction of exergy. In

addition, the amount of exergy destruction is high due to physical exergy changes as well as exergy destruction.

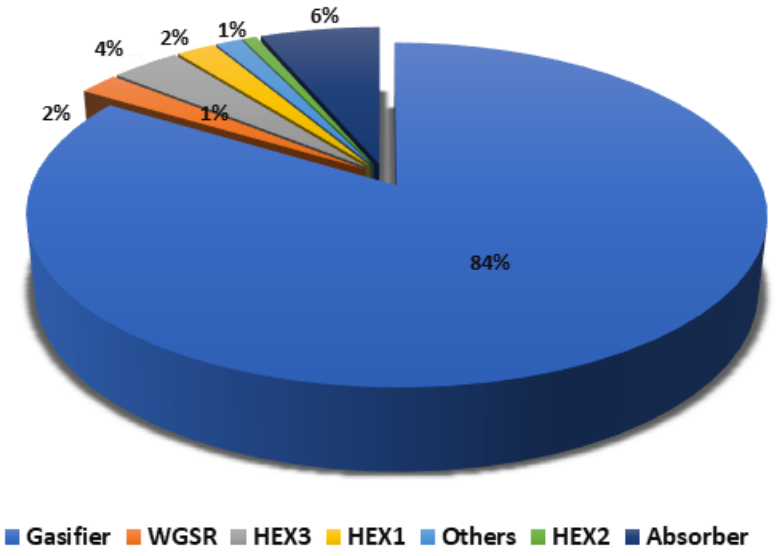

Figure 5.18 Exergy destruction ratios of main system components of system 2

The second multigeneration system, designed to use waste tire as fuel, is fed with a 20 kg/s steam feed rate and 12.2 kg/s waste tire at 203 °C. The gasification operation temperature is determined as 1250 °C. According to the calculations, the energetic and exergetic efficiencies of the system were calculated as 71.45% and 69.87%, respectively. The energy and exergy efficiencies for the previous system, multigeneration system 1, are 61.1% and 56.4%, respectively. The main reason for this improvement in energy and exergy efficiency is the combusting of syngas produced in the first multigeneration system. Combustion of syngas in the combustion chamber reduces the amount of hydrogen and ethanol produced, and energy losses are higher due to the use of an open Brayton cycle with the combustion chamber.

In Figure 5.19, the energy and exergy efficiency of subsystems in multigeneration system 2. The overall energy and exergy efficiencies for multigeneration system 2 are 71.45% and 69.87%, respectively, while the efficiencies of the individual subsystems are lower. Results show the advantage of multigeneration systems, in which subsystems are used together in terms of efficiency.

The thermal energy supplied to the system by the geothermal well is calculated using the balance equations of the heat exchanger 1. The steam feed rate of the gasifier is selected

as 12.62 kg per second, while the oxygen feed rate is accepted as 0.65 kg/s. The energy transmitted from the solar tower to the system is 28920.3731 kW to supply this steam at 203.1 °C. According to the calculations, the total net power generation of the system is 18752.6 kW.

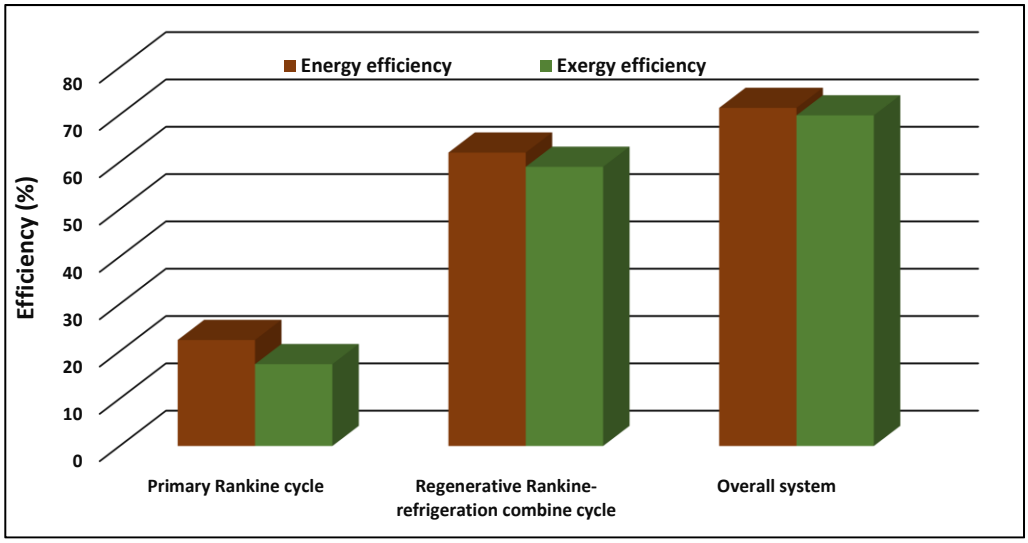

Figure 5.19 Energy and exergy efficiencies of sub-systems in system 2

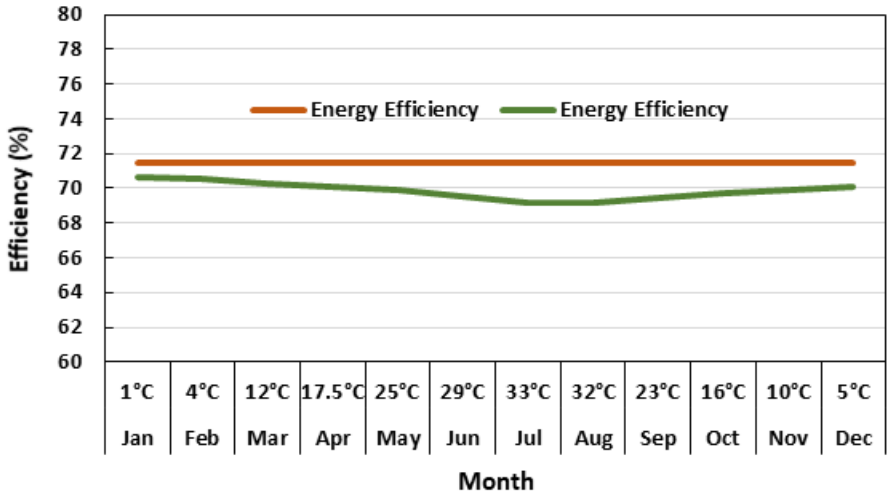

Figure 5.20 Overall energy and exergy efficiencies system 2 depending on average reference temperature

Figure 5.20 illustrates the changes in overall energetic and exergetic efficiencies depending on the reference temperature for multigeneration system 2. According to the calculations made, a slight decrease is observed in the exergy efficiency of the system depending on the rise in the accepted reference temperature. The exergy efficiency, about 70.67% at 1°C ambient temperature, decreased to 59.17% at 33°C reference temperature. No significant

effect on the energy efficiency of the reference temperature is observed. This is because the reference temperature has a negligible impact on the overall energetic efficiency expression.

5.5 System 2 Parametric Study Results

To improve the gasifier's efficiency, pure oxygen is utilized as a gasification agent. Numerous studies on the design and analysis of systems have been carried out. Many parametric studies are conducted to determine system efficiencies and useful outputs including hydrogen and ethanol, as a function of system inputs such as varying the steam feed rate, gasification temperature, and oxygen feed rate within the gasifier component. In addition, the effect of the waste tire feed rate on the overall system performance is examined. Since all multigeneration systems use the same method and utilize carbon-based feedstocks, the analysis of syngas compositions based on system operating conditions such as steam feed rate, gasification operating temperature, and oxygen feed rate is only done for system 1. This is because the method is the same for all systems, and the results are similar for syngas composition.

As shown in Figure 5.21, increasing gasification operating temperatures increase the hydrogen and ethanol produced. The water-gas reaction in Table 3.1 can explain the increase in hydrogen. As a result of this endothermic process, the steam injected into the gasifier decomposes and combines with carbon, producing carbon monoxide and water as a result. The increase in ethanol production is dependent on hydrogen.

Unlike the first proposed multigeneration system, ethanol is produced in the second multigeneration system by direct hydrogenation of carbon dioxide in an electrochemical synthesis reactor. However, ethanol production increases depending on the increase in gasification temperature. This is because rising gasifier temperatures increase the amount of carbon dioxide produced. In addition, since no hydrogen is consumed for ethanol production, hydrogen production is 3 kg/s, and it is much higher than the production capacity of multigeneration system 1.

As seen in Figure 5.22, the increase in gasification temperature increases ethanol and hydrogen production. As the temperature increases, the amount of carbon dioxide produced by the multigeneration system increases. The point to be noted here is that the temperature

increase increases the carbon dioxide production of the system; otherwise, the increase in the gasification operation temperature reduces the amount of carbon dioxide in the syngas. However, the amount of carbon monoxide increases directly to the temperature. Later, this carbon dioxide produced reacts with water in the water gas shift reaction, causing carbon dioxide production. Therefore, as the gasification operating temperature increases, the total amount of carbon dioxide produced by the system also increases.

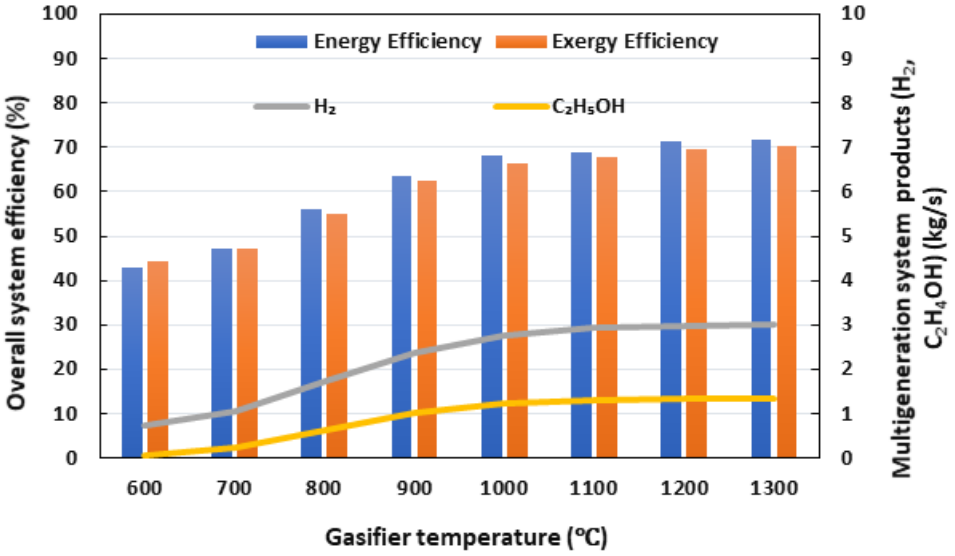

Figure 5.21 Effects of ethanol and hydrogen production rates and temperature on system efficiency for system 2

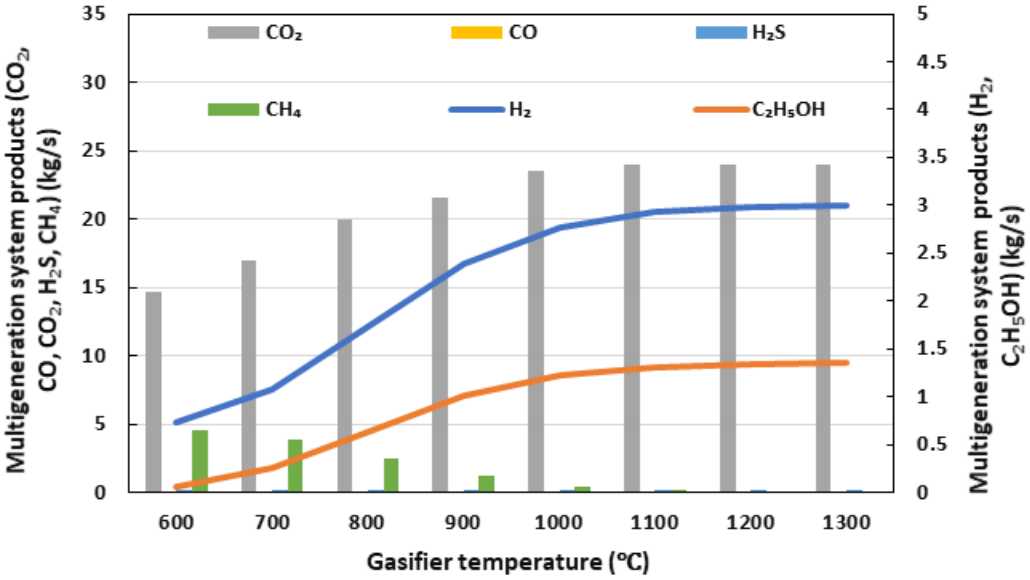

Figure 5.22 Effects of gasifier temperature on system products for system 2

Figure 5.22 illustrates the temperature-dependent ethanol production rate throughout the gasification process, as well as a comparison of ethanol production to other generated gases. Similar to the preceding figure, Figure 5.23 compares the temperature-dependent rise in hydrogen production to other generated gases.

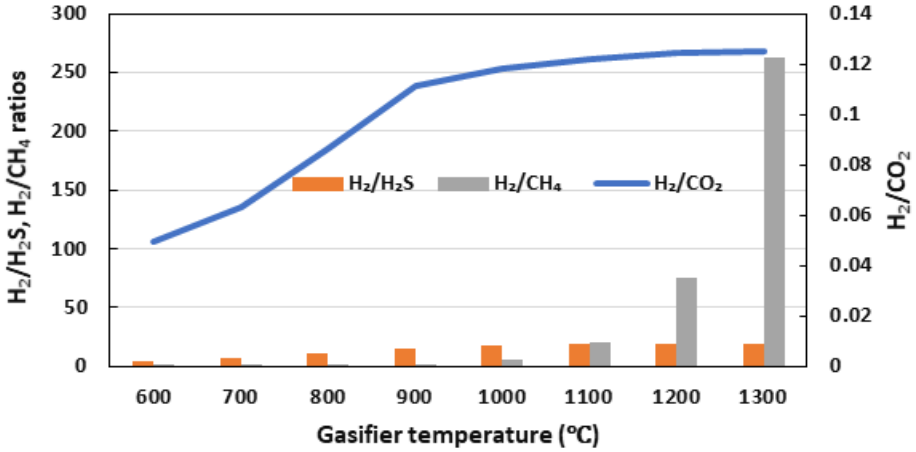

Figure 5.23 Effects of gasifier temperature on hydrogen production ratio for system 2

The variations in Figures 5.23 and 5.24 indicate that the hydrogen and ethanol synthesis rate is much greater than the rate of carbon dioxide generation at different temperatures. This increases the H/C ratio of the syngas by increasing the hydrogen content of the syngas much more than the carbon dioxide content of the gasification temperature increases. This reduces the amount of green gas released into the environment when the syngas is combusted, which helps the environment.

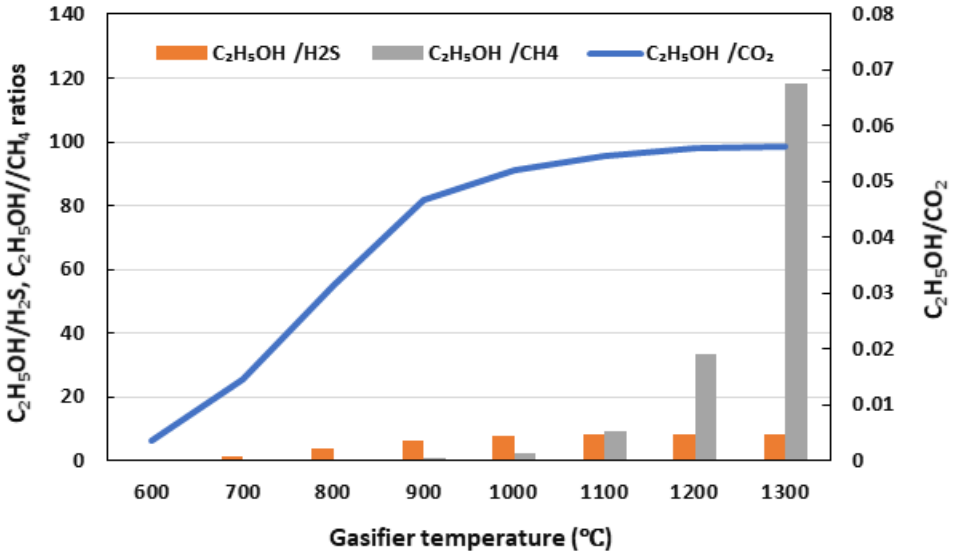

Figure 5.24 Effects of gasifier temperature on ethanol production ratio for system 2

Figure 5.25 illustrates the effect of steam feed rate on the energetic and exergetic efficiencies of the overall system. As the steam supply rate rises, the efficiency improves owing to the water-gas reaction given in table 3.1. However, the oxygen produced, and the hydrogen reacted with the carbon monoxide resulting in carbon dioxide production. Consequently, the carbon monoxide concentration in the syngas reduces while the carbon dioxide concentration rises. Accordingly, the amount of hydrogen produced in the water gas shift reaction decreases, but the increase in hydrogen is not the reduction of carbon monoxide by reacting with water in the water gas shift reaction, but the increase in the number of water molecules decomposed in the gasifier. Despite the rise in carbon dioxide in the syngas composition, clean syngas is devoid of carbon dioxide and monoxide due to the scrubber's carbon dioxide molecules. Due to a lack of carbon dioxide in the carbon hydrogenation reactor, the amount of ethanol generation in the multigeneration system 2 drops. Although there is a slight decrease in the increase in the energy and exergy efficiency of the system due to the reduced ethanol production, more hydrogen to be produced due to more steam supplied to the system increases the system's efficiency.

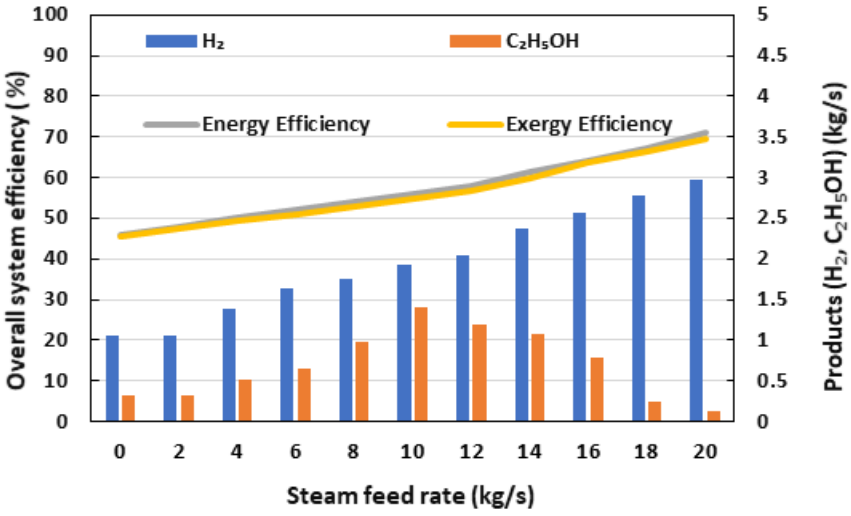

Figure 5.25 Effect of hydrogen and ethanol production rate and steam feed rate on overall system efficiencies for the system 2

The effects of oxygen feed rate on hydrogen and ethanol generation rate as well as on overall system efficiencies are illustrated in Figure 5.26. Since partial combustion occurs at low oxygen feed rates, sufficient carbon monoxide production increases and this carbon monoxide is transformed into hydrogen and oxygen with the water gas shift reaction. At this point, ethanol production for multigeneration system 2 is maximum. However, with

increasing oxygen feed rates, partial combustion returns to complete combustion and carbon monoxide production is reduced. Since carbon dioxide cannot be produced in the water gas shift reaction, ethanol production decreases for the designed system. With the decrease in ethanol production, the hydrogen used for ethanol production is not converted to ethanol and the number of hydrogen increases. With the decrease in ethanol production, the hydrogen used for ethanol production cannot be converted to ethanol, and the amount of hydrogen increases slightly. However, due to the decrease in the amount of carbon monoxide produced with the increasing amount of oxygen, less hydrogen is produced in the water gas shift reaction. Therefore, hydrogen production decreases with increased oxygen feed rate.

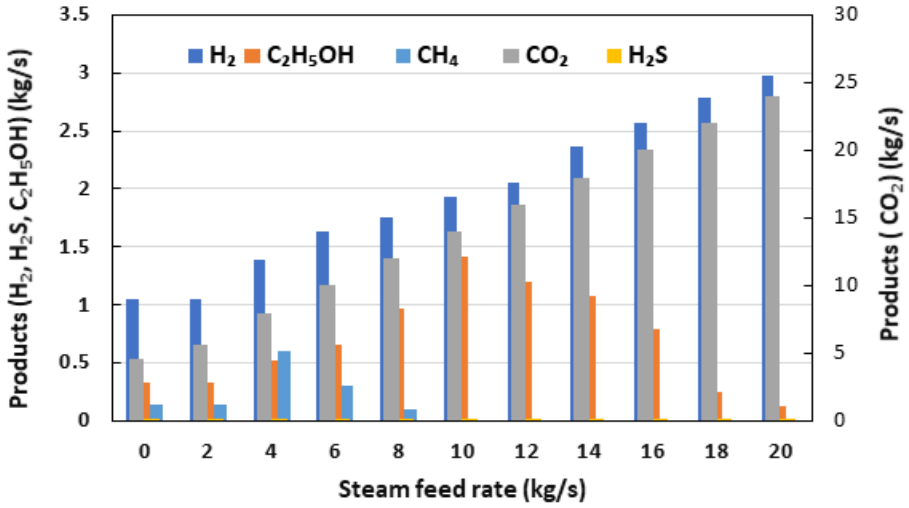

Figure 5.26 Effects of steam feed rate on outputs for system 2

The effects of oxygen feed rate on hydrogen and ethanol generation rate as well as on overall system efficiencies are illustrated in Figure 5.27. Since partial combustion occurs at low oxygen feed rates, sufficient carbon monoxide production increases and this carbon monoxide is converted into hydrogen and oxygen with the water gas shift reaction. At this point, ethanol production for the multigeneration system is maximum. However, with increasing oxygen feed rates, partial combustion returns to complete combustion and carbon monoxide production is reduced. Since carbon dioxide cannot be produced in the water gas shift reaction, ethanol production decreases for the designed system. With the decrease in ethanol production, the hydrogen used for ethanol production is not converted to ethanol and the number of hydrogen increases. With the decrease in ethanol production, the hydrogen used for ethanol production cannot be converted to ethanol, and the amount

of hydrogen increases slightly. However, due to the decrease in the amount of carbon monoxide produced with the increasing amount of oxygen, less hydrogen is produced in the water gas shift reaction. Therefore, hydrogen production decreases with increased oxygen feed rate.

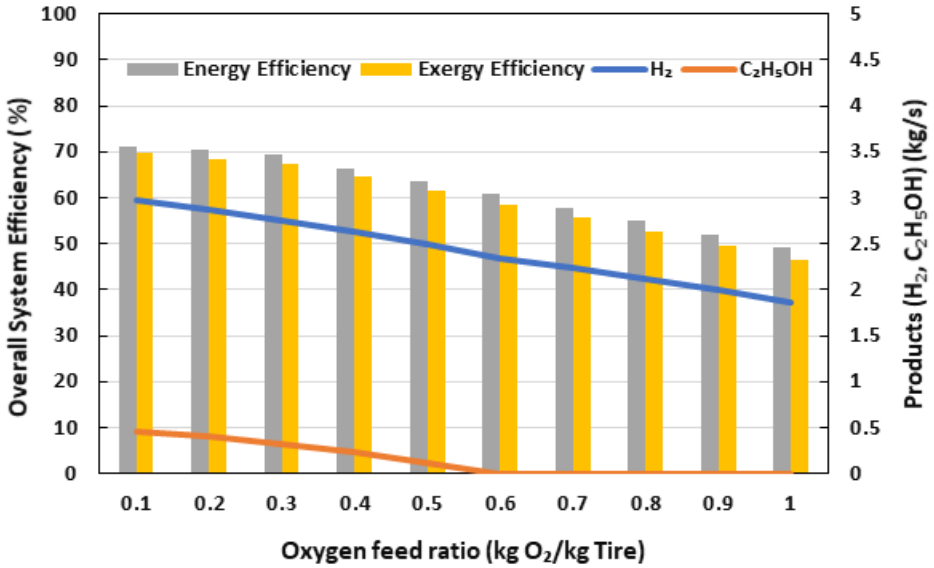

Figure 5.27 Effect of hydrogen and ethanol production rate and oxygen feed rate on overall system efficiencies for system 2

Table 5.4: System 3 state point values

State No	Substance	T (°C)	P (kPa)	ṁ (kg/s)	h (kJ/kg)	s (kJ/kgK)	ex (kJ/kg)
1	Oxygen	25	101.33	0.65	0	0	0
2	Oxygen	430.791	1550	0.65	394.64	0.118	359.48
3	Water	199.76	1550	10	851.2	2.33	255.31
4	Raw Syngas	1200	1550	23.89	2179.52	3.07	2051.53
5	Syngas	1200	1550	15.42	2438.87	3.01	2139.46
6	Hydrogen Sulfide	1200	1550	1.15	894.04	2.52	852.14
7	Syngas	1200	1550	14.27	4739.13	5.747	2750.19
8	Syngas	660	1550	14.27	3274.18	4.34	1504.35
9	Syngas	450	1550	14.27	2156.65	3.60	1111.67
10	Hydrogen+ Carbon Dioxide	450	1550	25.04	3652.19	0.22	1712.48
11	Hydrogen+ Carbon Dioxide	130.15	101.325	25.04	2382.51	0.15	232.74
12	Hydrogen+ Carbon Dioxide	130.15	101.325	12.52	2382.51	0.15	232.74
13	Ethanol	80	101.325	3.16	258.7	1.2	19.23

14	Hydrogen+ Carbon Dioxide	130.15	101.325	12.52	2382.51	0.15	232.74
15	Carbon dioxide + Water	130.15	101.325	11.14	103.52	0.42	476.59
16	Hydrogen	130.15	101.325	1.38	5462.14	57.13	159.36
17	Hydrogen	-252.6	101.325	1.38	450.9	22.4	367.12
18	Water	25	101.33	20.77	104.9	0.37	0.18
19	Water	25.06	1550	20.77	106.4	0.36	2.14
20	Water	199.76	1550	20.77	851.2	2.33	255.31
21	Water	199.76	1550	10.77	851.2	2.33	255.31
22	Water	84	130	7.2	351.9	1.123	25.03
23	Water	84.12	1650	7.2	353.6	1.123	27.12
24	Water	519.52	1650	7.2	3515	7.58	1303.38
25	Water	203.62	130	7.2	2881	7.73	628.14
25	Water	203.62	130	7.2	2881	7.73	628.14
26	Air	30	80	47	4.83	0.084	0
27	Air	253.89	410	47	231.59	0.17	179.79
28	Air	431.54	410	47	418.46	0.48	275.64
29	Air	201.77	80	47	178.24	0.54	18.19
30	Ammonia+Water	111	1547	30.32	308.5	1.468	18.73
31	Ammonia+Water	108.3	1547	4.53	1550	4.889	93.08
32	Ammonia+Water	108.3	1547	0.4	266.1	1.358	16.49
33	Ammonia+Water	43.9	1547	4.13	1294	4.175	71.98
34	Ammonia+Water	39.8	1547	4.13	189.8	0.655	14.13
35	Ammonia+Water	-15.33	234.8	4.13	189.8	0.7528	14.13
36	Ammonia+Water	-11	234.8	4.13	1258	4.881	71.69
37	Ammonia+Water	39.8	234.8	30.32	-42.53	0.472	0.01
38	Ammonia+Water	39.93	1547	30.32	-40.84	0.4725	0.07
39	Ammonia+Water	131.4	1547	26.19	404.2	1.657	25.17
40	Ammonia+Water	39.93	1547	26.19	-0.1823	0.5269	2.36
41	Ammonia+Water	40.2	234.8	26.19	-0.1823	0.5315	2.36

The effects of oxygen feed rate on the synthesis of carbon monoxide, hydrogen, ethanol, hydrogen sulphide, and methane in Multigeneration System 2 are shown in Figure 5.28. Unlike pyrolysis, gasification involves the combustion of oxygen. However, oxygen consumption is limited, and complete combustion does not occur. At low rates, oxygen generates heat in the environment through exothermic processes described by the R1 and R2 equations. Additionally, the R2 equation's partial combustion process raises the carbon monoxide content of the syngas. Since oxygen produces carbon dioxide and carbon monoxide at modest rates, the synthesis of hydrogen and ethanol rises. Suppose the oxygen

addition is maintained and the reaction progresses to complete combustion. In that case, the quantity of hydrogen produced in the water gas shift reactor reduces as the carbon monoxide content of the syngas drops.

Nonetheless, this drop is not dramatic because of the rise in gasification temperatures. After all, the presence of oxygen enhances exothermic processes. As a result, the quantity of hydrogen generated during the gasification process increases. Even though more carbon dioxide is removed from the syngas when scrubbed, the amount of ethanol made in the multigeneration 2 system drops.

According to the chemical balance equations, the increase in the manure feed rate, which is the fuel used in the system, increases the hydrogen and ethanol productions at the same rate. Figure 5.29 illustrates the effect of the tire feed rate provided to the system on the energy and exergy efficiencies of the system. In the study, calculations are made by increasing other gasification agents such as steam and oxygen in the same proportion with the increased manure feed rate. Other useful output amounts such as ethanol, hydrogen and electricity produced due to the increase in manure are raised at the same ratio. Since the consumption of energy-consuming units such as compressors and pumps does not or slightly increase, the efficiency also improves.

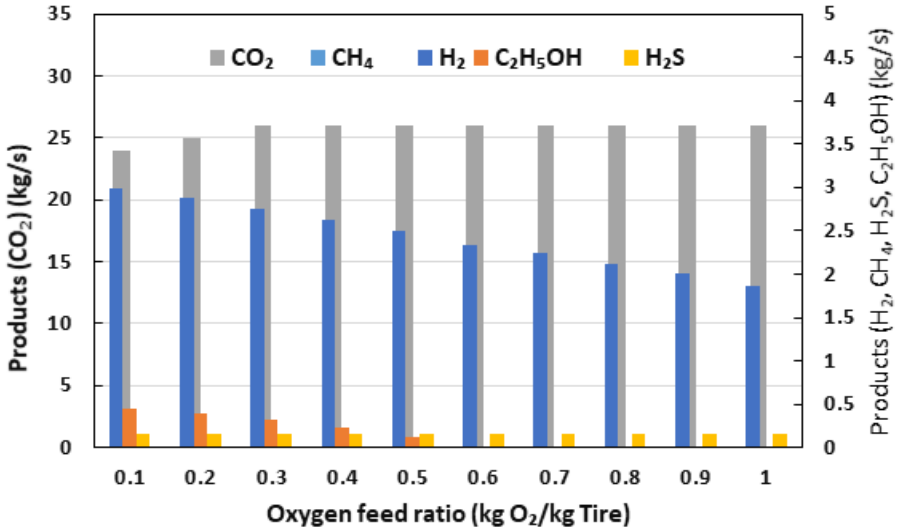

Figure 5.28 Effect of oxygen feed rate on outputs for system 2

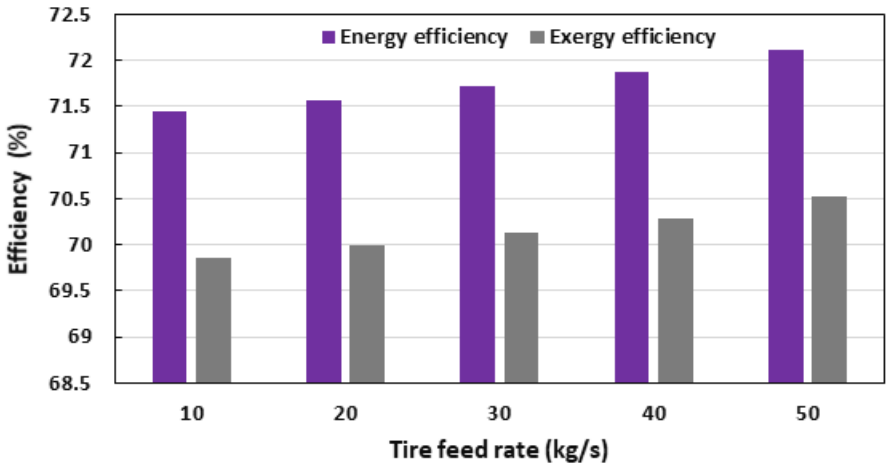

Figure 5.29 Overall energy and exergy efficiencies of system 2 depending on tire feed rate

5.6 System 2 Validation

To validate the presented simulation model, the system's energy and exergy efficiencies as a function of steam and oxygen feed rates derived from the Aspen Plus simulations are compared to the parametric findings of Gungor and Dincer [87]. Similar to multigeneration system 2, the shredded waste tire is utilized as a feedstock in their study. While the operating temperature is 1227 °C, the oxygen-fuel ratio has been selected as 1:10. Moreover, solar energy is utilized to produce steam as a gasifier agent. Furthermore, similar components such as water gas shift reactor, steam and gas turbines, compressors and condensers are used in their multigeneration system. Therefore, this study has been selected to compare energy and exergy efficiency results and deviations. In Figure 5.30, the comparison of energy and exergy efficiencies between multigeneration system 2 and reference system depending on altering steam feed rate. Results show that energy and exergy efficiencies increase depending on varying steam feed rates and both systems' findings are consistent with each other.

Similarly, Figure 5.31 illustrates the comparison of energy and exergy efficiencies between multigeneration system 2 and reference system depending on altering oxygen feed rate. Results show that energy and exergy efficiencies decrease depending on varying oxygen feed rates and both systems' findings are consistent with each other.

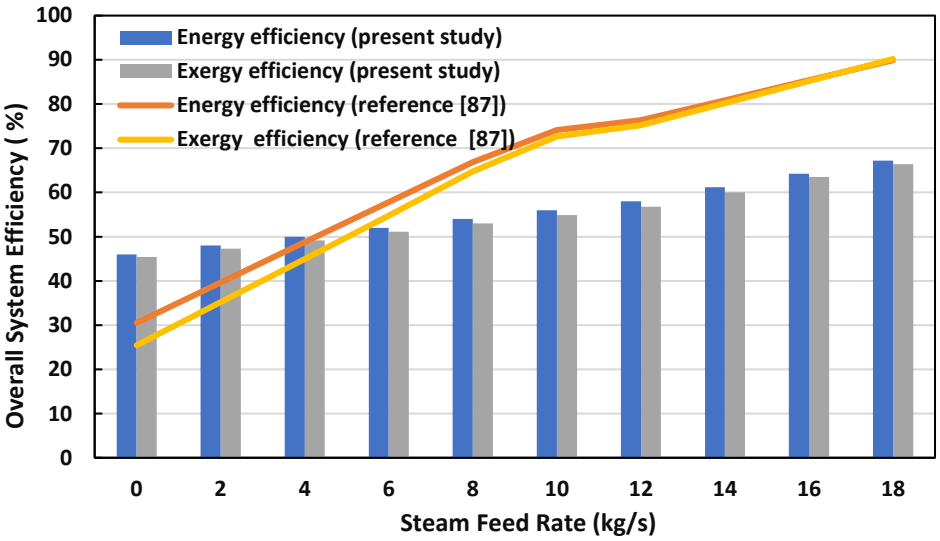

Figure 5.30 Comparison of system 2 and the reference system's energy and exergy efficiencies depending on the steam feed rate

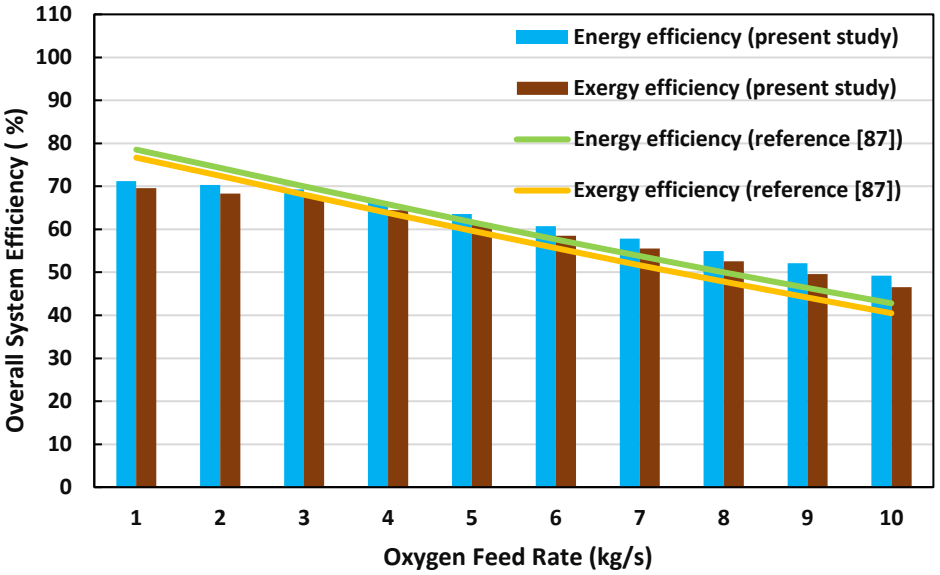

Figure 5.31 Comparison of system 2 and the reference system's energy and exergy efficiencies depending on the oxygen feed rate

To validate the created simulation model, the syngas compositions as a function of gasifier temperature derived from the Aspen Plus simulations are compared to the experimental findings of Portofino et al. [88].Waste tires and oxygen-enriched air are used in their study at temperatures ranging from 850 to 1000 °C. Figure 5.32 shows the comparison of hydrogen concentration between the simulation and the experimental results for multigeneration system 2. Similar to the experimental data, the Aspen Plus results indicate that hydrogen yield in the syngas composition increases as the gasification temperature

rises. There is an average of 5.12% differences between the experimental and simulation model according to experimental results. Results show that hydrogen volumetric composition increases depending on gasification operating temperature, and both studies' findings are consistent with each other.

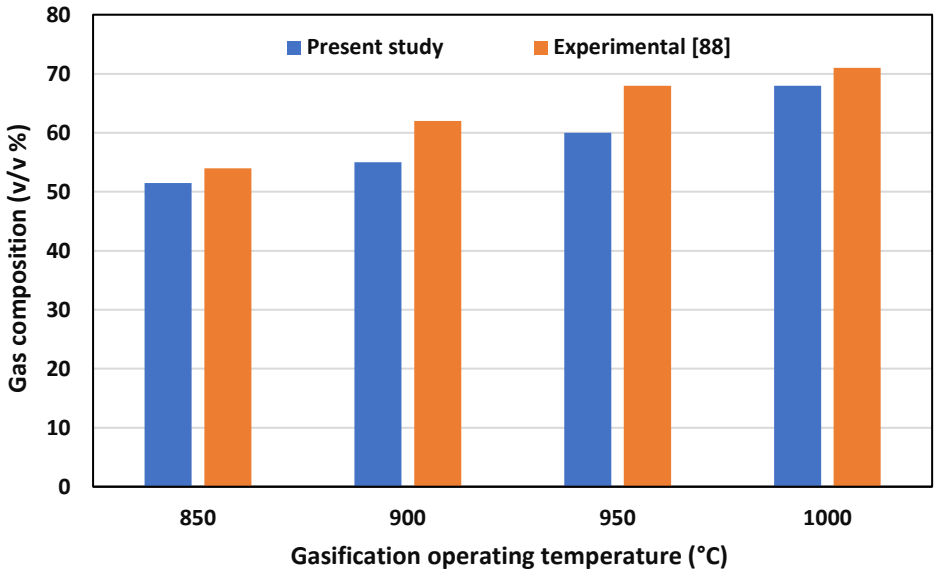

Figure 5.32 Comparison of hydrogen concentrations of syngas between the present study and the experimental for system 2

5.7 System 3 Thermodynamic Analysis Results

Figure 5.33 illustrates the main system components' rate of exergy destructions in multigeneration system 3. The highest exergy destruction occurs in the gasifier with 148229 kW. The main reason for this is that they have high temperatures, so irreversibility increases in the gasifier, resulting in more significant physical exergy destruction. In addition, the amount of exergy destruction is high due to physical exergy changes as well as exergy destruction.

The third multigeneration system, which is intended to run on lignite, is supplied with steam at 10 kg/s and coal at a rate of 20 kg/s at 199.76 °C. The temperature at which the gasification process begins is set at 1200 °C. Based on the computations, the system's energy and exergy efficiencies were determined to be 68.8% and 66.56%, respectively. Energy and energy efficiencies are 71.45% and 69.87%, respectively, for the prior system, multigeneration system 2. The primary cause for this efficiency decreases in energy and exergy efficiency compared to multigeneration system 2 is the hydrogen consumption for

ethanol production in the third multigeneration system. Since hydrogen produced in system 2 is not used for ethanol generation, there was no loss in the hydrogen produced in the system. Therefore, the energy and exergy efficiencies of multigeneration 2 are slightly better than multigeneration system 3.

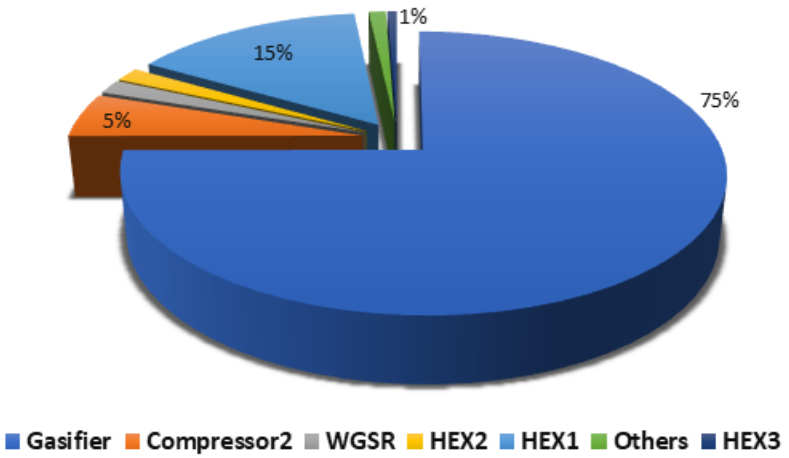

Figure 5.33 Exergy destruction ratios of main system components of multigeneration system 3

In Figure 5.34, the energy and exergy efficiency of subsystems in multigeneration system 3. The overall energy and exergy efficiencies for multigeneration system 3 are 68.8% and 66.56%, respectively, while the efficiencies of the individual subsystems are lower. Results show the advantage of multigeneration systems, in which subsystems are used together in terms of efficiency.

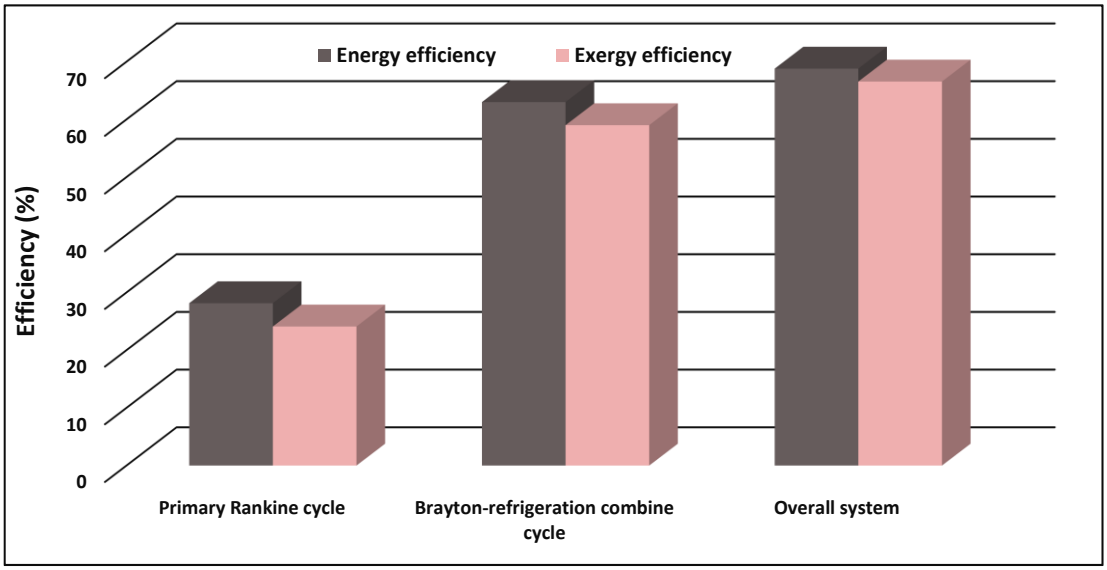

Figure 5.34 Energy and exergy efficiencies of sub-systems in multigeneration system 3

The thermal energy supplied to the system by the geothermal well is calculated using the balance equations of the heat exchanger 1. The steam feed rate of the gasifier is selected as 10 kg per second, while the oxygen feed rate is accepted as 0.65 kg/s. The energy transmitted from the solar tower to the system is 20905.55 kW to supply this steam at 199.8 °C. According to the calculations, the total net power generation of the system is 19254.3 kW.

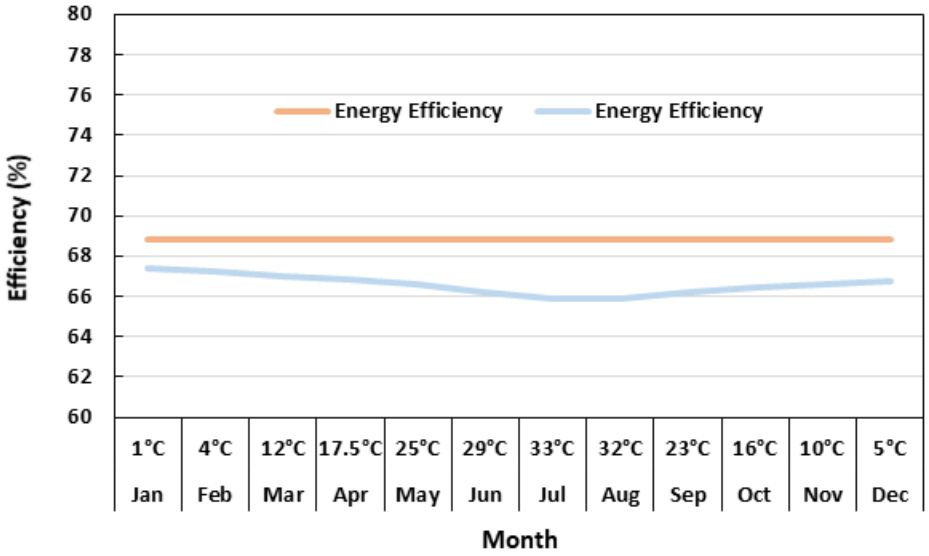

Figure 5.35 Overall energy and exergy efficiencies of system 3 depending on average reference temperature

Figure 5.35 illustrates the changes in overall energetic and exergetic efficiencies depending on the reference temperature for multigeneration system 3. According to the calculations made, a slight decrease is observed in the exergy efficiency of the system depending on the increase in the accepted reference temperature. The exergy efficiency, about 67.36% at 1°C ambient temperature, decreased to 65.86% at 33°C reference temperature. No significant effect on the energy efficiency of the reference temperature is observed. This can be explained by the fact that the reference temperature has no effect on the overall energy efficiency expression.

The ethanol production method in multigeneration system 3 is similar to multigeneration system 1, and in both systems, hydrogen is needed for the ethanol hydrogenation process of carbon dioxide.

5.8 System 3 Parametric Study Results

Similar to the other two systems, pure oxygen is used as the gasifier to increase the efficiency of the gasifier. Numerous parametric studies have been conducted on the design and analysis of systems. Several parametric studies have been undertaken to assess system efficiency and useful outputs, including ethanol and hydrogen, as a function of system inputs including steam feed rate, gasification temperature, and oxygen feed rate within the gasifier. Furthermore, the impact of low-grade lignite input rate on system performance is investigated. Due to the fact that all multigeneration systems use the same process and utilize carbon-based feedstocks, only system 1's syngas compositions are analyzed based on system operational parameters such as steam feed rate, gasification operating temperature, and oxygen feed rate. This is because the method is consistent across all systems and the findings for syngas composition are similar.

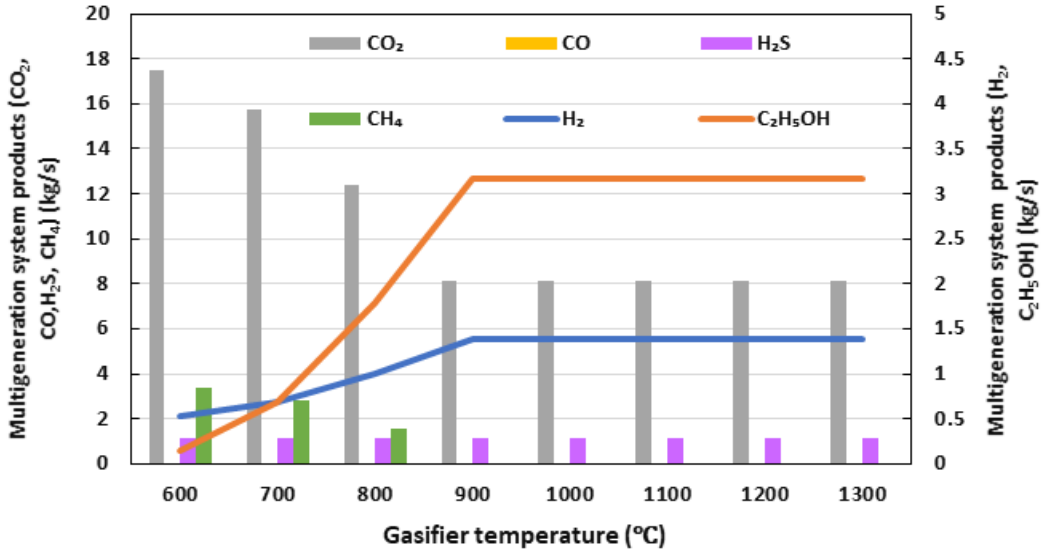

Figure 5.36 Effects of gasifier temperature on gasification products for system 3

As seen in Figure 5.36, increasing the temperature of the gasification process results in an increase in ethanol and hydrogen production. The amount of carbon monoxide produced by the multiple production systems rises depending on the gasification operating temperature. After the water gas shift reaction, carbon monoxide gas reacts with water to produce hydrogen and carbon dioxide. As ethanol is produced with some of this carbon dioxide and hydrogen, ethanol production increases. However, with increasing gasifier temperatures, ethanol and hydrogen production tends to remain constant for multigeneration system 3.

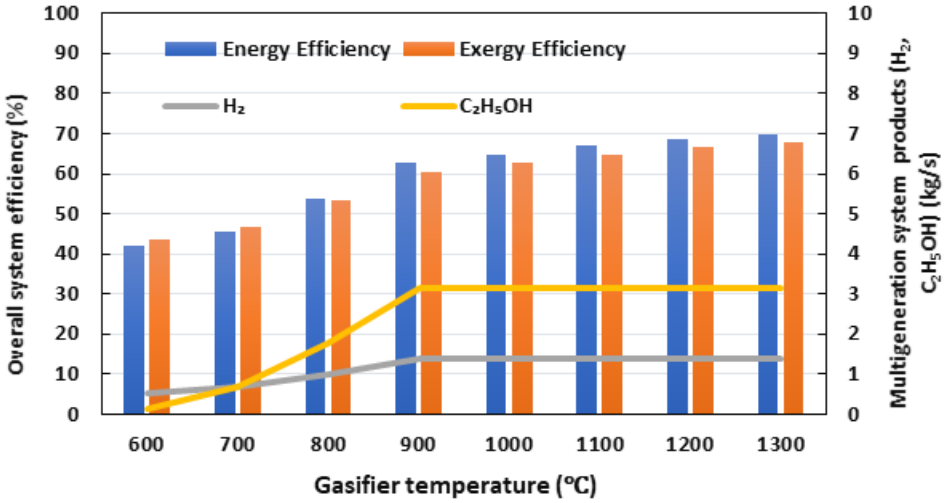

Figure 5.37 Effects of ethanol and hydrogen production rate, and temperature on system efficiency in system 3

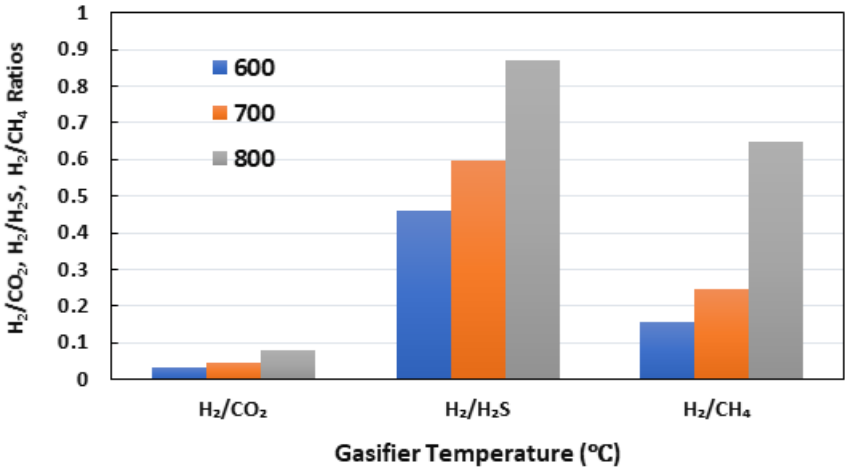

Figure 5.38 Effects of gasifier temperature on hydrogen production ratio of system 3

As shown in Figure 5.37, the amounts of ethanol and hydrogen generated enhance as the gasification operating temperature increases, benefiting system efficiency by increasing syngas temperature, which can be utilized in the turbine. Additionally, increased ethanol and hydrogen generation has a beneficial effect on efficiency. Therefore, increasing the temperature of the gasifier has a substantial effect on system efficiency, ethanol, and hydrogen generation, and on emissions of carbon dioxide reduction.

Figure 5.39 illustrates the temperature-dependent ethanol production rate throughout the gasification process, as well as a comparison of ethanol production to other generated gases. Similar to the preceding figure, Figure 5.38 compares the temperature-dependent rise in hydrogen production to other generated gases.

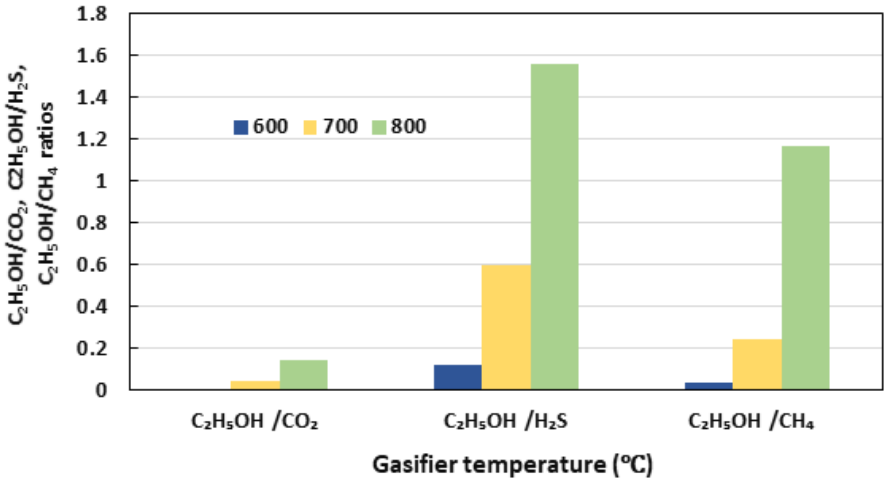

Figure 5.39 Effects of gasifier temperature on ethanol production ratio of system 3

The variations in Figures 5.38 and 5.39 indicate that the hydrogen and ethanol synthesis rates are higher than the rates of carbon dioxide generation at different temperatures. This enhances the hydrogen to carbon ratio of the products by raising the hydrogen content of the syngas much more than the carbon dioxide content of the gasification temperature rises. Therefore, the amount of green gas discharged into the environment is minimized when the syngas is combusted.

Figure 5.40 shows the relationship between the steam supply and the energy and energy efficiency of the system. As the steam feed rate increases, the hydrogen synthesis rate also increases. Despite the decreasing ethanol production, the efficiency rises up to a certain steam rate as hydrogen production increases then remain constant. Because depending on the increasing steam feed rate, the amount of carbon monoxide produced in the gasifier decreases after a certain point and negatively affects the amount of hydrogen produced in the water gas shift reaction.

Figure 5.41 illustrates the relationship between steam feed and the system's products. As the steam feed rate increases, the hydrogen synthesis rate increases depending on the water-gas reaction shown in Table 3.1. Nevertheless, as a result of this reaction, the released oxygen reacts with carbon monoxide and leads to the formation of carbon dioxide. Consequently, carbon monoxide in the syngas decreases while carbon dioxide increases. Therefore, the hydrogen produced in the water gas shift reaction decreases, but overall hydrogen production of the system increases since more steam is injected into the gasifier. Despite the increase in carbon dioxide in the syngas composition, since the scrubber will

capture these carbon dioxide molecules, clean syngas is deprived of carbon dioxide and monoxide. Although the amount of hydrogen increases with the steam feed rate, carbon dioxide is insufficient in the carbon hydrogenation reactor, so ethanol production declines in the designed multigeneration system 3.

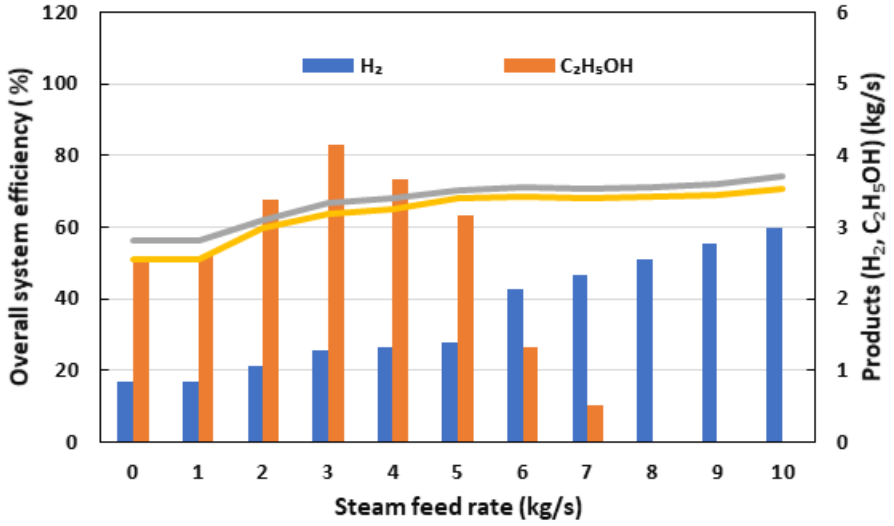

Figure 5.40 Effects of hydrogen and ethanol production rate and steam feed rate on overall system efficiencies for system 3

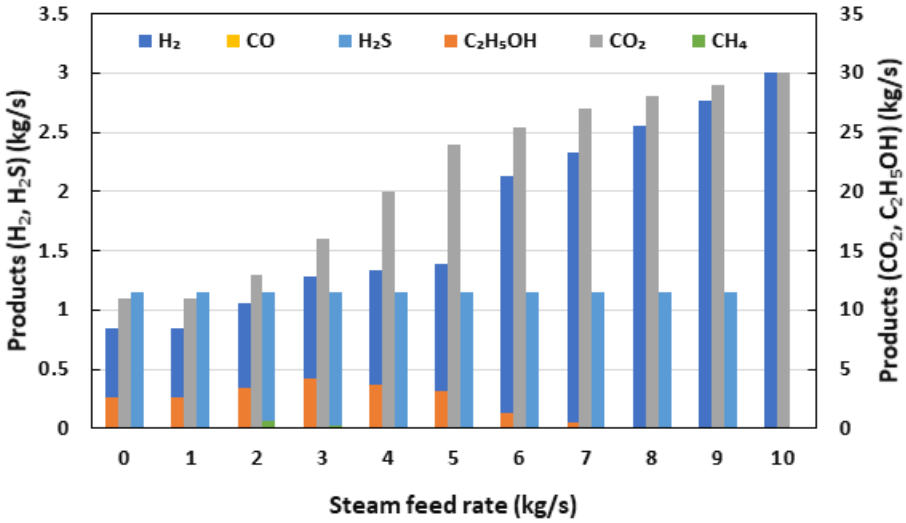

Figure 5.41 Steam feed rate effects on outputs in system 3

Figure 5.42 shows the effect of oxygen as a gasification agent on ethanol and hydrogen production rate and overall system efficiencies for the multigeneration system 3. The continuous increase in oxygen that feeds the gasifier increases carbon dioxide production and limits hydrogen production. Due to falling ethanol production and partially stable hydrogen production, energetic and exergetic efficiencies are slightly reduced.

Figure 5.43 shows the effect of oxygen as a gasification agent on carbon dioxide, hydrogen, ethanol, and energy and exergy. Increasing oxygen feed ratio raises the carbon dioxide in the syngas. Although the amount of hydrogen produced in water shift gas decreases due to decreasing carbon dioxide, the amount of hydrogen produced in the gasifier increases with increasing temperatures, and a balance occurs. Since the carbon dioxide produced is separated from the syngas by scrubbing, ethanol production decreases. Hydrogen production remains relatively constant for the multigeneration system 3. According to the chemical balance equations, the increase in the coal feed rate, which is the fuel used in the system, increases the hydrogen and ethanol productions at the same rate.

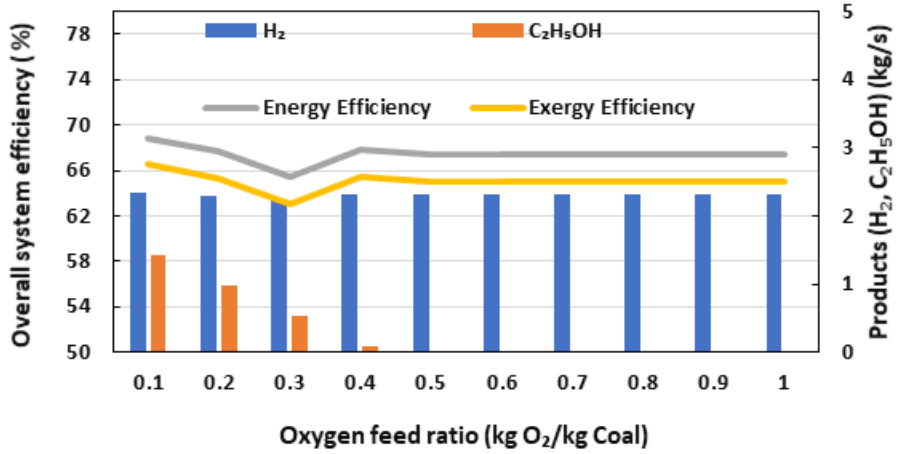

Figure 5.42 Effects of hydrogen and ethanol production rate and oxygen feed ratio on overall system efficiencies for system 3

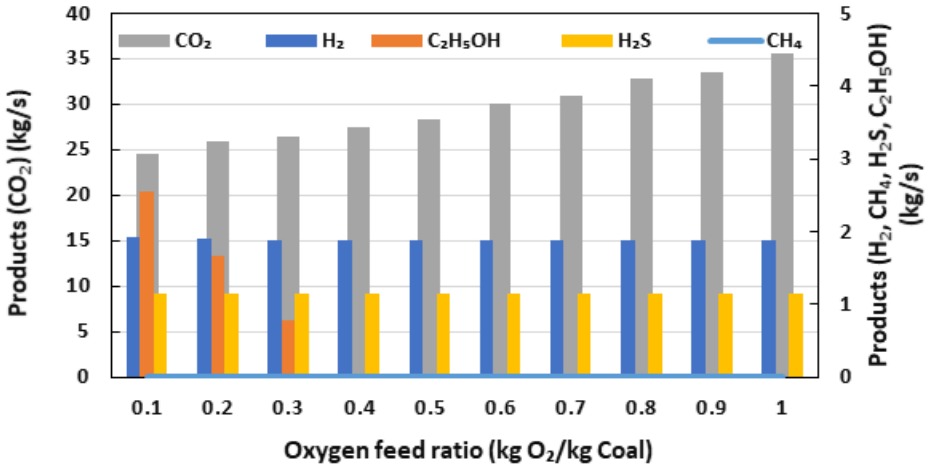

Figure 5.43 Effects of oxygen feed ratio on multigeneration system outputs for system 3

Figure 5.44 illustrates the effect of the lignite feed rate provided to the system on the energy and exergy efficiencies of the system. In the study, calculations are made by increasing other gasification agents such as steam and oxygen in the same proportion with the increased manure feed rate. Other useful output amounts such as ethanol, hydrogen and electricity produced due to the increase in manure are raised at the same ratio. Since the consumption of energy-consuming units such as compressors and pumps does not or slightly increase, the efficiency also improves.

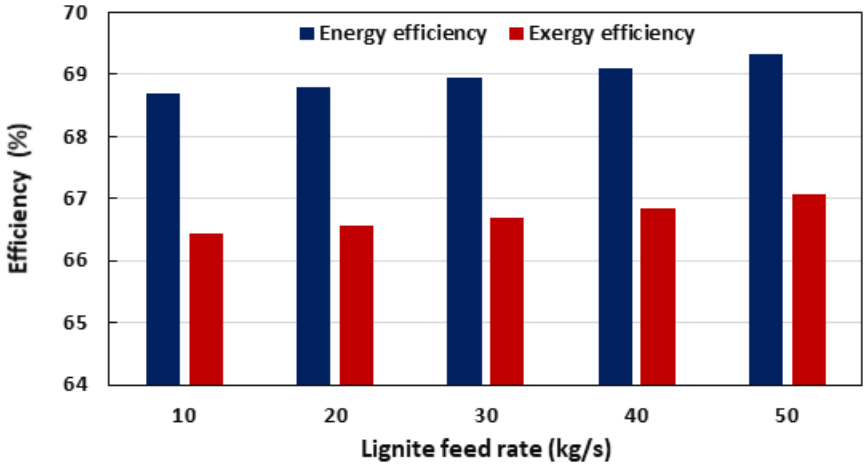

Figure 5.44 Overall energy and exergy efficiencies of multigeneration system 3 depending on lignite feed rate

5.9 System 3 Validation

To validate the presented simulation model, energy and exergy efficiencies of the overall system as a function of gasifier temperature derived from the Aspen Plus simulations are compared to the parametric results of Bicer and Dincer [89]. Similar to multigeneration system 3, low grade underground coals are utilized as a feedstock in their study. Moreover, the coal feedstock rate has been considered to be 20 kg/s in both studies. While the operating temperature is 550 °C, steam and oxygen feed rates are 33.55 kg/s and 15 kg/s, respectively. Furthermore, similar components such as water gas shift reactor, steam, gas cleaning unit, sulfur recorvery unit, compressors and condensers are used in their multigeneration system. Therefore, this study has been selected to compare energy and exergy efficiency results and deviations. In Figure 5.45, the comparison of energy and exergy efficiencies between multigeneration system 3 and reference system depending on altering gasification temperature. Results show that energy and exergy efficiencies increase depending on varying steam feed rates and both systems' findings are consistent with each

other. Alongside some subsystem differences, air usage instead of oxygen as a gasification agent causes energy and exergy efficiency to decrease compared to the third multigeneration system.

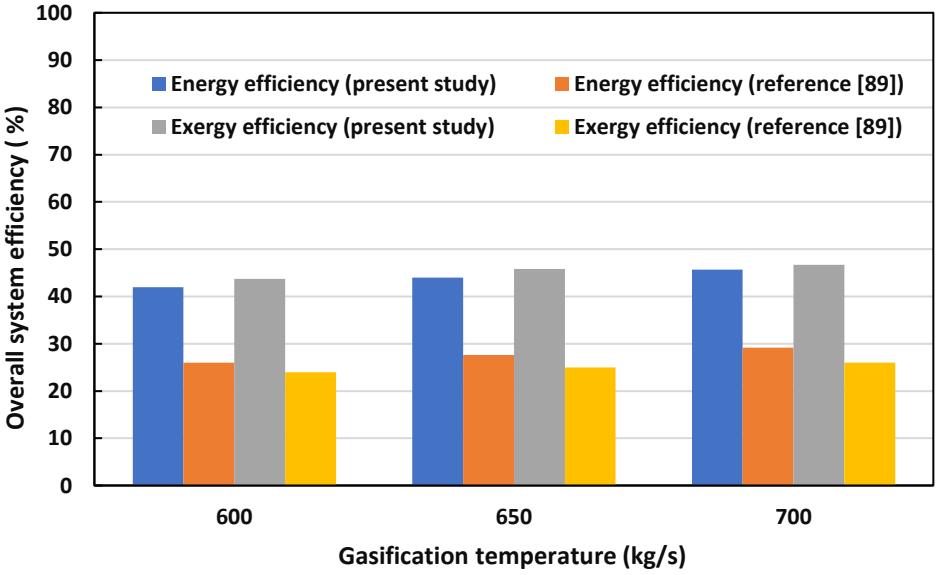

Figure 5.45 Comparison of system 3 and the reference system's energy and exergy efficiencies depending on the gasification temperature

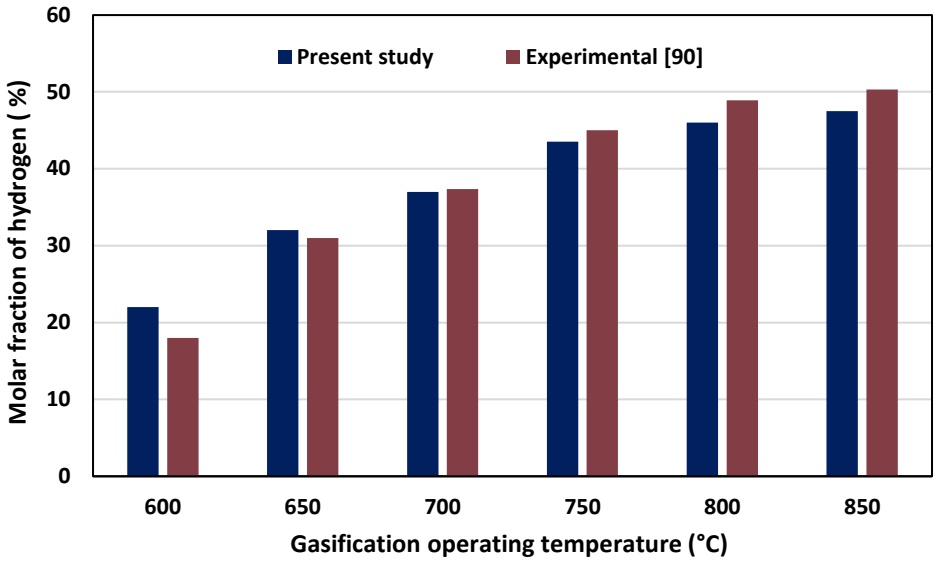

Figure 5.46 Comparison of hydrogen concentrations between the present study and the experimental for system 3

To verify the developed simulation model, the syngas compositions as a function of gasifier temperature are compared to the experimental results of Zhang et al. [90]. Lignite and oxygen-enriched air are utilized in their study at temperatures ranging from 600 to 850 °C.

Similar to the experimental data, the Aspen Plus results indicate that hydrogen molar fraction in the syngas composition increases as the gasification temperature rises. Figure 5.46 illustrates the comparison of hydrogen concentration between the simulation and the experimental results for multigeneration system 3. There is an average of 1.98% differences between the experimental and simulation model according to experimental results. Results show that hydrogen volumetric composition increases depending on gasification operating temperature, and both studies' findings are consistent with each other.

5.10 Thermodynamic Performance Comparison of Systems

In Figure 5.47, the amounts of hydrogen and ethanol produced by the systems are compared. According to calculations, multigeneration system 2 is the best option for hydrogen production, with a hydrogen production rate of 3.02 kg/s. In addition, the multigeneration system 3 is the best alternative for ethanol production, with an ethanol production rate of 1.58 kg/s. The reason for low hydrogen and ethanol generation in multigeneration system 1 is that half of the syngas generated is combusted in the combustion chamber.

In Figure 5.48, the systems are compared over their energetic and exergetic efficiencies, and it is found that the system with the best performance was multigeneration system 2. The energetic and exergetic efficiencies for system 2 are 71.45% and 69.87, in this order. In addition, the amount of hydrogen ethanol produced by the system is 71.45% and 69.87, respectively. In addition to these, the proposed system produces 3.02 kg/s hydrogen and 0.13 kg/s.

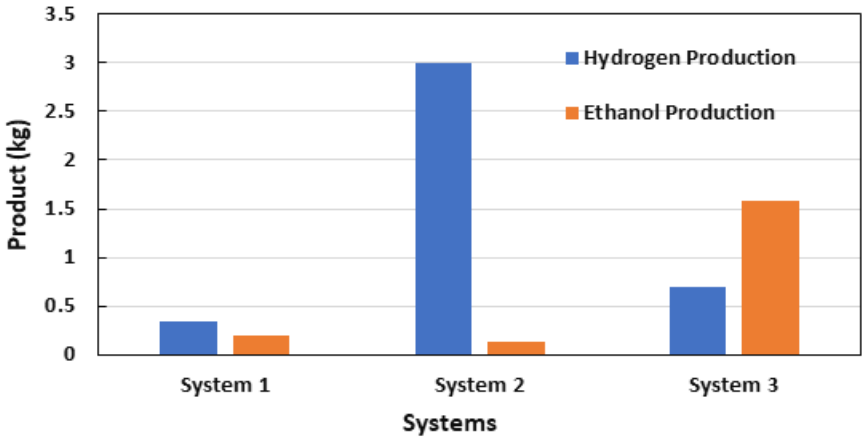

Figure 5.47 Comparison of ethanol and hydrogen production rates of all three systems

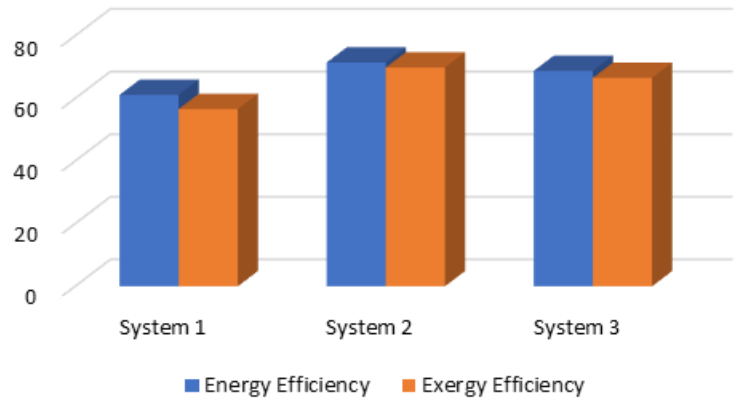

Figure 5.48 Comparison of energy and exergy efficiencies of all three systems

5.11 Cost Assessment Results for the System

Figure 5.49 illustrates the comparison of multigeneration systems in terms of cost-effectiveness. Since the internal rate of return rates are more than 5%, which accepted interest rate, is for all three system. The findings indicate that the third system can be the most cost-effective and feasible alternative, followed by the second and first systems. While multigeneration system 3 is the most viable application in terms of internal rate of return (IRR) and payback period (PBP), the second multigeneration system has more advantages according to net present value (NPV). Multigeneration system 3 requires less investment since it includes fewer components and equipment, such as a gasifier unit, cyclone separator, and ash handling.

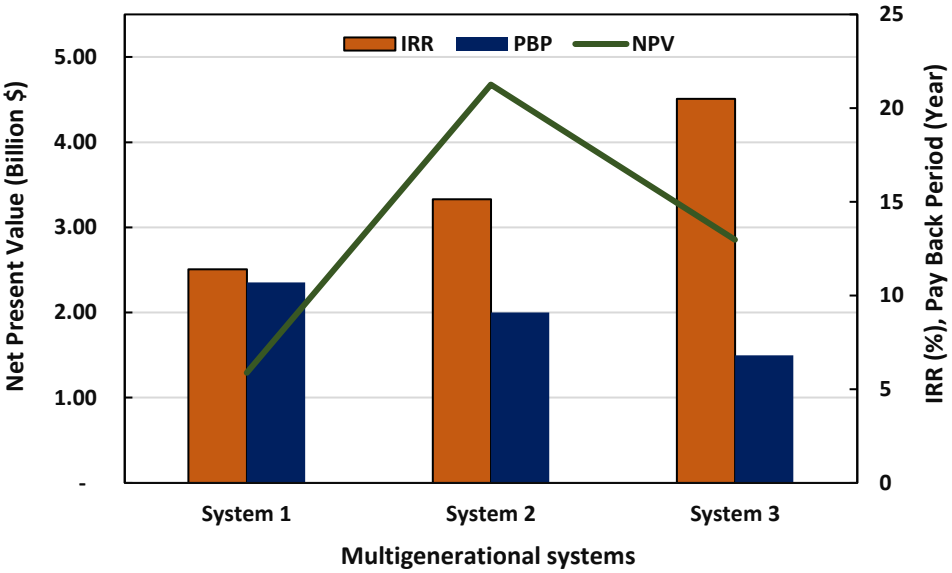

Figure 5.49 Cost-effectiveness comparison of all three systems

Moreover, multigeneration system 3 has fewer maintenance costs because the underground itself is a gasifier, and the ash produced is not handled. Hence, there is no additional ash disposal cost for the third multigeneration system. Therefore, the payback period is shorter for the third system. However, the second system has more advantages and is economically more viable in terms of net present value. The main reason for this is that the second system has a higher hydrogen production rate, which means more income in the long term.

Chapter 6. Conclusions and Recommendations

This thesis presents and evaluates three distinct integrated systems aimed at increasing the efficiency and sustainability of hydrogen and ethanol generation via the use of green and renewable resources. Such as solar and geothermal energy as well as gasifiable wastes. Each research included a reference scenario and a sensitivity analysis of the system and its variants in terms of energy and exergy techniques. The primary emphasis of this research is on energy and exergy efficiency in order to evaluate the system's operational performance. This approach enables comparisons of each system's operational performance. This chapter examines and summarises the significant conclusions from the thermodynamic study of the systems and their variations. This chapter also includes some ideas for prospective process improvements and future research paths.

6.1 Conclusions

Three different waste-to-energy integrated multigeneration systems are analyzed and investigated thermodynamically with an energetic and energetic approach. All three systems are designed for different scenarios, and parametric analyses are performed. Konya, Turkey, is considered to be the proposed location for the first multigeneration system. For the solar integrated waste energy system, animal manures from Konya are used as a gasification fuel, and thermodynamic analyses using ultimate and proximate are conducted. In addition, electricity and steam are produced from solar energy, and this steam is utilized as a gasification agent. Half of the syngas generated in gasification is utlized in the combustion chamber to produce electricity, heating and cooling. As a result of gasification, hydrogen and ethanol are produced, as well as sulfuric acid production as a by-product of gasification. The second system is a geothermal-based waste-to-energy system that is considered to be materialized in the Larderello geothermal field in southern Tuscany, Italy, which contains many geothermal fields and is considered to be the proposed location. The system is designed to be used in both the gasification unit and the water gas shift reactor, which is produced from geothermal energy. The third system aims to utilize Tuncbilek lignites in Turkey through underground coal gasification, and the system is designed accordingly.

In all three systems designed waste to energy multigenerations system, energy is taken from renewable sources, and six useful outputs are obtained, namely ethanol, hydrogen,

cooling, heating, sulfuric acid production and electricity. Following are the main conclusions from the thermodynamic study of the three integrated systems using an energy and exergy approach:

The first multigeneration system's net power production, cooling, and heating capacities are calculated to be 21179 kW, 43196 kW, and 3998 kW, respectively. In addition, the overall energy and exergy efficiencies of the proposed system are found as 61.1% and 56.6%, respectively. In multigeneration system 1, The primary Rankine cycle's energy and exergy efficiencies are determined to be 16.9 % and 11.2 %, respectively. These values are 56.75 % and 28.9 %, respectively, for the Brayton-Rankine combined cycle. Finally, the third Rankine-Absorption refrigeration cycle's energy and exergy efficiencies are computed to be 58.2 % and 38.3 %, respectively. The system produces 0.34 kg/s of hydrogen and 0.195 kg/s of ethanol, respectively.

The second multigeneration system's net power production, cooling, and heating capacities are calculated to be 18752 kW, 49236 kW, and 5363 kW, respectively. In addition, the overall energy and exergy efficiencies were calculated as 71.45% and 69.87. In addition to these, 3.02 kg/s hydrogen and 0.13 kgs ethanol are produced in the proposed system. The gasification unit, with a capacity of 137238 kW, has the highest rate of exergy destruction.

The third multigeneration system's net power production, cooling, and heating capacities are calculated to be 19254 kW, 39025 kW, and 4326 kW, respectively. Moreover, the designed system's overall energy and exergy efficiencies are calculated as 68.8% and 66.56%, respectively. While the system produces 0.69 kg/s of hydrogen, it can produce 1.59 kg/s of ethanol. The gasification unit, with a capacity of 148229 kW, has the highest rate of exergy destruction.

Multigeneration system 1 has 1.29 billion $ net present value over the 20 years. In addition, the payback period has been calculated as 10.7 years for multigeneration system 1. Moreover, the first system has an 11.4% internal return rate, which is more than double the interest rate accepted.

Unlike the first multigeneration system, the second multigeneration system has the highest NPV with 4.68 billion dollars in a 20-year period among all three systems. Furthermore, multigeneration system 2 has a 15.33% IRR and its payback period is 9.1 years.

The third multigeneration is the most viable, with the highest IRR, which is 20.49%, and the lowest PBP, which is 6.8 years, among all three systems. However, it is the second-best option in terms of NPV, at 2.85 billion dollars, in a 20-year time interval among all three options.

6.2 Recommendations

Energy has undoubtedly been one of humanity's most critical demands throughout history. Today, it is undergoing a transformation driven by governments and organizations worldwide focusing on sustainability. Sustainable development is a realistic goal. Numerous factors, however, need to be addressed. Consideration should be given to the ability to phase out fossil fuels as an energy source, assuring a transition to low-emission green energy sources, improving energy production efficiency, and reducing energy consumption. Solar, geothermal, wind, and tidal energy have all gained recognition as potential alternatives to fossil fuels in recent years. However, these resources, whose effectiveness varies according to solar radiation and wind speed parameters, raise specific worries about their sustainability. As a result, integrating renewable energy sources into systems presents unique sustainability issues owing to the state of the ecosystem. To overcome these challenges, integrated systems that combine many energy sources and generate energy-dense, transportable fuels such as hydrogen and ethanol, in addition to providing heating, cooling, and power generating, seem to be a viable option.

- Comprehensive life assessment study should be conducted to investigate and to developed systems will be important for future research.
- It is essential to carry out a comprehensive feasibility study on multigeneration systems in order to prevent or control the possible high investment costs as well as their detrimental environmental effects
- Multi-objective optimization techniques can be utilized to determine the optimum gasification parameters such as gasification operating temperature, steam, and oxygen feed rate of the waste-to-energy multigeneration system.

- The prototype for developed systems should be tested to confirm the accuracy of the theoretical findings and minimize the predictive effects in the calculations.
- Including multi-objective optimization research on how collective operational parameters affect the efficiency of waste-to-energy multigeneration systems would be beneficial and provide greater dependability.
- Conducting scale-up studies and developing prototypes of proposed systems to identify the pilot plant processes is crucial for designing a full-scale plant.

References

[1] I. Dincer and A. Abu-Rayash, “Energy sustainability,”. Elsevier, Jan. 2019, doi: 10.1016/C2018-0-04801-X.

[2] E. Holden, K. Linnerud, and D. Banister, “The Imperatives of Sustainable Development,” *Sustainable Development*, vol. 25, no. 3, pp. 213–226, 2017, doi: 10.1002/sd.1647.

[3] “Data.GISS: GISS Surface Temperature Analysis (GISTEMP v4).” https://data.giss.nasa.gov/gistemp/ (accessed Jan. 26, 2022).

[4] B. Turner, “Organisation for Economic Co-operation and Development (OECD),” *Statesman’s Yearb.*, no. February 2008, pp. 55–57, 2008, doi: 10.1007/978-1-349-74027-7_52.

[5] M. Ablain, A. Cazenave, G. Valladeau, and S. Guinehut, “A new assessment of the error budget of global Mean Sea Level rate estimated by satellite altimetry over 1993-2008,” *Ocean Science*, vol. 5, no. 2, pp. 193–201, 2009, doi: 10.5194/os-5-193-2009.

[6] IPCC, “Climate Change 2021: The Physical Science Basis,” 2021. [Online]. Available:https://www.ipcc.ch/report/ar6/wg1/downloads/report/IPCC_AR6_WGI_Full_Report.pdf.

[7] J. A. Church and J. M. Gregory, “Sea level change,” *Encyclopedia of Ocean Sciences*, pp. 493–499, 2019, doi: 10.1016/B978-0-12-409548-9.10820-6.

[8] J. Martinich and A. Crimmins, “Climate damages and adaptation potential across diverse sectors of the United States,” *Nature Climate Change*, vol. 9, no. 5, pp. 397–404, 2019, doi: 10.1038/s41558-019-0444-6.

[9] K. Ricke, L. Drouet, K. Caldeira, and M. Tavoni, “Country-level social cost of carbon,” *Nature Climate Change*, vol. 8, no. 10, pp. 895–900, 2018, doi: 10.1038/s41558-018-0282-y.

[10] N. S. Diffenbaugh and M. Burke, “Global warming has increased global economic inequality,” *Proceedings of the National Academy of Sciences U. S. A*, vol. 116, no. 20, pp. 9808–9813, 2019, doi: 10.1073/pnas.1816020116.

[11] P. E. V. De Miranda, *Hydrogen energy: Sustainable and perennial*. 2018.

[12] L. (International E. A. Cozzi and T. (International E. A. Gould, “World Energy Outlook 2021,” pp. 1–386, 2021, [Online]. Available: www.iea.org/weo.

[13] I. Energy Agency, “World Energy Outlook 2021,” 2021, Accessed: Mar. 11, 2022. [Online]. Available: www.iea.org/weo.

[14] “The Future of Hydrogen – Analysis - IEA.” https://www.iea.org/reports/the-future-of-hydrogen (accessed Jan. 27, 2022).

[15] I. Dincer and C. Acar, “Review and evaluation of hydrogen production methods for

better sustainability," *International Journal of Hydrogen Energy*, vol. 40, no. 34, pp. 11094–11111, 2014, doi: 10.1016/j.ijhydene.2014.12.035.

[16] I. Dincer and C. Acar, "Smart energy solutions with hydrogen options," *International Journal of Hydrogen Energy*, vol. 43, no. 18, pp. 8579–8599, 2018, doi: 10.1016/j.ijhydene.2018.03.120.

[17] "Trends in Solid Waste Management." https://datatopics.worldbank.org/what-a-waste/trends_in_solid_waste_management.html (accessed Mar. 02, 2022).

[18] UNEP and CCAC, *Global Methane Assessment Report*. 2021.

[19] "Energy and Civilization | The MIT Press." https://mitpress.mit.edu/books/energy-and-civilization (accessed Mar. 02, 2022).

[20] B. Fatih, "Canada 2022 - Energy Policy Review," p. 121, 2022, [Online]. Available: www.iea.org/t&c/.

[21] "Solar PV – Analysis - IEA." https://www.iea.org/reports/solar-pv (accessed Mar. 02, 2022).

[22] IRENA, *Renewable Capacity Statistiques De Capacité Estadísticas De Capacidad*. 2021.

[23] I. Dincer and M. Ozturk, "Geothermal Energy Sistems," *Elsevier*, p. 518, 2021.

[24] I. Dincer and C. Acar, "A review on clean energy solutions for better sustainability," *International Journal of Energy Research*, vol. 39, no. 5, pp. 585–606, Apr. 2015, doi: 10.1002/ER.3329.

[25] I. Dincer and C. Zamfirescu, "Sustainable energy systems and applications," *Sustainable Energy Systems and Applications*, pp. 1–816, Jan. 2012, doi: 10.1007/978-0-387-95861-3.

[26] J. Parraga, K. R. Khalilpour, and A. Vassallo, "Polygeneration with biomass-integrated gasification combined cycle process: Review and prospective," *Renewable and Sustainable Energy Reviews*, vol. 92, no. March, pp. 219–234, 2018, doi: 10.1016/j.rser.2018.04.055.

[27] H. Yağlı, C. Karakuş, Y. Koç, M. Çevik, İ. Uğurlu, and A. Koç, "Designing and exergetic analysis of a solar power tower system for Iskenderun region," *International Journal of Exergy*, vol. 28, no. 1, pp. 96–112, 2019, doi: 10.1504/IJEX.2019.097273.

[28] Y. Fang, M. C. Paul, S. Varjani, X. Li, Y. K. Park, and S. You, "Concentrated solar thermochemical gasification of biomass: Principles, applications, and development," *Renewable and Sustainable Energy Review.*, vol. 150, no. June, p. 111484, 2021, doi: 10.1016/j.rser.2021.111484.

[29] X. Zhang *et al.*, "Optimization analysis of a novel combined heating and power system based on biomass partial gasification and ground source heat pump," *Energy Conversation and Management*, vol. 163, no. January, pp. 355–370, 2018, doi:

10.1016/j.enconman.2018.02.073.

[30] S. Ciuta, D. Tsiamis, and M. J. Castaldi, “Gasification of waste materials : technologies for generating energy, gas, and chemicals from municipal solid waste, biomass, nonrecycled plastics, sludges, and wet solid wastes.”

[31] U. Kahraman and I. Dincer, “Performance analysis of a solar based waste to energy multigeneration system,” *Sustainable Energy Technologies Assessments*, vol. 50, no. August 2021, p. 101729, 2022, doi: 10.1016/j.seta.2021.101729.

[32] M. Shahbaz, T. Al-Ansari, A. Al-Nouss, and G. McKay, “Flowsheet development for the steam gasification of animal manure with subsequent CO2capturing using CaO: An Aspen Plus® modelling study,” *International Journal of Global Warming*, vol. 25, no. 3–4, pp. 259–270, 2021, doi: 10.1504/IJGW.2021.118999.

[33] O. Bamisile, Q. Huang, M. Dagbasi, M. Taiwo, and V. Adebayo, “Energy, exergy and environmental analyses of a biomass driven multi-generation system,” *International Journal of Exergy*, vol. 31, no. 3, pp. 249–267, 2020, doi: 10.1504/IJEX.2020.106454.

[34] M. Tańczuk, R. Junga, S. Werle, M. Chabiński, and Ziółkowski, “Experimental analysis of the fixed bed gasification process of the mixtures of the chicken manure with biomass,” *Renewable Energy*, pp. 1055–1063, 2019, doi: 10.1016/j.renene.2017.05.074.

[35] “End use definitions project tire-derived fuel (TDF).” [Online]. Available: www.ustires.org/scrap-tire-markets.

[36] B. Gungor and I. Dincer, “Development of a sustainable community with an integrated renewable and waste to energy system for multiple useful outputs,” *Journal of Cleaner Production*, vol. 312, no. March, p. 127704, 2021, doi: 10.1016/j.jclepro.2021.127704.

[37] A. Hasan and I. Dincer, “Comparative assessment of various gasification fuels with waste tires for hydrogen production,” *International Journal of Hydrogen Energy*, vol. 44, no. 34, pp. 18818–18826, 2019, doi: 10.1016/j.ijhydene.2018.11.150.

[38] E. B. Machin, D. T. Pedroso, and J. A. de Carvalho, “Energetic valorization of waste tires,” *Renewable and Sustainable Energy Reviews*, vol. 68, no. September 2016, pp. 306–315, 2017, doi: 10.1016/j.rser.2016.09.110.

[39] D. A. Bell, B. F. Towler, and M. Fan, *Front Matter*. 2011.

[40] E. P. Review, “Turkey 2021,” 2021.

[41] A. Reva and A. Blinderman, *Underground gasification of oil shale*. 2018.

[42] Y. Bicer and I. Dincer, “Development of a multigeneration system with underground coal gasification integrated to bitumen extraction applications for oil sands,” *Energy Conversation and Management*, vol. 106, pp. 235–248, 2015, doi: 10.1016/j.enconman.2015.09.020.

[43] F. Yilmaz, M. Ozturk, and R. Selbas, “Design and thermodynamic analysis of coal-gasification assisted multigeneration system with hydrogen production and liquefaction,” *Energy Conversation and Management*, vol. 186, no. December 2018, pp. 229–240, 2019, doi: 10.1016/j.enconman.2019.02.053.

[44] S. S. Seyitoglu, I. Dincer, and A. Kilicarslan, “Energy and exergy analyses of hydrogen production by coal gasification,” *International Journal of Hydrogen Energy*, vol. 42, no. 4, pp. 2592–2600, 2017, doi: 10.1016/j.ijhydene.2016.08.228.

[45] I. Dincer, C. O. Colpan, and M. A. Ezan, Eds., “Environmentally-Benign Energy Solutions,” 2020, doi: 10.1007/978-3-030-20637-6.

[46] N. Tukenmez, M. Koc, and M. Ozturk, “A novel combined biomass and solar energy conversion-based multigeneration system with hydrogen and ammonia generation,” *International Journal of Hydrogen Energy*, vol. 46, no. 30, pp. 16319–16343, 2021, doi: 10.1016/j.ijhydene.2021.02.215.

[47] O. Siddiqui, I. Dincer, and B. S. Yilbas, “Development of a novel renewable energy system integrated with biomass gasification combined cycle for cleaner production purposes,” *Journal of Cleaner Production*, vol. 241, p. 118345, 2019, doi: 10.1016/j.jclepro.2019.118345.

[48] M. Temiz and I. Dincer, “Concentrated solar driven thermochemical hydrogen production plant with thermal energy storage and geothermal systems,” *Energy*, vol. 219, p. 119554, 2021, doi: 10.1016/j.energy.2020.119554.

[49] M. Temiz and I. Dincer, “A unique ocean and solar based multigenerational system with hydrogen production and thermal energy storage for Arctic communities,” *Energy*, vol. 239, p. 122126, 2022, doi: 10.1016/j.energy.2021.122126.

[50] “Net Zero by 2050,” *Net Zero by 2050*, 2021, doi: 10.1787/c8328405-en.

[51] M. Ghazvini, M. Sadeghzadeh, M. H. Ahmadi, S. Moosavi, and F. Pourfayaz, “Geothermal energy use in hydrogen production: A review,” *International Journal of Energy Research.*, vol. 43, no. 14, pp. 7823–7851, 2019, doi: 10.1002/er.4778.

[52] M. Temiz and I. Dincer, “An integrated bifacial photovoltaic and supercritical geothermal driven copper-chlorine thermochemical cycle for multigeneration,” *Sustainable Energy Technologies and Assessments*, vol. 45, no. September 2020, p. 101117, 2021, doi: 10.1016/j.seta.2021.101117.

[53] J. W. Lund and A. N. Toth, “Direct utilization of geothermal energy 2020 worldwide review,” *Geothermics*, vol. 90, no. July, p. 101915, 2021, doi: 10.1016/j.geothermics.2020.101915.

[54] B. Gungor and I. Dincer, “Development of a waste-to-energy gasification system for sustainable communities,” *International Journal of Energy Research*. 2021, doi: 10.1002/er.7464.

[55] H. Ishaq and I. Dincer, “Comparative assessment of renewable energy-based hydrogen production methods,” *Renewable and Sustainable Energy Reviews.*, vol. 135, no. July 2020, p. 110192, 2021, doi: 10.1016/j.rser.2020.110192.

[56] R. P. Merchán, M. J. Santos, A. Medina, and A. Calvo Hernández, "High temperature central tower plants for concentrated solar power: 2021 overview," *Renewable and Sustainable Energy Review*, vol. 155, p. 111828, 2022, doi: 10.1016/j.rser.2021.111828.

[57] I. Dincer and Marc A. Rosen, *Thermal energy storage systems and applications*. Wiley, 2021.

[58] S. Heidenreich, M. Müller, and P. U. Foscolo, *Advanced Biomass Gasification: New Concepts for Efficiency Increase and Product Flexibility*. 2016.

[59] J. Karl and T. Pröll, "Steam gasification of biomass in dual fluidized bed gasifiers: A review," *Renewable and Sustainable Energy Review*, vol. 98, no. September, pp. 64–78, 2018, doi: 10.1016/j.rser.2018.09.010.

[60] I. Bianco, D. Panepinto, and M. Zanetti, "End-of-life tyres: Comparative life cycle assessment of treatment scenarios," *Applied Sciences*, vol. 11, no. 8, 2021, doi: 10.3390/app11083599.

[61] S. Heidenreich, M. Müller, and P. U. Foscolo, *Advanced Biomass Gasification: New Concepts for Efficiency Increase and Product Flexibility*. Academic Press, 2016.

[62] F. R. M. Nascimento, A. M. González, E. E. Silva Lora, A. Ratner, J. C. Escobar Palacio, and R. Reinaldo, "Bench-scale bubbling fluidized bed systems around the world - Bed agglomeration and collapse: A comprehensive review," *International Journal of Hydrogen Energy*, vol. 46, no. 36, pp. 18740–18766, 2021, doi: 10.1016/j.ijhydene.2021.03.036.

[63] I. Dincer and Y. Bicer, *Integrated energy systems for multigeneration*, 1st Edition. Elsevier, 2019.

[64] S. Bai, Q. Shao, P. Wang, Q. Dai, X. Wang, and X. Huang, "Highly Active and Selective Hydrogenation of CO2 to Ethanol by Ordered Pd-Cu Nanoparticles," *Journal of American Chemical Society*, vol. 139, no. 20, pp. 6827–6830, May 2017, doi: 10.1021/jacs.7b03101.

[65] "IMO 2020 – cutting sulphur oxide emissions." https://www.imo.org/en/MediaCentre/HotTopics/Pages/Sulphur-2020.aspx (accessed Mar. 05, 2022).

[66] Riyanto, S. Ramadan, S. Fariduddin, A. R. Aminudin, and A. K. Hayatri, "Conversion of Carbon Dioxide into Ethanol by Electrochemical Synthesis Method Using Cu-Zn Electrode," *IOP Conference Series Materials Science Engineering*, vol. 288, no. 1, 2018, doi: 10.1088/1757-899X/288/1/012136.

[67] G. Perkins, "Underground coal gasification – Part I: Field demonstrations and process performance," *Progress in Energy and Combustion Science*, vol. 67, pp. 158–187, 2018, doi: 10.1016/j.pecs.2018.02.004.

[68] G. Perkins, "Underground coal gasification – Part II: Fundamental phenomena and modeling," *Progress in Energy and Combustion Science*, vol. 67, pp. 234–274, 2018, doi: 10.1016/j.pecs.2018.03.002.

[69] P. F. Nelson, “The Coal Handbook: Towards Cleaner Production,” *Coal Handbook Towards Cleaner Production*, pp. 21–62, 2013, Accessed: Mar. 05, 2022. [Online]. Available:http://www.sciencedirect.com/science/article/pii/B978178242116050002 5.

[70] M. S. Blinderman and A. Y. Klimenko, “Underground coal gasification and combustion.”

[71] F. Fantozzi and P. Bartocci, “Integrated Gasification Combined Cycle (IGCC) Technologies,” *Integrated Gasification Combine Cycle Technology,*, pp. 145–180, 2017, Accessed: Mar. 05, 2022. [Online]. Available: http://www.sciencedirect.com/science/article/pii/B9780081001677000044.

[72] M. Ozer, O. M. Basha, G. Stiegel, and B. Morsi, “Effect of coal nature on the gasification process,” *Integrated Gasification Combine Cycle Technology*, pp. 257–304, 2017, doi: 10.1016/B978-0-08-100167-7.00007-X.

[73] E. Yağmur, E. H. Şimşek, Z. Aktaş, and T. Toğrul, “Effect of demineralization process on the liquefaction of Turkish coals in tetralin with microwave energy: Determination of particle size distribution and surface area,” *Fuel*, vol. 84, no. 18, pp. 2316–2323, 2005, doi: 10.1016/j.fuel.2005.05.004.

[74] “Aspen Plus | Leading Process Simulation Software | AspenTech.” https://www.aspentech.com/en/products/engineering/aspen-plus (accessed Aug. 04, 2021).

[75] “EES: Engineering Equation Solver | F-Chart Software : Engineering Software.” https://fchartsoftware.com/ees/ (accessed Aug. 07, 2021).

[76] I. Dincer, *Thermodynamics: A Smart Approach*. United Kingdom, 2020.

[77] H. Gu, Y. Tang, J. Yao, and F. Chen, “Study on biomass gasification under various operating conditions,” *Journal of Energy Institute*, vol. 92, no. 5, pp. 1329–1336, Oct. 2019, doi: 10.1016/j.joei.2018.10.002.

[78] “Turkish Statistical Institute (TURKSTAT).” https://www.tuik.gov.tr/Home/Index (accessed Aug. 07, 2021).

[79] Z. Akyürek, “Sustainable valorization of animal manure and recycled polyester: Co-pyrolysis synergy,” *Sustainability.*, vol. 11, no. 8, pp. 1–14, 2019, doi: 10.3390/su11082280.

[80] A. S. Augustine, Y. H. Ma, and N. K. Kazantzis, “High pressure palladium membrane reactor for the high temperature water-gas shift reaction,” *International Journal of Hydrogen Energy,*, vol. 36, no. 9, pp. 5350–5360, May 2011, doi: 10.1016/j.ijhydene.2011.01.172.

[81] H. Y. Ismail, A. Abbas, F. Azizi, and J. Zeaiter, “Pyrolysis of waste tires: A modeling and parameter estimation study using Aspen Plus®,” *Waste Manag.*, vol. 60, pp. 482–493, 2017, doi: 10.1016/j.wasman.2016.10.024.

[82] M. Tamborra, “European Commission, DG Research,” *Iccr-International.Org*, vol.

4, no. May, pp. 1–77, 2006, [Online]. Available: http://www.iccr-international.org/regionet/docs/ws3-tamborra.pdf.

[83] S. Szima *et al.*, "Techno-Economic Assessment of IGCC Power Plants Using Gas Switching Technology to Minimize the Energy Penalty of CO2 Capture," *Clean Technologies*, vol. 3, no. 3, pp. 594–617, 2021, doi: 10.3390/cleantechnol3030036.

[84] I. Dincer and Marc A. Rosen, *Exergy : energy, environment and sustainable development*, 3rd Edition. Elsevier Science, 2020.

[85] L. Liu *et al.*, "Experimental study of biomass gasification with oxygen-enriched air in fluidized bed gasifier," *Science of the Total Environment*, vol. 626, pp. 423–433, 2018, doi: 10.1016/j.scitotenv.2018.01.016.

[86] J. Li, S. Liao, W. Dan, K. Jia, and X. Zhou, "Experimental study on catalytic steam gasification of municipal solid waste for bioenergy production in a combined fixed bed reactor," *Biomass and Bioenergy*, vol. 46, pp. 174–180, 2012, doi: 10.1016/j.biombioe.2012.08.026.

[87] B. Gungor and I. Dincer, "Development of a sustainable community with an integrated renewable and waste to energy system for multiple useful outputs," *Journal of Cleaner Production*, vol. 312, Aug. 2021, doi: 10.1016/j.jclepro.2021.127704.

[88] S. Portofino *et al.*, "Steam gasification of waste tyre: Influence of process temperature on yield and product composition," *Waste Management*, vol. 33, no. 3, pp. 672–678, 2013, doi: 10.1016/j.wasman.2012.05.041.

[89] Y. Bicer and I. Dincer, "Energy and exergy analyses of an integrated underground coal gasification with SOFC fuel cell system for multigeneration including hydrogen production," *International Journal of Hydrogen Energy*, vol. 40, no. 39, pp. 13323–13337, 2015, doi: 10.1016/j.ijhydene.2015.08.023.

[90] B. Zhang, S. Guo, and H. Jin, "Production forecast analysis of BP neural network based on Yimin lignite supercritical water gasification experiment results," *Energy*, vol. 246, p. 123306, 2022, doi: 10.1016/j.energy.2022.123306.

[91] "Interesting Rates - RBC Royal Bank." https://www.rbcroyalbank.com/rates/interesting-rates.html (accessed Apr. 20, 2022).

[92] X. gang Zhao, G. wu Jiang, A. Li, and L. Wang, 'Economic analysis of waste-to-energy industry in China', Waste Management, vol. 48, pp. 604–618, 2016, doi: 10.1016/j.wasman.2015.10.014.